REACTOR MATERIALS

A Quarterly Technical Progress Review

Prepared for DIVISION OF TECHNICAL INFORMATION, USAEC, by
R. W. DAYTON, E. M. SIMONS, and ASSOCIATES, BATTELLE MEMORIAL INSTITUTE

Summer 1966

● VOLUME 9

● NUMBER 2

TECHNICAL PROGRESS REVIEWS

To meet the needs of industry for concise summaries of current atomic developments, the Atomic Energy Commission is publishing this series, Technical Progress Reviews. Issued quarterly, each of the reviews digests and evaluates the latest findings in a specific area of nuclear technology and science.

The five journals published in this series are:

Isotopes and Radiation Technology P. S. Baker, A. F. Rupp, and associates
Oak Ridge National Laboratory

Nuclear Safety Wm. B. Cottrell, W. H. Jordan, and associates
Oak Ridge National Laboratory

Power Reactor Technology
Argonne National Laboratory

Reactor Fuel Processing Stephen Lawroski and associates
Chemical Engineering Division, Argonne National Laboratory

Reactor Materials R. W. Dayton, E. M. Simons, and associates
Battelle Memorial Institute

See the back cover for availability information.

The views expressed in this publication do not necessarily represent those of the United States Atomic Energy Commission, its divisions or offices, or of any Commission advisory committee or contractor.

Availability of Reports Cited in This Review

Unclassified AEC reports are available for inspection at AEC depository libraries and are sold by the Clearinghouse for Federal Scientific and Technical Information, National Bureau of Standards, U. S. Department of Commerce, 5285 Port Royal Road, Springfield, Va., 22151. Some of the reports cited are not available owing to their preliminary nature; however, the information contained in them will eventually be made available in formal progress or topical reports.

Unclassified reports issued by other Government agencies or private organizations should be requested from the originator.

Unclassified British and Canadian reports may be inspected at AEC depository libraries. British reports are sold by the British Information Service, 45 Rockefeller Plaza, New York, N. Y.; Canadian reports (AECL series) are sold by the Scientific Document Distribution Office, Atomic Energy of Canada, Ltd., Chalk River, Ontario, Canada.

Classified U. S. and foreign reports identified in this journal as Classified may be purchased by properly cleared Access Permit Holders from the Division of Technical Information Extension, U. S. Atomic Energy Commission, P. O. Box 1001, Oak Ridge, Tenn., 37830. Such reports may be inspected at classified AEC depository libraries.

Contents

Reactor Materials

Vol. 9, No. 2

I Fuel and Fertile Materials

Uranium Metal and Alloys 73
Plutonium 74
Plutonium Compounds 77
Thorium 79
Metal–Ceramic Fuels 79
Coated-Particle Fuels 80
Uranium Oxide Fuels 81
Uranium and Thorium Carbides, Nitrides, Sulfides, and Phosphides . . 83
Basic Studies of Irradiation Effects in Fuel Materials 87
References 88

II Moderator Materials

Graphite 91
Beryllium Metal and Alloys 92
Beryllium Oxide 94
Solid Hydrides 96
References 98

III Nuclear Poisons

Metallic Poison Materials 99
Dispersion and Nonmetallic Poison Materials. 100
References 102

IV Cladding and Structural Materials

Corrosion 103
Metal–Water Reactions. 110
Radiation Effects in Nonfuel Materials . 111
Selected Mechanical Properties of Cladding and Structural Materials 117
Selected Metallurgical Aspects of Cladding and Structural Materials 123
Diffusion Studies 131
Ceramic Technology 132
References 133

V Special Fabrication Techniques

Melting, Casting, and Hot and Cold Working 138
Cladding 139
Pressure Bonding 142
Welding and Brazing 142
Nondestructive Testing 147
References 148

Issued quarterly by the U. S. Atomic Energy Commission. Use of funds for printing this publication approved by the Director of the Bureau of the Budget on October 14, 1963.

Reactor Materials is one of a series of quarterly technical progress reviews broadly covering the field of nuclear science and technology. Under the auspices of the USAEC Division of Technical Information, *Reactor Materials* is prepared by Battelle personnel from worldwide literature. It covers properties, behavior, and fabrication processes of materials applicable to nuclear reactor components and associated equipment.

The reader will recognize that the scope of this Review is too broad to permit detailed coverage of every topic. Rather, the authors and editors attempt to combine the highlights of significant new developments into an information summary of current research for both management and the technical specialist. As a rule, enough of the results are presented to define the research and summarize the findings. For readers desiring more information on any particular topic, a complete set of references is provided at the end of each section.

Each quarter a number of bibliographies, monographs, and books appear on subjects within the scope of *Reactor Materials*. Although the main purpose of this Review is to call attention to findings that are new and significant, such publications are noted in the text because they often represent excellent compilations of available information on important materials topics.

R. W. DAYTON
E. M. SIMONS
R. W. ENDEBROCK
Battelle Memorial Institute

Section

I

Reactor Materials

Fuel and Fertile Materials

Uranium Metal and Alloys

Unalloyed Uranium

On the basis of detailed studies of the fatigue of unalloyed uranium, British workers arrived at the following conclusions:[1]

1. The fatigue limit of worked and annealed uranium at room temperature is about 30,000 psi at 10^8 cycles of completely reversed stress. This is 39% of a tensile strength of 116,000 psi.

2. The endurance limit is raised by a cold-working step and by a decrease in the testing temperature.

3. Even though uranium is not usually notch sensitive under cyclic loading, the notch effect of a crack in protective plating can lower the fatigue life seriously.

4. The endurance limit of uranium is not affected seriously by a hydrogen atmosphere at room temperature, nor by the frequency of stress application. However, self-heating caused by internal friction could influence the fatigue behavior at high stresses and moderate frequencies if no cooling were used.

5. Like conventional metals, uranium shows precipitation on slip bands and does not undergo very much twinning during fatigue loading.

The oxidation of uranium by CO_2 that has been partially decomposed by ionizing radiation has been studied at the Japan Atomic Energy Research Institute.[2] It was found that the oxidation rate increased almost linearly with increasing percentage of decomposition of the CO_2. The oxidation rate at 500°C with 0.68% decomposed CO_2 was 18 times that with undecomposed CO_2. This difference is related to the oxygen content in the decomposed gas.

High-Uranium Alloys

The identification and distribution of intermetallic compounds found in as-cast and in as-cast and beta-quenched adjusted uranium (containing small precipitate-forming alloy additions) were studied by the British.[3] The precipitate consisted of a network of particles about 0.1 μ in diameter, distributed fairly uniformly throughout the matrix. A technique was developed for extracting precipitates for X-ray diffraction. At the edge of a specimen of adjusted uranium that had been soaked in the gamma phase and furnace cooled over a period of several days, two intersecting networks were observed, neither of which was associated with the alpha-uranium structure. It was considered likely that the coarser network resulted from a eutectoid reaction during the gamma–beta phase transformation. The network of smaller particles followed the beta grain boundaries.

The British also investigated the precipitates occurring in uranium–iron–aluminum alloys and their solution in the beta and gamma phases by measurements of electrical resistance and by metallography.[4] Iron dissolved rapidly in the beta phase. Some UAl_2 precipitates also dissolved, and those which did not do so became coarser. Both iron and aluminum dissolved very rapidly in gamma uranium. The gamma phase was shown to exist in equilibrium down to 710°C in adjusted uranium. The implications of these results with regard to grain refinement and swelling resistance of adjusted uranium were discussed.

Experimenters at Battelle–Northwest[5] were successful in utilizing electron microscopy to study particle-size–density distributions in dilute alloys of uranium. The results of a quantitative metallographic procedure using transmission electron micrographs agreed well with those obtained from replica electron microg-

raphy. The superior resolution inherent in the transmission technique permits the observation of particles normally too small to be resolved by replica methods.

A new phase in the uranium–molybdenum silicon system has been reported by Yugoslavian workers.[6] The $U_4Mo_5Si_3$ phase is hexagonal, with unit-cell dimensions $a = 5.37$ A and $c = 8.58$ A. This phase belongs to the $P6/mmc$ space group or a subgroup. A $U_4Cr_5Si_3$ phase was found to have a similar structure.

The effect of carbon on the melting point of uranium was studied by the National Lead Company of Ohio.[7] The melting point of high-purity uranium was found to be 1133 ± 3°C, whereas uranium containing 187 ppm, 615 ppm, and 857 ppm carbon showed a melting point of approximately 1137°C. Metallographic examinations indicated a peritectic at approximately 55 ppm carbon.

In other work[8] it was found that nitric acid etching removed nitrides and carbides from uranium metal.

An allotropic transformation[7] has been found in the U_3Si compound at 765 ± 3°C. The tetragonal U_3Si transforms to a cubic form isostructural with Cu_3Au, and this new form is stable to 930°C, the temperature of the peritectoid decomposition.

Low-Uranium Alloys

Canadian investigators[9] have found that the pronounced thermal effect observed on heating or cooling aluminum-rich aluminum–uranium alloys is due to a phase transformation occurring in the UAl_4 compound. The transformation observed in aluminum–20 wt.% uranium alloys occurred near the alpha-aluminum–UAl_4 eutectic temperature of 646°C, making it difficult to detect from heating curves. However, thermal and X-ray analyses indicated that, upon cooling, the high-temperature phase labeled beta UAl_4 precipitated during eutectic solidification.

General

A Russian publication, "Corrosion of Uranium and Its Alloys," is now available in translated form.[10]

Included in the transactions[11] of a meeting on X-ray diffraction are several papers dealing with uranium and uranium alloys: "Kossel Diffraction Patterns of a Uranium Single Crystal," "Effect of Alloying on the Quench-Induced Texture of Alpha-Uranium,"[12] "Texture Gradients of Various Degrees by NLO Processes," "Effect of Soller Slits on X-ray Intensity," and "Precise Pole Figure Measurements on Rolled Uranium Sheet." (M. S. Farkas)

Plutonium

Argonne National Laboratory (ANL) is continuing the development of metallic fuel alloys with studies of uranium–plutonium–fizzium (fissium), uranium–plutonium–zirconium, and uranium–plutonium–titanium alloys, In an irradiation experiment[13] to determine the effects of increased cladding thickness on extending the burnup capabilities of uranium–plutonium–fizzium, five specimens achieved calculated burnups as high as 8.7 at.% without failure. A sixth specimen developed a localized rupture. Irradiation conditions for the experiment are shown in Table I-1.

The phase relations in uranium–20 wt.% plutonium–fissium alloys have been extensively studied.[14] The solidus temperatures of these alloys decreased from about 930 to 800°C with additions of fissium up to 15 wt.%. An intermediate phase termed theta, which is thought to contain uranium, plutonium, and palladium, was

Table I-1 IRRADIATION CONDITIONS FOR HIGH-BURNUP URANIUM–PLUTONIUM–FIZZIUM SPECIMENS[13]

Fuel composition (balance uranium), wt.%	Jacket thickness, in.	Maximum fuel temp., °C	Maximum jacket temp., °C	Predicted maximum burnup to failure, at.%	Actual calculated burnup, at.%
10 Pu–10 Fz	0.015	590	510	5.0	7.1
10 Pu–10 Fz	0.020	610	530	5.9	7.1
15 Pu–10 Fz	0.015*	625	545	5.3	8.7
15 Pu–10 Fz	0.025	625	545	9.4	8.7
15 Pu–10 Fz	0.015	625	545	7.2	8.7
10 Pu–10 Fz	0.025	610	530	6.7	7.1

*Observed to have developed a localized jacket split.

present to the melting point in all the alloys. A U_2Ru phase was also present with the theta in most of the alloys; however, additions of zirconium to the fissium suppressed the formation of U_2Ru and instead formed zirconium–ruthenium. Alloys containing less than 10 wt.% fissium undergo transformations involving the three allotropic forms of uranium, gamma-prime (U_2Mo), eta, and zeta phases from the uranium–plutonium system, and two of the previously mentioned intermediate phases (either theta plus U_2Ru or theta plus zirconium–ruthenium). Less complicated transformation characteristics are exhibited by the alloys containing more than 10 wt.% fissium in that the formation of beta uranium is entirely suppressed and gamma-plus-theta phases are stable with either U_2Ru or zirconium–ruthenium from the melting point to about 550°C.

If the fissium system is simplified by disregarding the theta, U_2Ru, and zirconium–ruthenium phases, then this system appears to be similar to the uranium–plutonium–molybdenum system in the region of about 2 to 10 wt.% molybdenum and 20 wt.% plutonium. A pseudoternary system has been proposed, where the components are uranium, plutonium, and fissium. In this system, three four-phase reactions occur as follows:

$$\gamma + \beta + \eta \rightarrow \zeta \quad \text{at } 610°C$$

$$\beta + \gamma \rightarrow \zeta + \gamma' \quad \text{at } 555°C$$

$$\beta \rightarrow \alpha + \zeta + \gamma' \quad \text{at } 500°C$$

Quenching of alloys containing less than 10 wt.% fissium did not bring about the retention of gamma uranium as expected. Instead, a tetragonal modification of the gamma phase, called gamma-naught, and a distorted alpha resulted. Gamma was retained in alloys with more than 10 wt.% fissium. An increase in the sluggishness of the gamma transformation accompanied an increase in fissium content. Fuel pins of uranium–20 wt.% plutonium–10 wt.% fissium, prepared by injection casting, retained gamma phase at the top, but a considerable amount of the low-temperature phases (assumed to be alpha, gamma-prime, and zeta) appeared in the microstructure of the bottom section of the pins. Therefore a substantial range in properties may occur over the length of cast fuel pins from variations in the phases present.

Room- and elevated-temperature mechanical properties of uranium–plutonium–zirconium and uranium–plutonium–titanium alloys have been reported in greater detail than previously.[13,15] Results of compression and short- and long-time tensile tests are shown in Tables I-2 to I-4, respectively.

Solid-state transformations in a uranium–15 wt.% plutonium–10 wt.% zirconium alloy were investigated by dilatometry and, more extensively, by differential thermal analysis.[13] Results are shown in Fig. I-1. Hysteresis

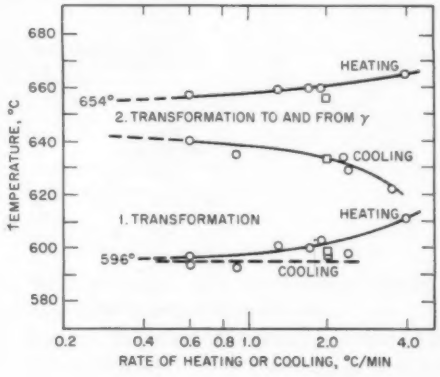

Fig. I-1 Solid-state transformations in uranium–15 wt.% plutonium–10 wt.% zirconium (uranium–12.9 at.% plutonium–22.5 at.% zirconium) as a function of heating and cooling rates.[13] ○, differential thermal analysis; □, dilatometry.

occurred in both transformations on heating but only in the higher temperature transformation on cooling. The hysteresis increased with increasing heating and cooling rates.

Mound Laboratory[16] has also begun investigations of uranium–plutonium–zirconium alloys. Although the work is directed toward the phase relations in the ternary system, preliminary studies have dealt mainly with binary systems. Results of studies of the uranium–plutonium binary system were essentially in agreement with published phase diagrams. Solidus temperatures of plutonium–zirconium alloys containing up to 25 at.% zirconium were found to be higher than those given in the literature (905°C at 25 at.% zirconium compared with the literature value of 840°C).

Viscosities of several liquid plutonium–cerium alloys have been measured at tempera-

Table I-2 ULTIMATE COMPRESSIVE STRENGTH OF URANIUM–PLUTONIUM–ZIRCONIUM AND URANIUM–PLUTONIUM–TITANIUM ALLOYS AT SELECTED TEMPERATURES[15]

Alloy, wt.%	Heat-treatment	Ultimate compressive strength, kg/mm² at indicated temp.				
		25 C	500 C	625 C	675 C	750 C
U–11.1 Pu–6.3 Zr	Hom.*	164		12	4.0	
U–12.3 Pu–14.1 Zr	Hom.	166			6.9	4.2
	As cast	164	>55	12	5.2	
U–16.6 Pu–6.3 Zr	As cast	127	>55	11	2.5	
U–15 Pu–10 Zr	As cast	129	48	11	5.6	
U–18.5 Pu–14.1 Zr	Hom.	116			5.6	
U–9.1 Ti	Hom.	145	115	80	65.0	35.0
	As cast	150	95	65	50.0	30.0
U–11.4 Pu–3.4 Ti	Hom.	96			6.3	
U–17.1 Pu–3.4 Ti	Hom.	96			3.8	
U–15 Pu–6.5 Ti	Hom.	130	37	13	6.3	4.2
	As cast	158	27	12	9.0	
U–15 Pu–10 Ti	Hom.	90	45	20	10.0	7.0
	As cast	120	40			
U–22.1 Pu–11.8 Ti	As cast	141	55	30	20.0	10.0

*Homogenizing heat-treatment: 1050 C for one week, oil quench for the alloys with less than 10 wt.% zirconium or titanium; and 950 C for one week, oil quench for alloys with less than 10 wt.% zirconium or titanium.

Table I-3 VARIATIONS OF TENSILE PROPERTIES WITH TEMPERATURE IN HOMOGENIZED AND QUENCHED* URANIUM–PLUTONIUM–ZIRCONIUM AND URANIUM–PLUTONIUM–TITANIUM ALLOYS[13]

Alloy, nominal wt.%			Temp., C	Tensile strength		Young's modulus (E), 1000 kg/mm²	Type of failure
				Ultimate, kg/mm²	Yield,† kg/mm²		
U	Pu	Zr					
82.6	11.1	6.3	25	18.1		17.4	Brittle
			675	1.2	1.1	1.4	Ductile
77.1	16.6	6.3	25	4.0		10.6	Brittle
			675	1.2	1.1	1.6	Ductile
67.4	18.5	14.1	25	7.7		13.0	Brittle
			675	2.9	2.8	1.9	Ductile
U	Pu	Ti					
90.9	0	9.1	25	14.7		22.7	Brittle
			675	26.3		3.0	Brittle
85.2	11.4	3.4	25	30.8		17.9	Brittle
			675	5.5	5.2	2.4	Ductile
75	15	10	675	7.0	6.5	3.0	Ductile

*All specimens were tested in creep prior to the tensile tests and therefore contain some (<5%) hot work.

†Yield strength at 0.2% offset. Brittle specimens did not attain this before fracturing.

Table I-4 TIME, MIN, TO ATTAIN 2% STRAIN IN URANIUM–PLUTONIUM–ZIRCONIUM AND URANIUM–PLUTONIUM–TITANIUM ALLOYS[13]

Alloy composition, wt.%			Load, kg/mm²	Temp., °C				
				600	625	650	675	700
U	Pu	Zr						
82.6	11.1	6.3	0.5				15	
			1.0				5	
			2.0				3	
			4.0		5		1	
77.1	16.6	6.3	0.5				10	
			1.0		5,000		1	
			2.0		210			
			4.0		10			
75	15	10	0.5			5,000		
			1.0		5,000	80		
			2.0		210	1		
			4.0		10			
67.4	18.5	14.1	0.5	100,000		5,000	45	40
			1.0	10,000		80	5	5
			2.0	800		1	1	1
			4.0	70				
U	Pu	Ti						
85.2	11.4	3.4	0.5					
			1.0		20,000		20,000	
			2.0		350		60	
			4.0		5		1	
75	15	10	0.5	400		110		45
			1.0	20		5		5
			2.0					
			4.0					

tures up to about 850°C. The resulting data fit the general equation

$$\log [10^5\ \eta(\text{poise})/T(°\text{K})] = [1000\ m/T(°\text{K}) - b]$$

Values for m and b, along with activation energy and liquidus temperature (as measured in the viscosimeter) are presented in Table I-5.

Table I-5 VISCOSITY DATA FOR PLUTONIUM–CERIUM ALLOYS[16]

Viscosity Equation: Log $[10^5\ \eta(\text{poise})/T(°\text{K})] = [1000\ m/T(°\text{K})] - b$

Alloy composition (balance Pu), at.%	m	b	Activation energy, cal/gram atom	Standard deviation, poise	Liquidus temp.,* °C
Unalloyed	1.1270	0.4191	5157	±0.001	
4.9 Ce	1.4070	0.5185	6438	±0.004	639
10.0 Ce	1.2528	0.4073	5733	±0.001	
13.9 Ce	1.2684	0.4951	5804	±0.002	636
16.5 Ce	1.2855	0.4841	5882	±0.001	628
22.0 Ce	1.2932	0.5028	5917	±0.001	659
34.4 Ce	1.0226	0.2369	4679	±0.001	692
40.8 Ce	1.1479	0.3574	5253	±0.001	703
50.6 Ce	1.2327	0.4757	5641	±0.001	721
75.0 Ce	0.9973	0.4208	4564	±0.001	743
100 Ce	0.8838	0.3927	4044	±0.003	

*As measured in the viscosimeter.

Further studies of the plutonium–cerium–iron ternary systems have resulted in some modification of the previously proposed ternary-phase diagram. The diagram incorporating these changes is shown in Fig. I-2.

Los Alamos has reported that the equilibrium temperature for the alpha-to-beta phase transformation of plutonium is 117.0 ± 0.5°C, on the basis of electrical-resistivity measurements of thin, high-purity plutonium specimens.[17]

The development of an a-c electrolytic technique for etching alpha, delta, and beta plutonium has been reported.[18] Use of the technique permits examination of microstructures under bright-field illumination, preserves the form of alpha microcracks, and delineates coring in stabilized delta and beta allotropes.

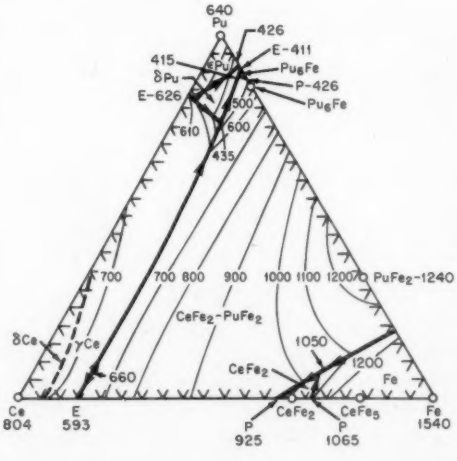

Fig. I-2 Plutonium-cerium-iron phase diagram.[16] E = eutectic; P = peritectic; numbers are °C; composition scales are atomic (5 at.%/division).

Plutonium physical-metallurgy studies at Battelle–Northwest[19] are continuing. Evidence that cold-worked alpha plutonium anneals at 105°C was obtained from determinations of subsequent alpha-to-beta transformation rates (deformation accelerates the alpha-to-beta transformation). The results also showed that the annealing process was complete after two weeks at 105°C.

The temperature dependence of the creep of beta plutonium, formed from both alpha and gamma, was determined at compressive stresses up to 10,000 psi. At 7500 and 10,000 psi, the creep activation energies for beta formed from gamma are 10 to 20% higher, respectively, than the corresponding values for beta formed from alpha. (V. W. Storhok)

Plutonium Compounds

Nuclear Materials & Equipment Corp.[20] has studied the thermal expansion of various PuO_2-containing oxides by the use of a high-temperature diffractometer. The results are presented in Table I-6.

Canadian workers, in studies involving aluminum–plutonium alloys and PuO_2, have found[21]

Table I-6 THERMAL-EXPANSION COEFFICIENTS OF PuO_2 MATERIALS[20]

Composition, wt.%	Constants in expression $\alpha = A \times 10^{-6} (1 + B \times 10^{-4}\, t)$, °C^{-1}	
	A	B
100 ThO_2 (standard)	8.6038	2.0925
100 ThO_2 (experimental)	8.9592	1.8334
100 $UO_{2.24}$	11.1442	0.0187
100 $UO_{2.08}$	9.6985	0.9796
$UO_{2.11}$ – 5 PuO_2	7.4189	7.8943
$UO_{2.13}$ – 12.5 PuO_2	9.0176	2.9893
$UO_{2.10}$ – 20 PuO_2	7.5353	13.8453
$UO_{2.09}$ – 35 PuO_2	7.7180	6.3313
$UO_{2.01}$ – 50 PuO_2	7.9772	5.9733
UO_2 – 80 PuO_2	7.7176	10.4012
100 PuO_2	6.7614	3.2460
100 PuO_2	6.7046	14.7319

that the $PuAlO_3$ compound tentatively identified as belonging to the rhombohedral crystal class is actually orthorhombic, with lattice parameters of $a = 3.750$, $b = 5.314$, and $c = 5.350$ A. They have also done experiments in which the only effect of a thermal gradient between 2310 and 1890°C across a UO_2–1 wt.% PuO_2 pellet was to grow columnar grains and homogenize microsegregation, and no plutonium migration occurred.

An improvement in quality of PuO_2 microspheres was noted by Mound Laboratory[16] as more dense feed material was used in plasma spheroidization studies; arc-melted oxide feed produced the most desirable structure.

In the course of plutonium oxide fabrication studies, Nuclear Materials & Equipment Corp. has noted that generally an oxidizing sintering atmosphere is desirable, that PuO_2 obtained from the nitrate is more sinterable, and that 0.4 to 1.0 mole % of SrO is an excellent sintering aid.[22] The same laboratory has established melting points[23] in the system UO_2–PuO_2–ZrO_2–CaO as shown in Table I-7.

The irradiation of specimens of undefined composition of PuO_2 mixed with sol–gel ThO_2 is reported by Oak Ridge National Laboratory.[24] A linear heat rating of 245 watts/cm and a burnup of 29,000 Mwd/ton resulted in a fission-gas release that was less than 5% of theoretical.

Table I-7 MELTING POINTS[23] IN THE SYSTEM UO_2–PuO_2–ZrO_2–CaO

Composition, vol.%				Melting point, °C
PuO_2	ZrO_2	UO_2	CaO	
10	25	65		2580
10	50	40		2542
10	75	15		2592
4	75	21		2686
10	40	40	10	2407

Compatibility[25] between $(UPu)O_2$ and the refractory metals has been evaluated by hot-stage microscopy in the temperature range 1300 to 2100°C. Results indicate that the mixed oxides react with the molybdenum, tungsten, tantalum, or niobium by oxidation of the metal and formation of a low-melting double salt of the metal and the heavy-metal oxides.

Studies of UN–PuN for fast reactor fuels continue at Battelle–Columbus.[26] There was no change in appearance of PuN that was heat-treated at 1800°C for 1 hr in helium, but its average grain size increased from 0.016 to 0.031 mm. At 2000°C for 30 min in helium, an appreciable weight loss occurred, and free plutonium was observed. Results indicate a decreasing solubility of plutonium in PuN as the temperature is lowered. The standard free energy of formation of PuN at 713°K is estimated at −59.4 kcal/mole.[27]

Studies of carbide fuels with potential refractory-metal containers[25] showed that the stoichiometric monocarbides react with refractory metals by carburization of the metal and formation of a liquid (uranium–plutonium) alloy at temperatures in the range of 1300 to 2100°C. Vapor-pressure studies of plutonium–carbon alloys at Los Alamos Scientific Laboratory[27] gave the following results: (1) for a 30 at.% carbon alloy in a tantalum cell, the cell failed prior to any meaningful results; (2) for a 50 at.% carbon alloy, good results were obtained in a tantalum cell, and the measured vapor pressures were given by $\log p$ (atm) $= -18{,}561/T + 5.096$; (3) for a 65 at.% carbon alloy, two results were obtained, with vapor pressures expressed by the equations

$$\log p \text{ (atm)} = -19{,}108/T + 3.465$$

and

$$\log p \text{ (atm)} = -17{,}142/T + 2.508$$

below and above 2020°K, respectively. Los Alamos workers[27] obtained a Gibbs free energy of formation of $(-6885 - 4.3\,T)$ cal/mole for PuC, and $(-15{,}438 - 13.3\,T)$ cal/mole for Pu_2C_3. In addition, they maintain that a $(UPu)C_{1.5}$ composition containing more than 30% Pu_2C_3 is stable as the solid-solution sesquicarbide structure.

Irradiations of 80%-dense vibratory-compacted carbide fuels at Argonne[15,28,29] have been performed at heat rates of 180 watts/cm, at cladding surface temperature of 550 to 675°C, and to burnups of 5.3 to 6.8 at.% of the heavy metal (1.4×10^{21} to 1.8×10^{21} fissions/cm^3). Specimens clad in stainless steel ruptured after a 14.3% diametral increase, whereas those clad in niobium–1 wt.% zirconium increased only approximately 0.1% diametrally and did not fail. Fission-gas release was dependent on carbon content. Typically, 20% was released at 650°C from PuC containing 4.24 wt.% carbon, less than 1% at 635°C from material containing 6.22 wt.% carbon.

Room-temperature microhardness values of 400 DPN were measured for PuP and PuS, whereas Pu_2S_3 is considered "much" harder.[13]

(W. M. Pardue)

Thorium

The solubility of plutonium in alpha thorium as a function of temperature was determined by point microanalysis of a biphase alloy,[30] with the use of samples containing approximately 50 at.% plutonium, annealed for times up to 1000 hr. The results showed that the solubility varies from 46 at.% at 600°C to 29.6 at.% at 400°C.

A summary of the properties of thorium, its alloys, and its compounds has been prepared by personnel at Oak Ridge. The report[31] includes physical and mechanical properties, as well as some potential uses for thorium. (R. L. Martin)

Metal-Ceramic Fuels

Cermet Fuels

Data reported by the British at the Third Geneva Conference indicated that high burnups (10 at.% of the uranium atoms) may be possible with a cermet fuel. Partially on the basis of these favorable results, emphasis on fuel compositions for future Brookhaven National Laboratory irradiation studies is being shifted from carbide to cermet fuels.[32] Cermet structures under consideration have fuel-matrix volume ratios of 80:20 to 60:40 and matrix materials of stainless steel, iron, and nickel. A 60:40 vol.% UO_2–iron cermet fabricated by cold pressing and sintering has been loaded into a capsule and sent to the Engineering Test Reactor (ETR) for irradiation. Another batch of 60:40 vol.% UO_2–stainless-steel cermet materials was ordered for low- and high-burnup irradiations at the ETR. By arc-melting prealloyed fragments, workers prepared spherical carbide cermets for irradiation and mechanical-property evaluations. Room-temperature compression tests showed an 80:20 vol.% $U_{0.9}Zr_{0.1}C_{0.98}$–molybdenum cermet specimen to break at three times the fracture load sustained by UC (4.7% carbon).

(R. A. Smith)

Dispersion Fuels

The loss of UO_2 from UO_2–molybdenum dispersions on heating was investigated at Los Alamos. The loss was measured as a function of temperature, time, and sample thickness. Despite the inhomogeneous nature of the solid dispersions, the results were treated by application of diffusion theory. The diffusion coefficient was found to vary with temperature as $D = 2.40 \times 10^{-3} \exp(-77{,}500/RT)$. The technique for treating these inhomogeneous systems was discussed, and the data indicated that UO_2 escaped along the molybdenum grain boundaries.[33]

Heat-treatments under oxidizing conditions have indicated that iron–15 wt.% chromium–4 wt.% aluminum–yttrium and iron–25 wt.% chromium–4 wt.% aluminum–yttrium alloys exhibited excellent oxidation resistance as cladding materials for various UO_2 and UN–iron, chromium, or iron–25 wt.% chromium dispersion fuels. Current results indicate[35] that specimens containing 40 vol.% UN–iron–25 wt.% chromium dispersions withstood 10,000 hr at 950°C without evidence of uranium diffusion at the surface. Plasma-arc spheroidized UO_2 was prepared from agglomerated UO_2 particles and was incorporated in several examples that showed relatively high surface-uranium intensities after 2500 to 2900 hr at 1100°C. Since the spherical UO_2 was expected to be the more stable fuel, new specimens were prepared and have accumulated 1800 hr at 750, 950, and 1100°C with no uranium diffusion detected. In addition, several iron–15 wt.% chromium–4 wt.% aluminum–yttrium clad 25 vol.% UO_2–iron specimens were prepared for irradiation testing in the Oak Ridge Research Reactor under high-burnup conditions. Briefly, the blended powders were cold pressed, sintered

in hydrogen at 1200°C, and hot-isostatically pressed at 1100°C to 98% of theoretical density. Following the machining step, the dense cores were cleaned and inserted in the iron–15 wt.% chromium–4 wt.% aluminum–yttrium cans that were electron-beam welded and hot-isostatically pressed at 1100°C under 700 kg/cm^2.

(D. L. Stoltz)

Coated-Particle Fuels

Particle Coating

Workers at Euratom are fabricating dispersion type fuel elements that consist of 100- to 250-μ-diameter particles of PuO_2 or $(U-Pu)O_2$ dispersed in a zirconium–niobium matrix.[36] To prevent reaction between the matrix and the fuel, the workers evaluated coatings of chromium, nickel, niobium, and molybdenum on the particles. Nickel coatings applied to fuel particles in an electrodeless nickel bath are reported to be particularly suitable. Coating rates of 8 to 10 μ/hr were found to be optimum. The coating method is readily adaptable for use in the glove boxes required for the handling of plutonium.

In another approach to the problem of coating PuO_2, vacuum-condensed coatings of chromium, iron, nickel, and molybdenum were evaluated.[37] This approach is also considered to be suitable for glove-box operation. Coating rates of 1 to 2 μ/hr were obtained by condensation of the metal vapor on particles contained in a vibrated pan located 5 to 7 mm below the vapor source. A third coating method considered was to coat fuel particles with molybdenum bisulfide or carbon by cycling the particles in a suspension of less than 0.1-μ-diameter coating material in Freon. It is suggested that other salts of metals could be applied as coatings from suspensions, with a subsequent in situ conversion of the salt to metal.

In work at Oak Ridge,[38] a study of porous-carbon coating, applied to 460-μ-diameter ThO_2 particles by pyrolysis of acetylene, was completed. Results of the study show:

1. A high acetylene supply rate is essential for producing a low-density coating. With pure acetylene the lowest density obtained was 0.6 g/cm^3.

2. Deposition temperature was not a significant variable with pure acetylene coating atmosphere at temperatures in the range of 950 to 1150°C.

3. Accessible porosity of coatings having a density of 0.6 g/cm^3 was 65% or greater. The pore-size distribution was determined and was found to depend only on density, regardless of coating thickness or coating conditions.

At Battelle–Columbus, work on characterization of pyrolytic carbon (PyC) fuel-particle coatings prepared with acetylene was concluded.[39] The microstructure of coatings prepared from acetylene appears to be related to coating temperature and reactant concentration in the same general manner as has been determined for coatings prepared from methane. However, the temperature boundaries between the coating structures, i.e., laminar, isotropic, and columnar, appear to be shifted toward lower temperatures when acetylene is used.

(N. D. Veigel)

Irradiation and Evaluation of Coated-Particle Fuels

Studies by Oak Ridge[38,40] and Battelle–Columbus on the irradiation behavior of PyC-coated oxide-fuel particles have continued. In postirradiation examinations at Oak Ridge of six batches of PyC-coated UO_2 fuels irradiated at high temperature (1350 to 1600°C) and up to 25 at.% burnup of the uranium, no failed coatings were observed. Coatings with inner porous layers of PyC showed no damage, whereas coatings without this inner buffer layer showed some damage to the inner layers but none to the outer coating. Close examination of one coating showed that its inner low-density PyC layer had shrunk to form a core-to-coating gap, as desired. At high burnup the UO_2 cores appeared more granular and showed some metallic inclusions but no growth.

At Battelle–Columbus[41] four sweep-gas experiments with PyC-coated large-diameter UO_2 cores were completed. In two of these experiments, the fuels, one with 79 μ of laminar PyC and the other with 113 μ of laminar PyC on 460-μ, 65% dense UO_2 cores, showed excellent performance, with fission-gas-release fractions (R/B) on the order of 10^{-8} after irradiations to 7.2 and 12.8 at.% burnup by fission, respectively, at 815°C. Two other fuels, one with 80 μ of laminar PyC and the other with 112 μ of laminar PyC coatings on 460-μ, 81% dense UO_2, showed good performance, with fission-gas

release fractions on the order of 10^{-6} after 6.2 and 8.7 at.% burnup by fission at 1100 and 815°C, respectively. Postirradiation examinations have been completed on three samples each of six lots of PyC-coated oxide fuels that were irradiated at temperatures of 500, 1050, and 1325°C. Descriptions of these fuels and their measured ^{133}Xe releases are given in Table I-8. The coating integrity appeared independent of fuel composition but was definitely improved by BeO or porous PyC inner buffer layers.

Investigators at Oak Ridge[42] have used a mathematical model to attempt to predict the performance of coated fuel particles considering various fuel-core, coating-structure, and irradiation parameters. They concluded that:

1. Fuel-particle coating may fail by (*a*) coating stresses produced by fuel swelling or fission-gas pressure, or (*b*) stresses in the outer coating from anisotropic expansion or fast-neutron damage.

2. Coatings on enriched-uranium cores irradiated to high burnup fail by (*a*), and failure may be prevented by the addition of inner void space equivalent to 2 or 3% of the fuel volume for each 1 at.% burnup.

3. Coatings on low-enriched uranium or thorium cores fail by (*b*), and failure may be prevented by the use of isotropic coatings.

4. Increasing the coating thickness such that the ratio of the inner to outer radius is 2 to 3 will not increase the coating life.

5. The fission-gas release from the fuel core is not a factor in coating failure if the rupture stress of the coating is greater than 20,000 psi.

(N. E. Miller)

Uranium Oxide Fuels

Properties and Behavior

Studies of the interfacial reaction between UO_2 and Zircaloy-2 at temperatures between 950 and 1575°K were performed at General Electric Company.[43] This reaction was found to proceed with the formation of oxygen-saturated alpha Zircaloy-2 and a gamma-uranium–beta-zirconium solid solution. The solid solution transformed on cooling to UZr_2 plus some gamma–beta solid solution. Alpha uranium containing zirconium in solution was also observed to form on cooling from the higher temperatures. The interaction between Zirca-

Table I-8 SUMMARY OF RESULTS OF POSTIRRADIATION EXAMINATION OF COATED-PARTICLE SPECIMENS[41]

Fuel material	Enrichment, %	Coating*		Irradiation temp., °C	Burnup, % ^{235}U	Fractional ^{133}Xe release, ppm	Coating failures,† %
		Material	Thickness				
UO_2	19.94	*d*-BeO	16				
		c-PyC	80	500	7.5	4.4	0.08
				1050	7.5	108	1.9
				1325	7.5	7.6	0.1
UO_2	19.94	*l*-PyC	71	500	7.5	43	0.3
				1050	7.5	1300	8.7
				1325	7.5	685†	4.6
$(Th,U)O_2$	18.8	*l*-PyC	69	500	7.0	176	2.0
				1050	7.0	316	3.7
				1325	7.0	1900	22.0
$(Th,U)O_2$	18.9	*p*-PyC	31	500	7.0	3.5	0.07
		l-PyC	80	1050	7.0	32	0.6
				1325	7.0	15	0.3
$(Th,U)O_2$	18.9	*p*-PyC	31	500	7.0	13	0.3
		l-PyC	79	1050	7.0	40	0.9
				1325	7.0	240	5.4
$(Th,U)O_2$	6.45	*p*-PyC	29	500	2.0	286	16.0
		l-PyC	77	1050	2.0	77	4.4
				1325	2.0	0.63	0.04

*In order of deposition; code used was as follows:
p-PyC = relatively porous pyrolytic carbon
l-PyC = laminar pyrolytic carbon
c-PyC = columnar pyrolytic carbon
d-BeO = dense BeO.
†Determined by comparing with the ^{133}Xe release from a similar sample with intentionally crushed coatings.

loy-2 and UO_2 differs from that between zirconium and UO_2, basically in the microstructure of the metallic reaction product. The extent of the interaction was found to be limited by oxygen diffusion in alpha Zircaloy-2.

Roellig[44] studied the reaction between UO_2 and aluminum. The presence of Al_2O_3 was found to accelerate this reaction. The reaction of UO_2 and TiO_2 was investigated in Yugoslavia.[45] In the composition range from 5 to 90 wt.% TiO_2, the compound $UO_2 \cdot 3TiO_2$ was observed when specimens were heated in argon at 1200, 1300, and 1400°C.

In the course of mechanical testing of UO_2 at Argonne,[28] it was observed that molecular hydrogen can dissociate at the surface of porous UO_2 and enter the lattice, where the hydrogen can then migrate by solid-state diffusion. The presence of the hydrogen in the lattice leads to an increase in the tensile strength of the UO_2, with a subsequent loss of ductility.

Schmitz and Lindner[46] have measured the diffusion of the actinide elements, ranging from thorium to americium, in dense sintered UO_2 compacts at temperatures between 1250 and 1600°C. The diffusion coefficient as a function of temperature can be expressed as

$$D = D_0 e^{-Q/RT} \quad \text{cm}^2/\text{sec}$$

where the appropriate constants for the different species are summarized in Table I-9.

(R. H. Barnes)

Table I-9 CONSTANTS[46] FOR DIFFUSION OF THE ACTINIDES IN UO_2

Element	D_0, cm^2/sec	Q (activation energy), kcal/gram-mole
Thorium	0.16	98
Protactinium	2.5	107.6
Uranium	0.9	104
Neptunium	2.9	109
Plutonium	0.2	98
Americium	0.03	92

Preparation of Fuel Bodies

Investigators at Nuclear Materials & Equipment Corp.[47] have prepared fuel compositions containing 6 to 10 vol.% PuO_2 in conjunction with 25, 50, and 75 vol.% ZrO_2, the remainder being UO_2. Preparation of the feed stock, from which fuel pellets could be fabricated, was accomplished by both coprecipitation and mechanical blending of the individual component powders.

Coprecipitation of the feed material was carried out from a nitrate solution to form an amorphous product that was thermally decomposed in a N_2-8 vol.% H_2 atmosphere at 740°C. Workers prepared the blended feed material by dry ball-milling the component powders, granulating them in paste form, and presintering the granules at 1700°C for 8 hr.

Pellets were pressed from both types of feed material and sintered for 8 hr at 1700°C in a N_2-8 vol.% H_2 atmosphere. The authors found that both materials resulted in a single-phase face-centered cubic structure, with the exception of the blended material containing 75 vol.% ZrO_2. This material contained approximately 20 vol.% of a monoclinic ZrO_2-rich phase.

Enriched UO_2 pellets with a grain size less than 100 μ have been prepared at Chalk River.[48] Pellets having a grain size of 35 μ were first prepared by a sintering step at 1765°C for 26 hr in hydrogen. These pellets were heated to 1500°C in vacuum and then to 2150°C in A–10 vol.% helium and held at 2150°C for 4 hr before being cooled to room temperature.

Subsequent examinations revealed that the average grain size was approximately 104 μ; however, metallic uranium was present in the specimens. The pellets were therefore heated to 1450°C in hydrogen in the presence of hyperstoichiometric UO_2 as a source of oxygen. Final pellets were free from metallic uranium, exhibited a density of 10.8 g/cm^3, and had an average grain size of 104 μ. (T. R. Wright)

UO_2-Water Reactions

The finding of a significant reaction between UO_2 and water has prompted further study at Argonne.[15] Experiments with unclad UO_2 were performed at 1 atm pressure and 1500°C and were designed to evaluate the rate and extent of reaction of typical high-density UO_2 pellets with flowing steam. The samples consisted of pressed and sintered cylinders of UO_2 (>95% of theoretical density), ½ in. in diameter by ½ in. high. Each cylinder weighed about 19.2 g. The amount of oxidation was determined by four independent methods: sample weight gain during an experiment, gravimetric analysis (subsequent controlled oxidation of sample residues to U_3O_8), X-ray diffraction, and hydrogen evolution.

The atomic ratios of oxygen to uranium were calculated from the results of each of the four methods of analysis. Good agreement between the methods was obtained. A plot of the final composition (oxygen-to-uranium ratio), taken from the weight-gain data, as a function of the square root of time is shown in Fig. I-3. The reaction rate follows an apparent parabolic law for the first 70 min and then tapers off at a final composition of about $UO_{2.17}$. In one experiment the pressed and sintered UO_2 pellet was crushed to powder before exposure to steam. No difference in the behavior of this sample was noted.

The results of the isothermal experiments confirm the reaction of UO_2 with steam. The reaction is relatively slow at 1500°C and probably would not contribute a large quantity of hydrogen following a loss-of-coolant accident in a UO_2-fueled power reactor.

(A. W. Lemmon, Jr.)

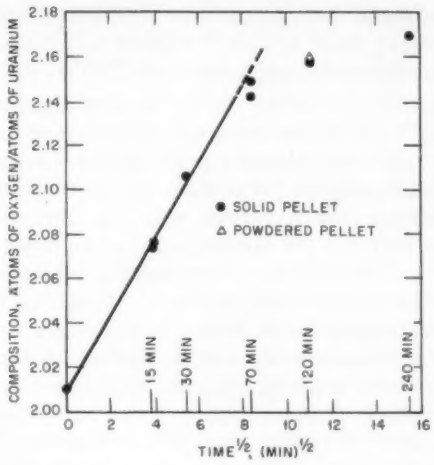

Fig. I-3 Oxygen-to-uranium ratio after exposure of UO_2 to steam at 1500°C and 1-atm pressure.[15]

Uranium and Thorium Carbides, Nitrides, Sulfides, and Phosphides

Fabrication

Workers at Harwell[49] have developed techniques for the production of US, UN, and UP by the reaction of uranium metal with hydrogen sulfide, nitrogen, and phosphine, respectively. Oxygen impurities occur in US as the oxysulfide UOS, and in UN and UP as the oxide UO_2. Cold pressing and vacuum sintering of US is facilitated by the formation of a eutectic between US and UOS. Vacuum sintering of UP and UN above 1800°C can lead to liquid-phase sintering through the formation of free uranium metal. Maximum densities of 92 to 94%, 84%, and 89% of theoretical have been obtained for US, UN, and UP, respectively, by cold-pressing and sintering steps. A hot-pressing technique is described which has produced specimens with densities greater than 95% of theoretical for all three compounds, although all of the specimens were cracked to varying degrees.

A process was developed by workers at Argonne[50] for the preparation of UC by precipitation from a liquid metal. The process involved dissolution of uranium in a zinc solution containing 14 to 18 wt.% magnesium, followed by the addition of a carbonaceous material at about stoichiometric quantities for UC formation. The melt is stirred for 8 to 19 hr at 800°C. The UC is allowed to settle for 3¾ hr, and then the bulk of the supernatant liquid metal (zirconium–magnesium) is drawn off the settled UC powder. The UC is then vacuum outgassed to remove the residual magnesium and zinc. The yield of UC was 83.5% of the calculated theoretical yield. Preliminary results indicate that UC with an oxygen content of 0.2 wt.% can be produced and that the UC can be fabricated to a high density.

French workers[51] describe a pilot-scale electron-beam furnace designed for continuous melting and casting of uranium–carbon alloys. The equipment allows the melting and casting processes to be automatically controlled, the cooling being carried out under vacuum and the discharge being effected without breaking the vacuum. In a preproduction run of 20 kg of slugs, the composition of practically all the pieces was controlled within ±0.1 wt.% carbon. The capacity of the furnace was 2.2 kg/hr.

Using published free-energy data, Gens, at Oak Ridge, has written a report[53] on the yield of uranium nitride per mole of nitrogen introduced over heated uranium dioxide and carbon. From the calculations the yield of UN per mole

of nitrogen introduced over UO_2 plus carbon increases from 6×10^{-19} mole to 0.13 mole as the temperature increases from 1000 to 2000°K.

Proceeding on the basis of Gens' calculations,[53] Oak Ridge workers[54] undertook to prepare UN microspheres from urania–carbon–gel microspheres. A method was developed for preparing urania–carbon sols and converting these sols into gel microspheres. Two methods were investigated for converting the gel microspheres into UN microspheres: (1) heating the gel microspheres in nitrogen to produce uranium nitride directly and (2) heating in argon to produce uranium carbide, then in nitrogen to produce uranium nitride from the carbide. Both methods appear promising. Problems arise when attempts are made to carry out the reaction $UO_2 + 2C + \frac{1}{2} N_2 \rightarrow UN + 2CO$. The microspheres rapidly develop a thin, mirrorlike surface layer of UN that impedes the entry of more nitrogen to the interior of the microspheres. The coating can be rendered pervious to nitrogen if it is temperature cycled, so that higher nitrides are alternately formed and decomposed in the coating.

In the second method the gel spheres are first converted to UC when they are heated in an argon atmosphere and then to nitride when they are heated in a nitrogen atmosphere. The final product contains the same amount of carbon as the UC intermediate product.

(D. S. Acuncius)

Properties and Behavior

As a part of a study of the thermodynamic properties of the uranium–carbon system,[55] Los Alamos has redetermined the solubility limits of UC in liquid uranium and the solubility limits of carbon in UC_2. The results, which are considerably more extensive than those obtained in previous studies, are in excellent agreement with the generally accepted phase diagram. Some of these data are shown in the following tabulation:

UC + U boundary		UC_2 + C boundary	
Composition, C/U	Temp., °C	Composition, C/U	Temp., °C
0.560	2250	1.927	2384
0.314	2007	1.905	2044
0.146	1784	1.883	1815
0.041	1420	1.866	1587

Other data were obtained showing that the two-phase region of UC plus UC_2 exists up to 2100 to 2150°C, which is also in agreement with the accepted phase diagram. Vapor-pressure studies allowed a systematic determination of activities. At 2100°C the activity of carbon changes from 0.08 to 0.65 in UC and from 0.65 to 1.0 in UC_2, as the compositions of the respective compounds change from slightly hypostoichiometric to slightly hyperstoichiometric. The free energy of formation of UC also varies correspondingly at 2300°K from 14 to 27 kcal per mole of uranium.

Argonne reports[13] that UC_2 dissolves about 50 mole % US.

The British found[56] that the solidus temperature between UC and tungsten is at 2050°C.

Workers at Battelle–Columbus report[57] that, at 1705°C, UC containing excess carbon reacts with tungsten and tungsten–0.6 wt.% niobium alloy to form a reaction zone but that, when the excess carbon is depleted, the reaction stops. At 1705°C, UN did not react at all with these tungsten alloys. A molybdenum-base alloy, TZM, did not react with UC or UN at 1705°C. However, at 1870°C, a tungsten–15 wt.% molybdenum alloy reacted with UC to form a liquid. Tantalum-base alloys reacted with UC to form TaC and Ta_2C at 1370°C. A tantalum-base alloy reacted with UN to form liquid uranium at 1540°C. A niobium-base alloy reacted with both UC and UN at 1370°C to form liquid uranium.

Pratt & Whitney Aircraft has issued a series of reports summarizing studies of the physical and mechanical properties of UC and UN. The thermal conductivity of UC is essentially constant at 0.23 watt/(cm)(°C) from 100 to 2000°C at compositions from 4.7 to 5.3 wt.% carbon.[58] The thermal conductivity of UN rises, from 0.16 watt/(cm)(°C) at 200°C to 0.26 watt/(cm)(°C) at 1600°C.[59] The partial pressure of nitrogen[60] over UN from 1910 to 2265°K is given by: $\log P \text{ (atm)} = 8.279 - 2.874 \times 10^4 T^{-1}$. Compressive creep rates for UC and UN were determined at temperatures from 1100 to 1350°C. As shown in Tables I-10 and I-11 and Figs. I-4 and I-5, creep rates of UN at 6000 psi are about three times those of UC over this temperature range.[61] Over the temperature range from 1500 to 1870°C, the self-diffusion rate[62] of ^{15}N in UN is given by: $D^N (\text{cm}^2/\text{sec}) = 2.6 \times 10^{-4} \exp(-55{,}000/RT)$.

Table I-10 CREEP RATES OF URANIUM CARBIDE[61]

Test	Composition C, wt.%	O, ppm	N, ppm	Temp., °C	Stress, 1000 psi	Creep rate, hr^{-1}
			Standard Tester			
UC(a)	4.9	1850	400	1100	10	6.5×10^{-5} (2.0×10^{-5})*
UC(b)	4.9	1850	400	1300	6	1.6×10^{-4}
UC(c)	4.9	1850	400	1300	8	3.1×10^{-4} (1.6×10^{-4})*
			Incremental Tests			
UC(d)	4.85	495	260	1200	6	6.57×10^{-5}
				1250	6	1.05×10^{-5}
UC(e)	4.5	3200	1150	1100	6	1.43×10^{-4}
				1125	6	1.90×10^{-4}
				1150	6	2.42×10^{-4}
				1175	6	3.26×10^{-5}
				1200	6	5.23×10^{-4}
				1225	6	6.88×10^{-4}
				1250	6	8.88×10^{-4}
				1275	6	9.44×10^{-4}
				1300	6	1.66×10^{-3}

*Values obtained after adjustment to 6000 psi using relation $\dot{\epsilon} = A\sigma^{2.3}$.

Table I-11 CREEP RATES OF URANIUM NITRIDE[61]

Test	Composition C, ppm	O, ppm	N, wt.%	Temp., °C	Stress, 1000 psi	Creep rate, hr^{-1}
UN(a)	1100	2600	5.25	1100	6	4.93×10^{-5}
				1125	6	7.05×10^{-5}
				1150	6	9.76×10^{-5}
UN(b)	1100	2600	5.25	1100	6	
				1125	6	4.28×10^{-5}
				1150	6	7.23×10^{-5}
				1175	6	1.42×10^{-5}
				1200	6	2.15×10^{-5}
UN(c)	1100	2600	5.25	1100	6	5.42×10^{-5}
				1125	6	8.09×10^{-5}
				1150	6	1.07×10^{-4}
				1175	6	1.58×10^{-4}
				1200	6	2.40×10^{-4}
				1225	6	3.34×10^{-4}
				1250	6	3.91×10^{-4}
UN(d)	1100	2600	5.25	1100	8	1.61×10^{-4}
				1125	8	2.25×10^{-4}
				1150	8	3.69×10^{-4}
				1175	8	8.33×10^{-4}
				1200	8	7.88×10^{-4}
				1225	8	1.04×10^{-3}
				1275	8	2.33×10^{-3}
				1300	8	3.14×10^{-3}
				1350	8	4.84×10^{-3}
UN(e)	1550	430	5.20	1100	8	Limit of extension-measuring device reached before second-stage creep achieved
UN(f)	1550	430	5.20	1100	6	8.51×10^{-4}
				1125	6	9.28×10^{-4}

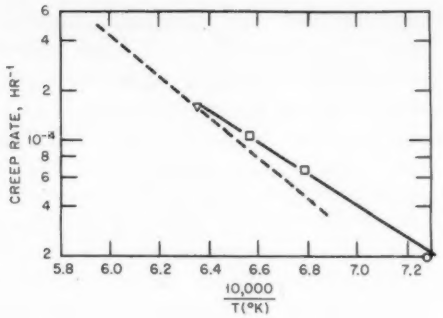

Fig. I-4 Compressive creep of uranium carbide (4.9 wt.% carbon).[61] ○, test UC(a) 1100°C isothermal; ▽, test UC(b) 1300°C isothermal; □, test UC(d) 1200 to 1250°C incremental; - - -, Norreys.

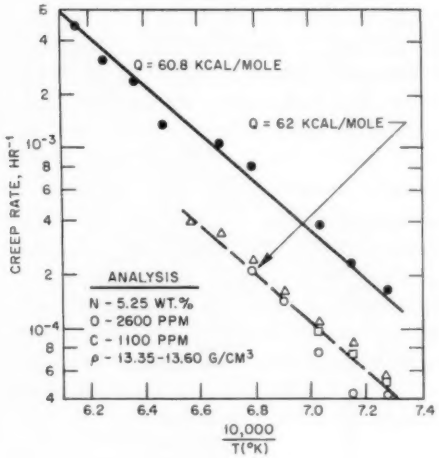

Fig. I-5 Compressive creep of uranium nitride.[61] □, test UN(a) 6000 psi; ○, test UN(b) 6000 psi; Δ, test UN(c) 6000 psi; ●, test UN(d) 8000 psi.

An irradiation of four specimens of hypostoichiometric UC at surface temperatures of 650 to 735°C and centerline temperatures of 1090 to 1270°C produced a rather dramatic illustration of the deleterious effects of the presence of metallic uranium in UC at these temperatures. The specimens were 0.49 in. in diameter and 2.5 in. long, bonded to type 304 stainless steel with sodium, and irradiated to a maximum burnup of 19,200 Mwd per metric ton of uranium. According to Atomics International workers,[63] the fuel specimens swelled more than 10% in diameter, burst their claddings, and showed uranium metal and fission-product redistribution toward the fuel surfaces.

Uranium mononitride samples of various densities were irradiated at surface temperatures up to 750°C to fission burnups of up to 6.3 at.% of the uranium (2.2×10^{21} fissions/cm^3). According to Battelle–Columbus,[64] the samples, which were clad in 0.201-in.-ID 0.260-in.-OD stainless steel, showed diameter changes of between 1.3 and 4%, density changes of between 3.5 and 6.2%, and gas release of between 0.1 and 26% of the amount produced. The gas releases could not be correlated with porosity or fabrication techniques. Of 20 samples, two showed melted areas in the claddings. These areas were attributed to reaction between the claddings and free uranium in the samples.

The British[56] have irradiated 11 samples of UC–15 wt.% PuC at surface temperatures up to 1040°C and center temperatures up to 1610°C to burnups of up to 5.5 at.% of the metal atoms. The samples ranged in carbon content from 4.0 to 5.3 wt.% (two appreciably hypostoichiometric and two appreciably hyperstoichiometric). The samples were 1 in. long, 0.26 to 0.30 in. in diameter, and ranged in density from loose powder to castings. They were wrapped in 0.006-in.-thick tantalum foil and placed in Nimonic 90 cans, and the assemblies were inserted in holes in mild-steel blocks. All samples, except the loose-powder samples, swelled sufficiently to achieve good thermal contact between the cladding and the steel blocks. Four of the Nimonic 90 cans cracked, and the only sample containing 4 wt.% carbon swelled its mild-steel matrix block as well. Samples containing free uranium showed enhanced fission-gas release compared with releases from stoichiometric and hyperstoichiometric materials. The effect of porosity on fission-gas release was insignificant.

Kempter and Merryman[65] found that the thermal-expansion coefficient of $(U_{0.3}Zr_{0.7})C_{0.97}$ is 7.78×10^{-6}/°C from 25 to 1000°C. This is appreciably lower than that of UC.

Oak Ridge workers[66] found that the thermal-expansion coefficients of UC_2–ThC_2 alloys from 40 to 1000°C decrease from 13.2×10^{-6}/°C at 25 wt.% ThC_2 to 8.4×10^{-6}/°C at 100% ThC_2.

According to Atomics International workers, U_3Si_2 has a uranium density of 11.3 g of uranium per cubic centimeter, a melting point of 1660°C, a thermal conductivity of 0.05 cal/(sec)(cm)(°C) at 1000°C, good oxidation resistance, and a tetragonal crystal structure.[67] Irradiation of slightly substoichiometric U_3Si_2

at a surface temperature of 700°C to a burnup of 7300 Mwd per metric ton of uranium produced a density decrease of 6.4%, a diameter change of 2.3%, and a gas release of 2.6%. This behavior is appreciably poorer than that of UO_2, UC, and UN, but better than that of metallic uranium. (W. Chubb)

Basic Studies of Irradiation Effects in Fuel Materials

Metals

It was shown by the British[68] that a critical temperature range exists where dislocation movement may contribute to enhanced swelling during the irradiation of alpha uranium. This range is one in which the temperature is sufficiently low for deformation to be caused by internal stresses resulting from irradiation growth, but still high enough to permit the fission-gas bubbles to move along with dislocation lines at speeds that enhance the rate of bubble coalescence. An analysis is presented which permits an assessment of the conditions under which swelling may become unacceptably large.

At Harwell,[69] replica taken from cathodically vacuum-etched and fractured uranium surfaces have been compared with the results from thin-film electron microscopy. Only cleavage surfaces of the fractures gave indications consistent with the bubble distributions obtained with thin-film microscopy. With 7500 A bubbles, the thin-film technique is no longer reliable. These studies yielded an experimental value of 1000 ± 500 ergs/cm^2 for the surface energy of alpha uranium.

A Japanese review of diffusion coefficients of xenon and krypton in uranium shows trends of effects due to cycling through transformation temperatures, neutron exposure, and experimental parameters such as the type of atmosphere used.[70]

Ceramics

In the United Kingdom, krypton-bubble diffusion in thin UO_2 samples has been studied by electron microscopy after injection in a heavy-ion accelerator.[71] The results indicate that bubbles migrate bodily in a temperature gradient, small bubbles migrating more rapidly than large ones. This and other evidence indicates that surface diffusion is the principal mechanism. Further work is planned to measure surface diffusion rates.

At Harwell, 5×10^{15} small gas bubbles/cm^3 are observed[72] in UO_2 after 2.2×10^{19} fissions/cm^3. These precipitate on annealing at 1100°C and appear to grow from 25 to 100 A in diameter at 1500°C by diffusion from the matrix. Grain-boundary migration sweeps up these bubbles at between 1800 and 2000°C. Dissolution of bubbles up to 300 A in diameter has been observed on reirradiation. At a dose of 1.6×10^{20} fissions/cm^3, bubbles appear to grow by coalescence and by dislocation sweeping. Precipitates, believed to be solid fission products, are observed.

Harwell workers demonstrated[73] that bubbles can migrate bodily in reactor materials under the influence of various driving forces and by various mechanisms. Directed migration due to temperature gradients, stress gradients, and moving dislocation lines or grain boundaries is more important than Brownian motion, except perhaps in the case of a short furnace anneal. Small bubbles are dominated by the behavior of dislocation lines; as their size increases, the temperature gradient becomes more important. However, if the material is a good thermal conductor, the temperature gradients are not important, even in the reactor.

In poor conductors (for example UO_2) the behavior is more complex, different models being required for each temperature zone. In the low-temperature zone, the bubbles are small and the temperature gradient is not important. At high temperatures the temperature gradient drags bubbles from dislocations, and they migrate up the temperature, becoming trapped upon the grain boundaries from where gas is released periodically. At higher temperatures the bubbles are dragged off the grain boundaries by the temperature gradient, and columnar grains are produced as the bubbles migrate, there being virtually complete gas release from this region. It is concluded that the bubbles migrate predominantly by a surface-diffusion mechanism, and only when the bubbles become large does an evaporation mechanism take over.

Hyperstoichiometric uranium carbide,[74] single-crystal specimens have been irradiated to doses of up to 5.4×10^{16} fissions/cm^3 at about 130°C. A dose of 1.4×10^{16} fissions/cm^3 results

in observable clusters in the UC phase, the size and number of which increase with dose. Observable point-defect clusters are only formed in the UC_2 platelets after the higher dose studied. On annealing, the point-defect clusters in both UC and UC_2 phases start to disappear above 700°C. On annealing at 1200 and 1300°C, however, the clusters in the UC matrix grow and become resolvable as loops. It is believed that the point defects are interstitial and that vacancies become mobile at 700°C to produce recombination. A model is proposed for the formation of interstitial loops, which is consistent with the observed loop behavior.

(F. A. Rough)

References

1. P. D. Tilbury, The Fatigue of Uranium, British Report AWRE-O-65/65, August 1965.
2. K. Taketani and K. Ikawa, Study of the Behavior of Punctured Fuel Element for Calder Hall Type Reactor. 5. Oxidation of Uranium by Partially Decomposed Carbon Dioxide, *J. Nucl. Sci. Technol. (Tokyo)*, 2: 241-244 (July 1965).
3. A. F. Smith, The Identification and Distribution of Intermetallic Compounds in Adjusted Uranium, *J. Inst. Metals*, 93: 454-455 (August 1965).
4. P. H. Dixon, F. H. Fern, and B. R. Butcher, The Solution of Precipitates in Very Dilute Uranium-Iron-Aluminum Alloys, *J. Inst. Metals*, 93: 423-428 (August 1965).
5. B. Mastel, T. K. Bierlein, and C. L. Corey, Electron Microscope Studies of Second Phase Particles in Dilute Alloys of Uranium, USAEC Report BNWL-SA-90, Pacific Northwest Laboratory, Mar. 3, 1965.
6. M. Sikirica and Z. Ban, New Phase in the System Uranium-Molybdenum-Silicon, in *New Nuclear Materials, Including Nonmetallic Fuels*, Symposium Proceedings, Prague, 1963, Vol. II, pp. 229-233, International Atomic Energy Agency, Vienna, 1963 (STI/PUB/77).
7. R. Burgett (Ed.), Summary Technical Report for the Period July 1–September 30, 1965, USAEC Report NLCO-965, National Lead Company of Ohio, Oct. 20, 1965.
8. P. L. Blum, G. Silvestre, and H. Vangoyeau, Metallography Concerning the Existence of an Allotropic Change to Cubic U_3Si Within the Uranium-Silicon System, USAEC Report NLCO-tr-6 [translated from *Compt. Rend.*, 260: 5538-5541 (May 24, 1965)].
9. O. J. C. Runnels and R. R. Boucher, Transformations in UAl_4 and $PuAl_4$, *Trans. AIME*, 233: 1726-1732 (September 1965).
10. V. V. Gerasimov, Corrosion of Uranium and Its Alloys, Report JPRS-31728 (TT-65-3223), translated from *Korroziya Urana i Ego Splavov*, Moscow, Atomizdat, 1965.
11. W. G. Jolley and W. I. Clark (Eds.), Papers and Proceedings of the Meeting on Applications of X-Ray Diffraction in the Atomic Energy Field, Richland, Washington, February 25–26, 1965, USAEC Report RL-REA-2595, Pacific Northwest Laboratory, October 1965.
12. K. R. Riggs and N. F. Neumann, Effect of Alloy Additions on the Quench-Induced Texture of Alpha-Uranium, USAEC Report MCW-1491, Mallinckrodt Chemical Works, Apr. 16, 1965.
13. Argonne National Laboratory, Reactor Development Program Progress Report, September 1965, USAEC Report ANL-7105, Oct. 20, 1965.
14. O. L. Kruger, Phase Studies of U-20 Wt.% Pu-Fs Alloys, USAEC Report ANL-6974, Argonne National Laboratory, May 1965.
15. Argonne National Laboratory, Reactor Development Program Progress Report, October 1965, USAEC Report ANL-7115, Nov. 23, 1965.
16. L. J. Wittenberg and G. R. Grove, Reactor Fuels and Materials Development — Plutonium Research: April–June 1965, USAEC Report MLM-1283, Mound Laboratory, Dec. 10. 1965.
17. J. W. Anderson, R. R. Gilmore, and W. J. Maraman, Studies of the Equilibrium Temperature for the Plutonium Alpha-Beta Transformation, USAEC Report LA-DC-7278, Los Alamos Scientific Laboratory, 1964.
18. K. A. Johnson, The Alternating Current Electroetching of Alpha, Delta, and Beta Plutonium, USAEC Report LA-DC-6691, Los Alamos Scientific Laboratory.
19. Pacific Northwest Laboratory, Metallurgy Research Section, Quarterly Progress Report, July–September, 1965, USAEC Report BNWL-166, Oct. 15, 1965.
20. J. Roth and E. K. Halteman, Thermal Expansion of Coprecipitated $(U,Pu)O_2$ Powders by X-Ray Diffraction Techniques, USAEC Report NUMEC-2389-9, Nuclear Materials & Equipment Corp., October 1965.
21. Atomic Energy of Canada Limited, unpublished, 1965.
22. M. D. Houston, Sintering Behavior of Plutonium Dioxide, USAEC Report NUMEC-2389-6, Nuclear Materials & Equipment Corp., 1964.
23. Nuclear Materials & Equipment Corp., UO_2-PuO_2-ZrO_2 Fuel Development Program, Progress Report, July 1–September 30, 1965, USAEC Report NUMEC-3505-8, Oct. 21, 1965.
24. A. R. Olsen, D. A. Douglas, Y. Hirose, J. L. Scott, and J. W. Ullmann, Properties and Prospects of Thoria-Base Nuclear Fuels, USAEC Report ORNL-P-1724, Oak Ridge National Laboratory, November 1965.
25. W. Batey, D. M. Donaldson, and M. B. Finlayson, The Compatibility of Mixed Oxides and Carbides with Refractory Metals, British Report TRG-Report-1038, July 16, 1965.
26. R. W. Dayton and S. J. Paprocki, Progress Relating to Civilian Applications During October 1965, USAEC Report BMI-1748 (Del.), Battelle Memorial Institute, Nov. 1, 1965.
27. Los Alamos Scientific Laboratory, Quarterly Status Report on Advanced Reactor Technology (ART) for Period Ending July 31, 1965, USAEC Report LA-3370, Aug. 31, 1965.
28. Argonne National Laboratory, Fuels and Materials Development Program, USAEC Quarterly Progress Report for Period Ending June 30, 1965.
29. Argonne National Laboratory, Reactor Development Program Progress Report, July 1965, USAEC Report ANL-7082, Aug. 24, 1965.

30. A. Y. Portnoff and D. Calais, The Solubility of Plutonium in Alpha Thorium, *J. Less-Common Metals*, 9: 74-76 (1965).
31. S. Peterson, R. E. Adams, and D. A. Douglas, Jr., Properties of Thorium, Its Alloys, and Its Compounds, presented at the IAEA Panel on Utilization of Thorium in Power Reactors, Vienna, June 14-18, 1965.
32. Brookhaven National Laboratory Annual Report, July 1, 1965, USAEC Report BNL-929, November 1965.
33. P. Wagner, Loss of UO_2 From Molybdenum-UO_2 Cermets by High-Temperature Diffusion, *J. Less-Common Metals*, 9: 40-47 (1965).
34. Deleted.
35. General Electric Company, Nuclear Materials and Propulsion Operation, High-Temperature Materials Program Progress Report No. 53, Part A, USAEC Report GEMP-53A, Nov. 26, 1965.
36. C. Sari and I. Lafontaine, Preparation and Coating of Spherical Particles of PuO_2 and $(U-Pu)O_2$ Mixtures, Special Report No. 19, USAEC-Euratom Report EURAEC-1391 (EUR-2350), Société Belge pour l'Industrie Nucléaire and Centre d'Étude de l'Énergie Nucléaire.
37. C. Sari and J. Pivato, Coating UO_2 Particles, USAEC-Euratom Report EURAEC-1392, Société Belge pour l'Industrie Nucléaire and Centre d'Étude de l'Énergie Nucléaire.
38. Oak Ridge National Laboratory, unpublished, Nov. 4, 1965.
39. M. F. Browning, D. A. Vaughn, J. F. Dettore, and J. M. Blocher, Jr., Characterization of Pyrolytic-Carbon Fuel-Particle Coatings Prepared With Acetylene, USAEC Report BMI-1735, Battelle Memorial Institute, July 19, 1965.
40. Oak Ridge National Laboratory, unpublished, Oct. 6, 1965.
41. R. W. Dayton and S. J. Paprocki, Progress Relating to Civilian Applications During August 1965, USAEC Report BMI-1742 (Del.), Battelle Memorial Institute, Sept. 1, 1965.
42. J. W. Prados and J. L. Scott, Mathematical Model for Predicting Coated-Particle Behavior, USAEC Report ORNL-TM-1405, Oak Ridge National Laboratory, March 1966.
43. L. N. Grossman and D. M. Rooney, Interfacial Reaction Between UO_2 and Zircaloy-2, USAEC Report GEAP-4679, General Electric Company, Atomic Power Equipment Department, April 1965.
44. H. E. Roellig, Compatibility of Uranium Dioxide and Aluminum. I. Kinetic Studies of the Uranium Dioxide-Aluminum Reaction in Mixed Powder Compacts, *Kernenergie*, 19(6): 685-691 (1963).
45. L. M. Manojlovic, M. M. Ristic, and S. S. Malcic, High Temperature Reaction in the UO_2-TiO_2 System, in *New Nuclear Materials, Including Nonmetallic Fuels*, Symposium Proceedings, *Prague*, Vol. I, pp. 245-249, International Atomic Energy Agency, Vienna, 1963 (STI/PUB/77).
46. F. Schmitz and R. Lindner, Diffusion of Heavy Elements in Nuclear Fuels: Actinides in UO_2, *J. Nucl. Mater.*, 17: 259-269 (1965).
47. Nuclear Materials & Equipment Corp., PuO_2-ZrO_2-UO_2 Fuel Development, Progress Reports NUMEC-3505-5, -8, -11, and -14, available from Clearinghouse for Federal Scientific and Technical Information.
48. Atomic Energy of Canada Limited, unpublished, Sept. 30, 1965.
49. M. Allbutt, A. R. Junkison, and R. G. Carney, Preparation and Fabrication of the Mononitride, Phosphide, and Sulphide of Uranium, British Report AERE-R-4903, August 1965.
50. Argonne National Laboratory, Chemical Engineering Division Semiannual Report, July-December 1964, USAEC Report ANL-6925, May 1965.
51. J. Trouve, R. Genard, A. Treillou, and A. Accary, Pilot-Scale Electron-Bombardment Furnace and Continuous Casting. Application to the Trial Preparation of 20 kg of Uranium Monocarbide Rods, British Translation AERE-Trans-1033 (from French Report CEA-R-2587, August 1964).
52. Deleted.
53. T. A. Gens, Thermodynamic Calculation of the Yield of Uranium Nitride During Carbothermic Reduction of Uranium Oxide in the Presence of Pure Nitrogen or Nitrogen Mixed With Hydrogen or Inert Gas, USAEC Report ORNL-TM-1264, Oak Ridge National Laboratory, Sept. 16, 1965.
54. T. A. Gens, D. M. Helton, and S. D. Clinton, Laboratory Preparation of Uranium Nitride Microspheres by a Sol-Gel Technique, USAEC Report ORNL-3879, Oak Ridge National Laboratory, November 1965.
55. E. K. Storms, A Mass Spectrometric Study of the Vapor Pressure of $U_{(g)}$ and $UC_{2(g)}$ Over Various Compositions in the Uranium-Carbon System, USAEC Report LA-DC-6953, Los Alamos Scientific Laboratory, 1965.
56. L. E. J. Roberts and J. Williams, United Kingdom Atomic Energy Authority, unpublished, August 1965.
57. F. E. McGrath, J. A. DeMastry, and M. S. Farkas, Metallography of Ceramic Fuel and Refractory Metal Compatibility Couples, USAEC Report NMI-5025 (Pt. I), pp. 39-58, Nuclear Metals, Inc., August 1965.
58. B. A. Hayes and M. A. DeCrescente, Thermal Conductivity and Electrical Resistivity of Uranium Monocarbide, USAEC Report PWAC-480, Pratt & Whitney Aircraft—CANEL, Division of United Aircraft Corp., October 1965.
59. B. A. Hayes and M. A. DeCrescente, Thermal Conductivity of Electrical Resistivity of Uranium Mononitride, USAEC Report PWAC-481, Pratt & Whitney Aircraft—CANEL, Division of United Aircraft Corp., October 1965.
60. P. A. Vozzella and M. A. DeCrescente, Thermodynamic Properties of Uranium Mononitride, USAEC Report PWAC-479, Pratt & Whitney Aircraft—CANEL, Division of United Aircraft Corp., October 1965.
61. M. H. Fassler, F. J. Huegel, and M. A. DeCrescente, Compressive Creep of UC and UN. Part I, USAEC Report PWAC-482, Pratt & Whitney Aircraft—CANEL, Division of United Aircraft Corp., October 1965.
62. T. J. Sturiale and M. A. DeCrescente, Self-Diffusion of Nitrogen in Uranium Mononitride, USAEC Report PWAC-477, Pratt & Whitney Aircraft—CANEL, Division of United Aircraft Corp., September 1965.
63. R. D. Hahn, The High-Temperature Irradiation Behavior of Hypostoichiometric Uranium Monocarbide, USAEC Report NAA-SR-11134, Atomics International, Aug. 31, 1965.

64. R. L. Martin, W. J. Zielenbach, V. W. Storhok, D. L. Keller, and J. E. Gates, Radiation Stability of Uranium Mononitride, USAEC Report BMI-1731, Battelle Memorial Institute, June 29, 1965.
65. C. P. Kempter and R. G. Merryman, Thermal Expansion of a UC-ZrC Solid Solution, *J. Chem. Phys*, 43: 1736-1738 (September 1965).
66. Oak Ridge National Laboratory, Gas-Cooled Reactor Program Semiannual Progress Report for Period Ending March 31, 1965, USAEC Report ORNL-3807, June 1965.
67. H. Shimizu, The Properties and Irradiation Behavior of U_3Si_2, USAEC Report NAA-SR-10621, Atomics International, July 25, 1965.
68. M. V. Speight and G. W. Greenwood, The Effect of Dislocation Movement in Enhancing Swelling in α-Uranium During Irradiation, *J. Nucl. Mater.*, 16: 327-332 (July 1965).
69. J. E. Bainbridge and B. Hudson, On the Techniques for Observing Fission Gas Bubbles in Uranium, British Report AERE-R-4965, June 1965.
70. R. Nagusaki and S. Kawasaki, Behavior of Krypton and Xenon in Uranium Metal. Release of Krypton and Xenon from Metallic Uranium, British Translation AERE-Trans-1034 [from *Nippon Genshiryoku Gakkaishi*, 6: 646-655 (1964)].
71. G. K. Williamson and R. M. Cornell, The Behavior of Fission Product Gases in Uranium Dioxide, *J. Nucl. Mater.*, 13(2): 278-280 (1964).
72. A. D. Whapham and B. E. Sheldon, Electron Microscope Observation of the Fission-Gas Bubble Distribution in UO_2, British Report AERE-R-4970, July 1965.
73. R. S. Barnes and R. S. Nelson, Theories of Swelling and Gas Retention in Reactor Materials, British Report AERE-R-4952, June 1965.
74. B. L. Eyre and M. J. Sole, On the Formation and Behaviour of Point Defect Clusters in Neutron Irradiated Uranium Carbide, British Report AERE-R-4956, June 1965.

Section

II

Reactor Materials

Moderator Materials

Graphite

The diffusion of barium, strontium, and cerium through various grades of polycrystalline graphite has been studied by British investigators.[1] The diffusion of barium and strontium in CYX-165 and HX30 graphites, and of barium in G5 graphite and pyrographite, was studied by the use of an electron microprobe. The diffusion of cerium in HX30 graphite was studied by a sectioning technique. The CYX165 graphite was a furfural-alcohol-impregnated and baked material having a surface area of approximately 3 to 5 m^2/g, a density of 1.7 g/cm^3, and a pore-size distribution wherein the majority of the pores had entrance diameters of less than 1 μ. The G5 graphite was very different from CYX165. Its density was 1.58 g/cm^3, surface area was in the range of 0.3 to 0.5 m^2/g, and pore-size distribution peaked at 1.5 to 4 μ. The HX30 graphite was a material with a narrow pore-size distribution, with most pores having entrance diameters of 55 to 10 μ. Both as-formed pyrographite and pyrographite annealed at 2700°C were used for the few barium-diffusion experiments.

The British investigators concluded that the movement of these metals through polycrystalline graphite and pyrographite occurs by activated surface diffusion, combined possibly with vapor-phase migration, through microstructural defects. Furthermore, they concluded that, in graphite containing ungraphitized material, the bulk of the mass transfer occurs along the surface of this component.

A unique combination of properties has been reported for graphites formed by hot-isostatic compaction of graphite powders.[2] Product graphites exhibited high degrees of isotropy, densities up to 99% of theoretical, and moderate tensile strengths. The values of isotropy, density, and strength combined in such hot-isostatically formed samples have not previously been achieved by other processes for forming bulk graphite shapes. The potential for combined irradiation stability and low permeability makes these new graphites of special nuclear interest. Thus more detailed characterization including irradiation behavior is planned for these materials. A secondary factor of significance in this reported research is the use of neutron diffraction to determine isotropy of graphite samples. This is believed to be the first reported application of neutron diffraction for this specific purpose. The pronounced advantage over X-ray diffraction is the much greater depth of sample penetration possible with neutrons as compared with X rays.

The high-temperature reaction of hydrogen and graphite has been studied up to 3450°K at Brookhaven.[3] Test temperatures were achieved by high current pulses of 0.01- to 10-sec duration. The results indicate that, above 3000°K, graphite vaporizes to C_n radicals, which react with hydrogen in the vapor phase. The C_2H_6 and C_3H_8 are minor stable intermediates, but above 3350°K the final product is C_2H_2. Below 3350°K, heat loss is by radiation and thermal conduction, but above 3350°K, vaporization absorbs most of the heat. Thus temperatures greater than 3350°K are required to carry out the endothermic formation of C_2H_2 efficiently.

British researchers have reported data indicating substantial radiation-induced creep in graphite, as well as data supporting the superior irradiation stability of isotropic graphite.[4] The experiments were carried out to a maximum dose of approximately 3.8×10^{22} neutrons/cm^2 in the temperature range 260 to 500°C. In-pile creep experiments demonstrated the existence of a steady-state creep in both PGA graphite and the isotropic graphite, which is capable of producing tensile strains of several percent.

The significance of this is that it provides a mechanism for relieving internal strain in highly rated reactor graphite and thereby prevents fracture due to differential dimensional changes. Dimensional data indicate that, at very high doses, the volume of isotropic graphite remains nearly constant. In the case of PGA (standard reactor graphite), there is an expansion of several percent in the perpendicular direction and a contraction of 10% in the parallel direction. Creep data are summarized in Table II-1. Dimensional changes are illustrated in Figs. II-1 and II-2, which compare PGA with the isotropic graphite.

(M. C. Brockway)

Table II-1 RADIATION CREEP OF GRAPHITE[4]

Neutron dose, 10^{22} neutrons/cm^2	Irradiation temp., °C	Stress, psi		Creep strain, %
		Initial	Final	
Type B (Isotropic) Graphite				
1.31	385	1150	2340	1.09
1.50	385	1200	2160	1.23
1.50	385	1050	3040	1.25
1.31	385	1100	2410	1.13
0.72	430	1050		0.52
0.95	430	1100		0.88
1.07	430	1100		1.17
1.07	430	1100		1.27
2.13	480	1200	3720*	2.24
2.40	460	1100	740*	2.67
2.38	440	1250	†	(2.34)
2.09	415	900	†	(1.75)
PGA Graphite				
1.66	265	430‡		**
		465§		**
2.04	310	360‡		**
		935¶		1.61
2.19	350	555§		0.81
		910¶		2.05
2.04	385	595§		0.90
		875¶		1.32
1.66	420	990¶		0.65
		965¶		1.08
1.58	>295	1180		>1.50
1.54	>340	1430		>1.38
1.39	360	1570		>1.33
1.18	375	1340		1.26
0.95	380	1300		1.96

*Specimen cracked.
†Specimen broken.
‡One-quarter strain rate.
§One-half strain rate.
¶Full strain rate.
**Strain not significant.

Beryllium Metal and Alloys

Beryllium Alloys

Investigators at Lockheed recently studied the beryllium-rich end of binary systems of beryllium with silver, aluminum, chromium, copper, and iron.[5] A study of the morphology

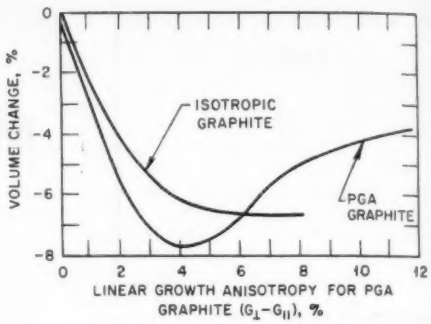

Fig. II-1 Volume changes in graphite.[4] ($G_\perp$ and $G_{||}$ refer to dimensional changes perpendicular and parallel, respectively, to extrusion direction.)

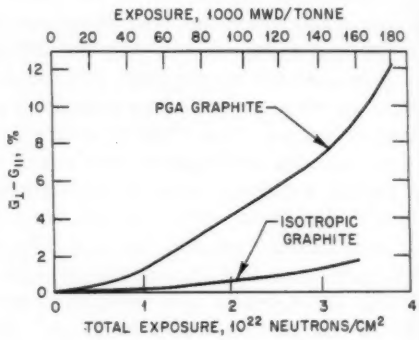

Fig. II-2 Variation in growth anisotropy of graphite with irradiation exposure.[4] ($G_\perp$ and $G_{||}$ refer to dimensional changes perpendicular and parallel, respectively, to extrusion direction.)

of some of the second-phase particles commonly observed in commercial beryllium was a secondary objective. The elements chosen are either major impurities or are being used for ductile-matrix or solid-solution-strengthened alloys. Higher purity materials currently available allowed more accurate determination of the systems than was possible in previous investigations.

In the beryllium–copper system, the previously established form of the diagram was found to be correct, but the solubility limit was found to be 2 at.% higher. The eutectoid temperature was determined to be 1090°C (1995°F), and some missing portions of the diagram were completed. Maximum solubility of aluminum in beryllium was approximately 0.02 at.%. Only minor changes were noted in the beryllium–iron

system, including a slight increase in the eutectoid temperature. Maximum solid solubility of silver in beryllium was 0.048 at.% at 1010°C (1850°F). Silver compounds were observed to have very slow decomposition rates. Chromium was found to be soluble in beryllium up to 0.076 at.% at 1220°C (2230°F).

The technique for diffusion-coupled preparation necessitated melting some binary alloys. The Lockheed report describes some outstanding metallography on these alloys. Predictions of rates of phase formation and decomposition are made on the basis of metallographic evaluation.

Physical Metallurgy

Pechiney has reported on the properties of SR beryllium, which is the highest purity commercial beryllium available.[6a] In general, cast and extruded materials were characterized by low tensile strength and low ductility at low temperatures. These properties were improved by additions of calcium, yttrium, titanium, and zirconium, which refined the grain structure. Conversion of the metal to powder and reconsolidation also improved the mechanical properties. However, in the cast and extruded metal, it was difficult to achieve a recrystallized grain size smaller than 30 μ.

In the range 400 to 700°C (750 to 1290°F), cast and extruded SR beryllium showed a decrease in tensile properties. Additions of solid-solution-strengthening alloys, such as iron and palladium, improved these properties. Aluminum was noted to be particularly detrimental to high-temperature properties by interfering with the precipitation process caused by overaging.

The author proposes several methods to improve the mechanical properties of high-purity beryllium: (1) production of finer and more homogeneous grain size, (2) addition of certain soluble metallic elements, (3) thermal treatment to minimize the role of unavoidable impurities, or (4) ternary alloying, which the author feels needs more investigation.

In a joint paper by the French Atomic Energy Commission and Pechiney, the recrystallization of commercial beryllium and beryllium–calcium alloys was reported.[6b] Commercial-purity beryllium that was cast, extruded, and swaged was used in this study. Recrystallization was defined as the restoration of an as-annealed microhardness and an equiaxed grain. Swaging at 400°C (750°F) permitted complete recrystallization to be achieved in 6 hr at 750°C or in 2 hr at 800°C (1470°F) on comparable reductions. On the other hand, metal swaged at 600°C (1110°F) recrystallized in less than 1 hr at 750°C (1380°F), and grain growth was experienced after 30 min at 775°C (1425°F). Recovery was experienced in metals swaged at 700°C (1290°F).

In the investigation it was found that recrystallized grain sizes of less than 25 μ could not be obtained in the broad range of parameters investigated. Deformation in the specimens swaged at 400°C was accompanied by a precipitation reaction. The precipitates were not taken back into solution during annealing at 700 to 800°C. Swaging at 600 and 700°C gave deformation, which was accompanied by polygonization that provided recrystallization nuclei. The fiber texture developed by the swaging step was only partly destroyed after a 1-hr anneal at 800°C. However, the extrusion texture was restored after 19 hr at 800°C. In general, the room-temperature ductility increased with decreasing as-annealed grain size.

Freibel at Rocky Flats observed microstructure changes in wrought vacuum-cast beryllium by the use of a hot-stage metallograph.[7] Specimens of various thermomechanical histories were heated at the rate of 10°C/min on the hot stage. It was noted that recrystallization, grain growth, and elimination of mechanical twins started in the range 600 to 750°C, depending on fabrication history. Grain growth was very rapid above 815°C. In this material it was impossible to eliminate all twins with prolonged heating.

Analysis

The Materials Advisory Board issued a report from one of its subpanels covering the analysis for impurities in beryllium.[8] Oxygen determination in both the commercial-purity (>500 ppm) and high-purity ranges was the major problem. Also, nitrogen below 10 ppm and carbon below 100 ppm caused problems. Some round-robin work is currently being done, but the committee recommended more of this effort. Once the most reliable technique is determined, standards should be produced so direct comparisons can be made among laboratories. The report also gives a review of various

analytical techniques for determination of impurities in beryllium.

Corrosion

Investigators at Harwell[9] examined the effect of prior irradiation on the oxidation of beryllium in CO_2. Both Pechiney- and Brush-source beryllium were irradiated to 1.2×10^{20} and 2.8×10^{21} neutrons/cm^2, respectively. When swelling due to nuclear transmutation was less than 5%, there was no appreciable increase in the corrosion rate. On the other hand, maximum oxidation occurred in specimens that swelled the most. This increase in oxidation was accompanied by the development of an intergranular void network caused by the swelling. This provided, initially, an increased surface area exposed to the CO_2 environment.

Component Fabrication

Pratt & Whitney investigated joining and compatibility of niobium–1 wt.% zirconium and type 316 stainless steel with beryllium armor.[10] These materials, which are candidates for space radiator systems, were studied in the range 540 to 760°C. On the basis of lap-shear-strength tests and on 3000-hr compatibility data, silver was found to be the only suitable brazing material for joining the components. A maximum service temperature below 760°C should be specified for silver-bonded systems, since a brittle compound is formed after long exposure at this temperature. Barrier layers to prevent compound formation were investigated, but they also inhibited bonding.

(H. D. Hanes)

Beryllium Oxide

Information on the irradiation behavior of beryllium oxide plus beryllium-metal additions and of beryllium oxide plus alumina and silica was reported by General Electric researchers.[11] Postirradiation data were reported for samples irradiated at 100°C to dosages up to about 5×10^{20} neutrons/cm^2 ($E \geq 1$ Mev). The compositions included NGK-grade* BeO with 2 wt.% beryllium metal added; UOX-grade BeO with 1 and 2 wt.% beryllium; and Thermalox 995A, a nuclear-grade BeO containing 0.2 wt.% Al_2O_3 and 0.1 wt.% SiO_2 fabricated by Brush Beryllium. Interest in the compositions containing beryllium was based on their small grain size and strength, a combination which offered some possibility of good resistance to microcracking. The results are summarized in Table II-2, and expansions of UOX + beryllium additions are shown in Fig. II-3.

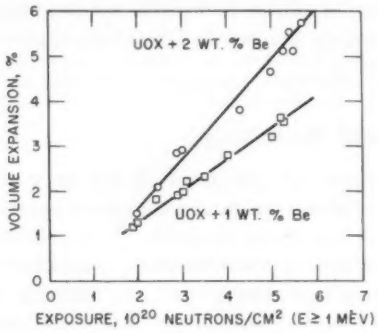

Fig. II-3 Expansion in UOX-grade BeO compositions containing 1 and 2 wt.% additions of beryllium metal[11] irradiated at approximately 100°C.

The two UOX compositions with beryllium additions appeared to undergo microcracking at dosages of 1.0 to 1.5×10^{20} neutrons/cm^2 ($E \geq 1$ Mev) — somewhat lower than previously reported for BeO of similar grain size without the additive. The larger expansion of the composition with the higher beryllium content also suggests that the beryllium is detrimental, but the data are not conclusive. Both of the beryllium-containing compositions were hot pressed. In general, hot-pressed materials have exhibited poorer microcracking behavior than comparable extruded or cold-pressed and sintered materials.

The NGK + 2 wt.% beryllium composition, also hot pressed, underwent microcracking at a dosage between 1.5 and 2.0×10^{20} neutrons/cm^2 ($E \geq 1$ Mev). The expansion is presented in Fig. II-4. The dosage at microcracking and the expansion curve are similar to BeO of similar grain size.

The Thermalox 995A composition exhibited somewhat superior performance. The plot of

*Product of NGK Insulators, Ltd., Nagoya, Japan.

Table II-2 EXPANSION IN BeO COMPOSITIONS[11] IRRADIATED AT 100°C

Table II-2 EXPANSION IN BeO COMPOSITIONS[11] IRRADIATED AT 100°C

Specimen description											
				Expansion, %					Modulus of rupture at room temperature		
Composition	Grain size, μ	Nominal density, g/cm³	Exposure, 10^{20} neutrons/cm² ($E \geq 1$ Mev)	Length	Diameter	Volume	Volume increase from density measurements, %	Increase in open porosity,*%	10^3 psi	10^3 kg/cm²	Percent of unirradiated value
UOX + 1 wt.% Be (hot-pressed)	9	2.98	1.9	0.4	0.4	1.2	1.2	0.4	22.1	1.55	71
			2.0	0.5	0.4	1.3	1.2	0.3			
			2.4	0.6	0.6	1.8	1.6		16.0	1.12	52
			2.9	0.7	0.6	1.9	1.7	0.6			
			3.0	0.8	0.6	2.0	1.8	0.6			
			3.1	0.8	0.7	2.2	2.2	0.7	17.0	1.20	55
			3.5	0.9	0.7	2.3	2.5	1.3			
			4.0	1.0	0.9	2.8	2.4	1.2	9.8	0.69	32
			5.0	1.2	1.0	3.2	2.9	1.4	8.3	0.58	27
			5.2	1.3	1.1	3.5	3.2	1.3			
			5.3	1.2	1.1	3.4	3.4	1.7	8.1	0.57	26
UOX + 2 wt.% Be (hot-pressed)	12	2.96	2.0	0.5	0.5	1.5	1.4	0.9	11.0	0.77	29
			2.5	0.7	0.7	2.1	0.9	1.1	7.4	0.52	19
			2.9	1.0	0.9	2.8	2.5	1.8			
			3.0	1.1	0.9	2.9	2.8		4.3	0.30	11
			4.3	1.4	1.2	3.8	4.0		3.3	0.23	9
			5.0	1.7	1.5	4.7	4.6	3.0	2.1	0.15	6
			5.3	1.9	1.6	5.1	4.9	2.9			
			5.4	2.0	1.7	5.4	5.4	3.4	1.8	0.13	5
			5.5	1.9	1.6	5.1	4.9	3.4	0.6	0.04	2
			5.7	2.1	1.8	5.7	5.8	2.5			
NGK + 2 wt.% Be (hot-pressed)	5	2.97	1.9	0.3	0.3	0.9	0.9	0.3	27.2	1.91	69
			2.1	0.3	0.3	0.9			21.9	1.5	56
			2.4	0.4	0.4	1.2	1.2	0.9	20.4	1.43	52
			2.9	0.6	0.5	1.6	1.5	0.9			
			3.0	0.6	0.6	1.8			4.7	0.33	12
			3.0	0.6	0.7	2.0	1.8	1.2			
			4.0	0.9	1.0	2.9	3.0		11.8	0.83	30
			5.1	1.1	1.2	3.5	3.3	2.2	3.5	0.25	9
			5.5	1.6	1.5	4.6	4.6	2.7	1.8	0.13	5
			5.8	1.6	1.6	4.8	4.8				
			5.8	1.5	1.4	4.3	4.9	3.6			
			5.9	1.4	1.5	4.4	4.6	2.3			
UOX + 0.2 wt.% Al_2O_3 + 0.1 wt.% SiO_2 (Thermalox 995A) (cold-pressed, sintered)	10	2.92	1.7	0.2	0.2	0.6	0.5	~0	41.0	2.88	151
			1.8	0.2	0.2	0.6	0.7	0.2			
			2.1	0.3	0.3	0.9	0.9	0.4	34.9	2.45	128
			2.2	0.3	0.3	0.9	1.0	2.0			
			2.9	0.4	0.4	1.2	1.3	2.5	36.8	2.59	135
			3.0	0.4	0.4	1.2	1.4	3.3	28.9	2.03	106
			3.5	0.5	0.5	1.5	1.6	2.6	21.0	1.48	77
			3.6	0.6	0.6	1.8	1.9	2.9	22.6	1.59	83
			4.0	0.7	0.7	2.1	2.3	4.0			
			4.0	0.6	0.6	1.8	1.6	3.3	14.1	0.99	52
			4.2	0.8	0.7	2.2	2.4	3.3	19.1	1.34	70
			4.6	0.7	0.8	2.3	2.4	3.1	14.8	1.04	54
			4.9	0.8	0.9	2.6	2.6	3.9	16.8	1.18	62
			5.1	0.9	0.9	2.7	2.9	3.7	12.8	0.90	47
			5.2	0.9	0.9	2.7	2.6	4.0	16.0	1.12	59
			5.5	1.0	0.9	2.8	3.1		12.9	0.91	47
			5.8	1.1	1.1	3.3	2.6	3.5	6.9	0.48	25

*This value is the difference between the % open porosity before and after irradiation.

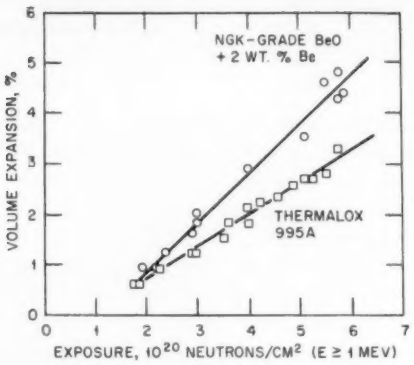

Fig. II-4 Expansion in BeO compositions[11] irradiated at 100°C. (Thermalox 995A is composed of UOX-grade BeO + 0.2 wt.% Al_2O_3 + 0.1 wt.% SiO_2.)

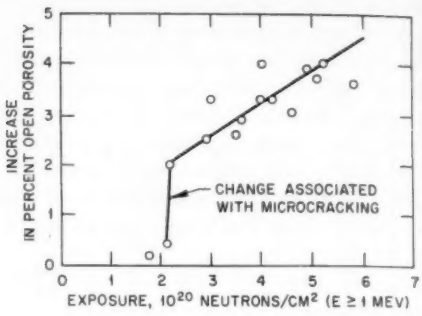

Fig. II-5 Increase in percent open porosity in Thermalox 995A composition of BeO irradiated[11] at 100°C.

porosity vs. exposure shown in Fig. II-5 indicates that microcracking occurred at about 2×10^{20} neutrons/cm^2 ($E \geq 1$ Mev). This exposure is 0.2 to 0.3×10^{20} neutrons/cm^2 higher than previously reported for comparable-grain-size material. The strength of Thermalox 995A appeared equal to that of unirradiated material up to a dosage of about 3×10^{20} neutrons/cm^2. This is roughly a 50% higher dosage than that at which previous materials retain original strength. Volume expansion at approximately 5×10^{20} neutrons/cm^2 was about 1% less than that for previous materials.

Solid Hydrides

Zirconium Hydride

In a summary of hydride properties and their potential applications, Van Houten and Baxter[12] reported that unclad samples of zirconium hydride with an N_H of 6.0 retained their dimensional stability and more than 95% of their hydrogen content after more than 1000 hr in Mach 0.2 air at 650°C.

The self-diffusion of zirconium in epsilon-phase zirconium hydride has been measured at Atomics International.[13] The diffusion coefficient was found to increase from about 4×10^{-12} cm^2/sec at 800°C to 10^{-11} cm^2/sec at 900°C, with some dependence on the grain size of the material. Electron micrographs of thin sections of the epsilon zirconium hydride show a structure believed to be characteristic of ordered domains within the interstitial lattice.

Fission-gas mobility studies have established that the migration of xenon through the hydride lattice is by a more complicated process than simple diffusion. Impurities in the zirconium hydride provide sites for heterogeneous nucleation and prevent simple diffusion of rare-gas atoms.

Yttrium Hydride

Hydrogen absorption isotherms for the yttrium–hydrogen system have been determined in the temperature ranges 250 to 350°C and 650 to 950°C up to 1-atm pressure by Yannopoulos and associates.[14] The isotherms for the higher temperature range are shown in Fig. II-6, with

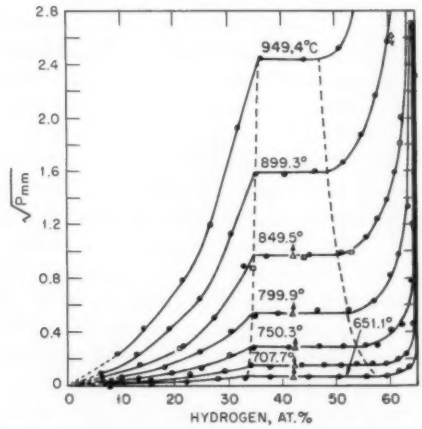

Fig. II-6 Experimental isotherms for the system yttrium–hydrogen: ●, absorption points; □, repeat absorption points; ⇳, desorption points obtained by raising the temperature; ⇲, desorption point obtained by lowering the temperature from the 949.4° isotherm.[14]

the dotted lines giving the estimated phase boundaries. Three solid-solution phases, with composition limits of $YH_{0.55}$, $YH_{1.972}$, and $YH_{2.7}$, are indicated by the data. The heat of formation value of –54.3 kcal/mole of hydrogen in two-phase regions agrees with data reported previously by Aldermaston (–54.2) but differs markedly from that of Denver Research Institute (–44.4). Partial molal heats of solution of hydrogen were calculated also.

Titanium Hydride

Crack-free titanium hydride having an N_H of 8.0 to 8.5 has been reported by Van Houten and Baxter.[12] They achieved this product by hydriding titanium that had been hot forged (810 to 1000°C) and cold rolled. Specimens with an N_H of 7.2 were held at 540°C in static furnace air for 2500 hr and gained only 0.145% in weight. No significant loss of hydrogen was detected, and very little redistribution occurred. Modulus-of-rupture tests on the thermal-stability specimens showed that titanium hydride has outstanding strength and ductility at temperatures above 350°C and is capable of retaining useful engineering properties after prolonged exposure under normal atmospheric operating conditions.

Lithium Hydride

A summary report on the application of lithium hydride to Systems for Nuclear Auxiliary Power (SNAP) reactors has been published by Atomics International.[15] The technology of lithium hydride casting is described as a method for fabricating reactor neutron shielding. The background, development, and current status are presented. The casting process and shield casting hardware are described in detail. The casting method is capable of consistently producing lithium hydride of purity greater than 97.5 wt.% and density 94% of theoretical.

Scandium Hydride

The hydrogen absorption isotherms for the scandium–hydrogen system in the range 600 to 1050°C up to 1-atm pressure were determined by Liebermann and Wahlbeck.[16] The isotherms are shown in Fig. II-7, with dotted lines indicating the phase boundaries. Two solid-solution phases with boundaries at $ScH_{0.55}$ and $ScH_{1.96}$ at 600°C were found. No trihydride phase was detected. In general, the system resembles the transition-metal hydrides.

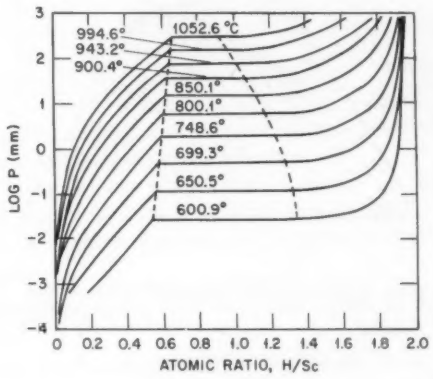

Fig. II-7 Experimental isotherms for the scandium–hydrogen system.

Hydrided Yttrium Alloys

Clad hydrided yttrium–5 wt.% chromium alloy with an N_H of 5.1 to 5.3 was tested in air for periods of 10,000 to 11,000 hr by Van Houten and Baxter.[12] No core cracking occurred in the first 5000 hr, in spite of relatively severe thermal cycles. Limited core cracking was observed in all the specimens after 10,000 hr, but this cracking had no effect on the dimensional stability of the specimens or on their hydrogen retention. Other samples reactor tested in air at 900°C for 5100 hr to an estimated thermal-neutron exposure of 1.3×10^{20} neutrons/cm^2 showed no evidence of distortion or weight loss. Further reactor exposure is in progress.

The equilibrium hydrogen pressures of the scandium–yttrium–hydrogen system were determined at 700, 800, and 900°C by Liebermann and Wahlbeck.[17] The data indicate a large primary solid-solution region of hydrogen in scandium–yttrium alloys, plus a three-condensed-phase region. The latter region shows limited miscibility of the two metal dihydrides. The ternary phase diagram at 700°C for the system is shown in Fig. II-8. For scandium–yttrium alloys of at least 60 at.% yttrium, evidence for a trihydride phase was found at 242°C. Thermodynamic properties of the system were calculated also.

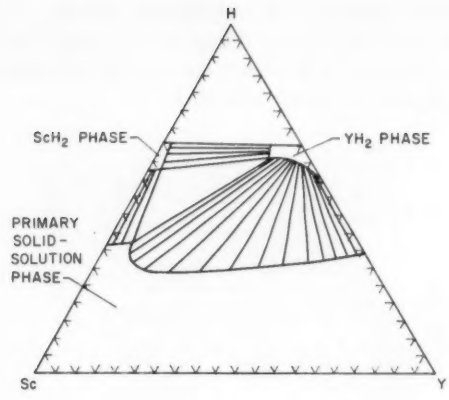

Fig. II-8 Scandium–yttrium–hydrogen phase diagram[17] at 700°C. (Tie lines were not experimentally determined.)

References

1. R. L. Faircloth, F. C. W. Pummery, and B. A. Rolls, Diffusion of Barium, Strontium, and Cerium in Various Grades of Reactor Graphite, British Report DP-Report-358, July 1965.
2. D. C. Carmichael, P. D. Ownby, and E. S. Hodge, Hot Isostatic Compaction of Graphite, USAEC Report BMI-1746, Battelle Memorial Institute, Oct. 5, 1965.
3. Brookhaven National Laboratory, Annual Report, July 1965, USAEC Report BNL-929, November 1965.
4. A. J. Perks and J. H. W. Simmons, Dimensional Changes and Radiation Creep of Graphite at Very High Neutron Doses, British Report AERE-R-5044, September 1965.
5. M. L. Hammond, A. T. Davinroy, and M. I. Jacobson, Beryllium-Rich End of Five Binary Alloys, Report AFML-TR-65-223, Lockheed Missiles and Space Co., August 1965.
6. Papers presented at the International Conference on Beryllium Metallurgy, Grenoble, France, May 17–20, 1965.
   a. J. M. Logerot, Mechanical Characteristics of High-Purity Beryllium Obtained by Double Electrolysis.
   b. R. Dumas, D. Carpentier, J. Moriceau, and D. Francois, Contribution to the Study of Beryllium and of Beryllium–Calcium Recrystallization.
7. V. R. Freibel, Metallography of Wrought Vacuum-Cast Beryllium at Elevated Temperatures, USAEC Report RFP-544, Dow Chemical Co., Rocky Flats Division, Nov. 22, 1965.
8. National Academy of Sciences, National Research Council, Analysis for Impurities in Beryllium, Report MAB-203-M, July 1, 1965.
9. M. J. Bennett, N. W. Crich, P. L. Blythe, and J. E. Antill, The Oxidation of Irradiated Beryllium in Carbon Dioxide, *J. Nucl. Mater.*, 17(1): 60-72 (August–September 1965).
10. J. R. Stewart, Space Radiator Fabrication Development, USAEC Report PWAC-483, Pratt & Whitney Aircraft Division, United Aircraft Corp., Aug. 25, 1965.
11. General Electric Company, Nuclear Materials and Propulsion Operation, High-Temperature Materials Program Progress Report No. 52, Part A, USAEC Report GEMP-52A, Oct. 20, 1965.
12. R. Van Houten and W. G. Baxter, Titanium, Zirconium, and Yttrium Hydrides as Space Shielding Materials, *J. Spacecraft Rockets*, 2(3): 469-472 (May–June 1965).
13. Atomics International, Annual Technical Progress Report, AEC Unclassified Programs, Fiscal Year 1965, USAEC Report NAA-SR-11450, Nov. 10, 1965.
14. L. N. Yannopoulos, R. K. Edwards, and P. G. Wahlbeck, The Thermodynamics of the Yttrium–Hydrogen System, *J. Phys. Chem.*, 69(8): 2510-2515 (August 1965).
15. F. H. Welch, Lithium Hydride Technology. Volume II. Fabrication of Shadow Shields for SNAP Applications, USAEC Report NAA-SR-9400 (Vol. II), Atomics International, Sept. 30, 1965.
16. M. L. Liebermann and P. G. Wahlbeck, Thermodynamics of the Scandium–Hydrogen System, *J. Phys. Chem.*, 69(10): 3514-3519 (October 1965).
17. M. L. Liebermann and P. G. Wahlbeck, The Scandium–Yttrium–Hydrogen System, *J. Phys. Chem.*, 69(11): 3973-3980 (November 1965).

Section

III

Reactor Materials

Nuclear Poisons

Metallic Poison Materials

A slightly boronated (250 ppm) type 304 stainless steel was developed by The Babcock & Wilcox Co. to be used as a burnable-poison fuel cladding.[1] During formation of the boronated tubes, it was found that the material was extremely hot short and had to be handled carefully in forging and welding. Additions of boron, up to 750 ppm, had no effect on tensile properties or corrosion in high-purity water at 600°F. The irradiation-induced mechanical-property changes increased with increasing boron content. However, irradiation had no effect on the corrosion properties of the boronated stainless steel.

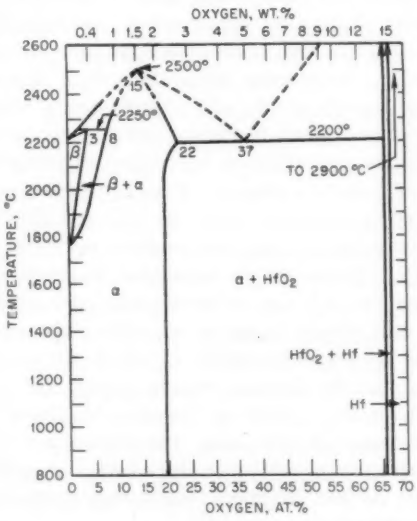

Fig. III-1 The hafnium–oxygen system.[2]

A partial hafnium–oxygen binary-system phase diagram has been constructed[2] (Fig. III-1). It was found that

1. The addition of oxygen raises the alpha–beta transformation temperature.
2. The alpha phase can dissolve up to 22 at.% oxygen at 2000°C and 20 at.% at 700°C.
3. A eutectic exists at 2200°C with 37 at.% oxygen.
4. HfO_2 has a limited homogeneity range of 66 to 66.7 at.% oxygen.

The hardness of hafnium increases considerably with the addition of oxygen up to 25 at.% oxygen.[2] Above 25 at.% oxygen, the hardness decreases until a composition of about 50 at.% oxygen is reached, after which the hardness again increases with increasing oxygen content. These effects are shown in Fig. III-2.

Studies at Harwell[3] indicate that the corrosion of hafnium in steam is very much pressure dependent, the corrosion rate decreasing sharply

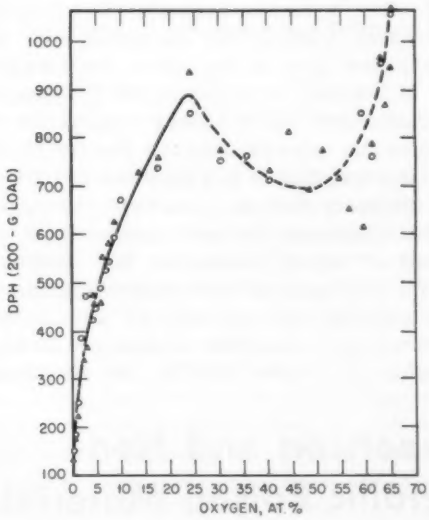

Fig. III-2 Hardness as a function of composition in the hafnium–oxygen system.[2] *Δ, specimens quenched from 1000°C; ○, specimens quenched from 1600°C.*

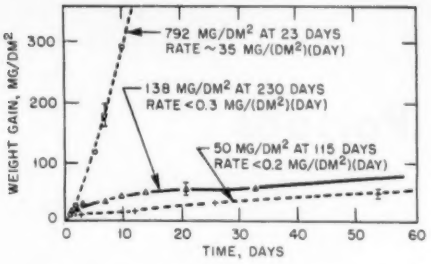

Fig. III-3 Weight gains for alpha-annealed hafnium in steam.[3] *--□--, in steam at 500°C, 1 atm; —Δ—, in steam at 500°C, 1000 psi; --+--, in steam at 500°C + H_3BO_3, 1000 psi; ⌈, typical spread of results at indicated weight gain.*

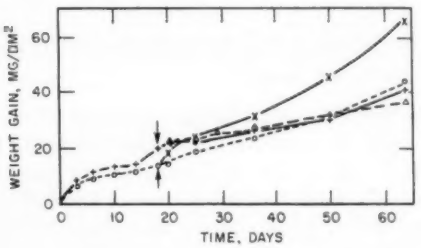

Fig. III-4 Weight gains for alpha-annealed hafnium in oxygen at 500°C (with transfers 1 atm = 1000 psi).[3] *○, 1 atm; +, 1000 psi; ×, 1 atm transferred to 1000 psi at ↑; Δ, 1000 psi transferred to 1 atm at ↓.*

with increasing pressure, as illustrated in Fig. III-3. Also, it can be seen that the addition of boric acid inhibits the corrosion rate still further. As seen in Fig. III-4, the corrosion rate of hafnium in oxygen at 500°C appears to be independent of pressure, except for the samples that were exposed at 1 atm for 18 days and then transferred to a pressure of 1000 psi. This suggests that the protective film formed at low pressures is more porous than that formed at higher pressures. The addition of 10 at.% aluminum or chromium to hafnium–25 wt.% tantalum and hafnium–12 wt.% niobium improved the oxidation resistance of these alloys[4] in static air at 2500°F. (M. Kangilaski)

Dispersion and Nonmetallic Poison Materials

The fabrication of HfO_2–aluminum and aluminum–boron control rods was described in a report[5] issued by Battelle–Northwest. Aluminum powder (–200 +325 mesh) was mixed with varying amounts of either HfO_2 or elemental boron. Three rods were fabricated by cold-pressing pellets of ball-milled mixtures of HfO_2 and aluminum powders. A simpler procedure was employed for four boron–aluminum rods, in which the ball-milled powders were tamp packed into Zircaloy-2 tubes and cold swaged.

A recent Atomics International report[6] describes the reference design and development information for the Mark IV control-rod assembly for the Sodium Graphite Reactor (SGR). This rod consists of dysprosium oxide packed to a density of 5.5 g/cm³ in the annulus formed by an inner core of graphite and an outer tube of Hastelloy X, which also serves as the structural support member. Results of elevated-temperature wear and compatibility tests indicated that the component materials were suitable for SGR operating environments. In-pile data are needed to provide information concerning the effects of long-term irradiation of this combination of materials.

The results of studies concerned with the corrosion resistance of europium molybdate and its compatibility with iron, nickel, and chromium were recently reported.[7] Workers prepared europium molybdate powder for corrosion studies by arc melting, oxidizing 16 hr at 1000°C, and then crushing to –325-mesh powder. Specimens possessing both face-centered cubic (fcc) and rhombohedral crystal structures were prepared and their corrosion resistance compared with that of unoxidized as-arc-cast material. The specimens were tested in distilled water at 100 and 250°C for varying times, and the results indicated only small differences in corrosion resistance between the fcc and rhombohedral structures for all the times considered. The as-arc-cast material appeared stable at 100°C but exhibited considerably larger weight gains at 250°C. Compatibility tests for the fcc and rhombohedral material with iron, chromium, and nickel showed that crystal structure had no significant effect on the chemical reactivity of the europium molybdate.

Development studies for the High Flux Isotope Reactor (HFIR) control element were also reported in this Oak Ridge annual report.[7] Procedures for fabricating the inner and outer cylinders were established such that finished components would meet the required tolerances. Clad segments containing regions of aluminum–

33 vol.% Eu_2O_3 and aluminum–tantalum were first fabricated to size by hot- and cold-rolling steps. These segments were then explosively formed into curved segments, four of which were subsequently seam welded together to form a preform cylinder. Explosives were again used to size the welded preforms to close tolerances. It has been possible to maintain tolerances to within ±0.015 in. of a nominal diameter of 17.842 in. over a 66-in. length.

Aluminum-clad specimens containing europium oxide and europium molybdate dispersed in aluminum were irradiated at 140°F to determine their dimensional stability. After exposure for one year to thermal- and fast-neutron doses of 1.3×10^{21} and 0.9×10^{21} neutrons/cm^2, respectively, only the specimen containing molybdate exhibited any swelling. Elastic moduli and creep-resistance data were determined for the europium- and tantalum-bearing portions of the control plates. In addition, it was found that significant stress relaxation occurred in the tantalum–aluminum specimens during irradiation.

The preparation and properties of solid solutions of titanium, zirconium, niobium, and tantalum carbides with hafnium carbides were described in a Russian journal.[8] The binary carbides were synthesized by powder-metallurgy techniques from powder produced by reduction of oxides with carbon. Compacting at 2560 psi (180 kg/cm^2) and sintering for 30 min at 2200°C produced a product that had 75% of the theoretical density. This sintered product was next pulverized, compacted at 4270 psi (300 kg/cm^2), and then sintered at 2700°C for 5 min to produce a product that was 96% dense. Thermal-expansion and microhardness measurements were made on these binary solid-solution carbides. Correlation of the data showed that changes in physical properties of the solid solutions are determined by the relation between the electronic-acceptor capacity of the metal atom and the probability that stable electronic configurations of the d^5 type will be formed.

The hafnium–carbon binary phase diagram was studied[9] by the use of metallographic and X-ray diffraction techniques. A single intermediate phase, HfC, was found and its boundaries defined. The most refractory composition was at 47.5 at.% carbon with a melting point of 3830°C. A peritectic reaction, in which hafnium was formed from HfC and hafnium-rich liquid, was found at 2240°C. The hafnium melting point was 2208°C, and the solubility of carbon in hafnium at this temperature was 10.5 at.%.

A British patent[10] describes how spherules of B_4C can be formed by one of two methods. In one method, finely divided B_4C is mixed with a finely divided inert isolating material. This mixture is rapidly heated in an inert atmosphere to 2300 to 2700°C. Upon cooling, the B_4C spherules solidify from the molten carbide. As an alternative, particles of boron or the oxide can be mixed and heated in the presence of an isolating medium containing enough carbon to form B_4C. Suitable isolating media include carbon, graphite, and boron nitride.

Vaporization characteristics of EuC_2 were studied and the results presented in a recent report.[11] A pure specimen of EuC_2 was synthesized from the elements, and its vaporization behavior was determined by means of a precise Knudsen effusion cell. The existence of a stable $EuC_{2.00}$ phase was confirmed, and the equilibrium vapor was found to consist only of europium, presumably in monatomic form. The europium pressure followed the relation

$$4.757 \log P \text{ (atm)} = \frac{-67{,}390}{T(^\circ\text{K})} + 27.4$$

The EuC_2 heat of formation was determined to be

$$\Delta H^\circ_{298} = -30.6 \text{ kcal/mole} \pm 4.5$$

Progress in the casting of high-melting-point metal–carbon alloys, which may be used for elevated-temperature physical-property measurements, was described in a recent report.[12] Tensile specimens of tantalum–HfC have been produced, and it became apparent that pressures of 1 atm or greater would be required to maintain the desired hafnium and carbon composition. A new furnace is being constructed which will incorporate design improvements developed from past experience in melting carbides.

Tensile tests were performed on 15 HfC–carbon castings as they were resistance heated in vacuum. Specimen temperature was measured by optical and thermocouple techniques. A strain rate of 0.0025 sec^{-1} was maintained

Table III-1 RESULTS OF TENSILE TESTS ON HAFNIUM CARBIDE CASTINGS[12]

Casting	Carbon, wt.%	Tensile strength		Modulus of elasticity		Remarks
		Psi	Temp., °C	10^6 psi	Temp., °C	
283	12.4	4,135	20			Broke at 1/16-in.-diameter gas hole
306	9.8	6,350	20			Failed in grips
287	8.9	12,450	20	33.7	20	Broke at 1/32-in.-diameter gas hole in center of specimen
276	10.4	15,890	1050	20.6	1050–1200	Broke at radius between gas hole and grip of specimen
278	10.8	15,300	1050	19.3	1050–1200	Broke at radius between gas hole and grip of specimen
298	12.5	18,300	1050	16.3	1050–1200	Broke at radius between gas hole and grip of specimen
277	9.9	18,720	1450	15.2	1450–1600	Broke at radius between gas hole and grip of specimen
286	10.8	16,080	1400	18.1	1400–1600	Broke at radius between gas hole and grip of specimen
292	10.5	13,850	1400			Broke at radius between gas hole and grip of specimen
265	10.0	18,700	2150	15.5	1950–2150	Broke at 1/16-in.-diameter gas hole in center of gauge section
267	11.3	16,340	2150	17	1950–2150	Broke at 1/16-in.-diameter gas hole in center of gauge section
308	11.6	16,350	2150			Broke at 1/16-in.-diameter gas hole in center of gauge section
275	10.0	12,580	2400	7.3	2100–2400	Broke at 1/16-in.-diameter gas hole in center of gauge section
279	11.4	11,895	2400	6.1	2100–2400	Broke at 1/16-in.-diameter gas hole in center of gauge section
297	11.5	13,510	2400	7.4	2100–2400	Broke at 1/16-in.-diameter gas hole in center of gauge section

constant throughout the tests. Stress–strain data were automatically recorded for each test. These data, along with test conditions, are summarized in Table III-1. It was found that no yielding occurred below 2150°C, but the curves for specimens tested at 2150 and 2400°C exhibited inflections indicative of limited ductility. However, the strain-measuring system did not record any reduction in area or elongation at fracture for any of the specimens.

(E. G. Smith, Jr.)

References

1. C. R. Johnson, Boron Stainless Steel Fuel Element Cladding in the Indian Point Reactor, in American Nuclear Society Meeting, San Francisco, November–December 1964, USAEC Report CONF-654-92.
2. R. F. Domagala and R. Ruh, A Study of the Hafnium–Oxygen System, Report ARL-65-138, Illinois Institute of Technology Research Institute, May 1965.
3. D. R. Silvester, J. V. Arthurs, C. E. Austing, and J. N. Wanklyn, The Corrosion of Hafnium in Steam and Oxygen at 500°C, British Report AERE-R-4706, July 1965.
4. R. J. Van Thyne, Development of Oxidation-Resistant Hafnium Alloys, Report IITRI-B6040-2, Illinois Institute of Technology Research Institute, July 15, 1965.
5. Battelle–Northwest, Ceramics Research and Development Quarterly Report, April–June 1965, USAEC Report BNWL-150.
6. Atomics International, Annual Technical Progress Report, AEC Unclassified Programs, Fiscal Year 1965, USAEC Report NAA-SR-11450, Nov. 10, 1965.
7. S. Peterson (Comp. and Ed.), Metals and Ceramics Division Annual Progress Report for Period Ending June 30, 1965, USAEC Report ORNL-3870, Oak Ridge National Laboratory, November 1965.
8. G. V. Samsonov and V. N. Paderno, Preparation and Properties of Solid Solutions of Titanium, Zirconium, Niobium, and Tantalum Carbides With Hafnium Carbides, *Izv. Akad. Nauk SSSR, Metal.*, No. 1: 180-188 (January–February 1965).
9. R. V. Sara, The Hafnium–Carbon System, *Trans. AIME*, 233: 1683-1691 (September 1965).
10. H. G. Sowman and J. R. Johnson, Boron Carbide Spherules, British Patent No. 1,001,360, August 1965.
11. R. H. Flowers, A Study of the Vapourization of Europium Dicarbide, British Report AERE-R-5012, August 1965.
12. Bureau of Mines, Albany Metallurgy Research Center, Quarterly Metallurgical Progress Report Number 28, August 1–September 30, 1965, Report USBM-RC-1205.

Section

IV

Reactor Materials

Cladding and Structural Marerials

Corrosion

Corrosion of Zirconium Alloys

A zirconium-alloy development program was conducted at Bettis Atomic Power Laboratory[1] to obtain an alloy with corrosion resistance superior to that of Zircaloy-2 in steam at temperatures above 750°F but with hydrogen pickup and corrosion resistance in water at least equal to that of Zircaloy-1. It was found that zirconium sponge-base alloys containing 0 to 0.5 wt.% tin and 1.5 wt.% iron plus chromium met the above requirements and possessed mechanical properties equivalent to those of Zircaloy-2. A ternary alloy containing 0.5 wt.% iron and 1.0 wt.% chromium appeared to have the best combination of overall properties.

The cracking of stressed zirconium alloys in $FeCl_3$ solutions was studied by Thomas and Allio.[2] The time to intergranular-cracking failure was found to decrease with increasing stress, increasing chloride concentration, and increasing hydrogen content of the metal. It is believed that cracks were initiated in the hydride phase by pileup groups of dislocations and were propagated in a corrosive medium by an electrochemical effect produced by a difference in energy between the matrix and the grain boundaries.

General Electric Company workers conducted a literature survey to assess the suitability of Zircaloy-2 and Zircaloy-4 as pressure tubes for use in the reactor core of their maritime nuclear-steam-generator concept. It was concluded that, on the basis of existing technology, both alloys possess adequate mechanical properties and corrosion resistance for the proposed application.[3]

(W. E. Berry)

Corrosion of Aluminum Alloys

The aqueous corrosion behavior of four high-silicon aluminum alloys was investigated at Battelle–Northwest.[4] On the basis of results of exposures to steam at 400°C and water at 360°C and the observed effects of galvanic couple, stress, and water velocity at 140°C, it was concluded that an aluminum–10 wt.% silicon–1 wt.% nickel–0.6 wt.% iron alloy exhibited the best overall corrosion resistance.

The effects of alloying with yttrium and zinc on the aqueous corrosion of aluminum were studied at Oak Ridge National Laboratory.[5] In tests conducted in water at 200°C, alloys containing 2 wt.% yttrium or 20 wt.% zinc exhibited greatly reduced corrosion rates. These alloys were free of the intergranular attack that normally was found in 99.999 wt.% aluminum under these conditions. Intermetallic phases in the yttrium alloy were believed to be anodic to the matrix, whereas intermetallics in the zinc alloys were believed to be cathodic.

The corrosion behavior in water at 330°C of electroless-plated nickel on aluminum alloys was studied at Battelle–Northwest.[6] The nickel-plated aluminum was compatible with semistatic deionized water and flowing *p*H 10 (NH_4OH) water but not with flowing *p*H 10 (LiOH) water. Corrosion rates of unclad aluminum in semistatic *p*H 10 water at 330°C were 17 mils/month with LiOH and 0.6 mil/month with NH_4OH.

(W. E. Berry)

Corrosion of Stainless Steels

The effects of surface treatment on the corrosion behavior of type 410, type 304, and 25-20 stainless steels in high-temperature water and steam were studied in Belgium.[7] At temperatures above 400°C, those surface treatments

which produced a cold-worked layer on the metal surface resulted in improved corrosion resistance. Surface roughness appeared to have no influence on corrosion behavior. Microprobe analyses of the cold-worked layers revealed that the oxide was enriched and the metal was depleted in chromium and manganese.

The oxidation of pure iron under bombardment by inert-gas ions was studied over the temperature range of −50 to 1200°C by French scientists.[8] They concluded that the mechanism of oxidation under ion bombardment is not fundamentally different from oxidation under conditions of thermodynamic equilibrium. Exceptions were an increase in oxidation kinetics and a difference in the growth of oxide crystallites under bombardment.

The effect of fast-neutron doses of 2×10^{20} neutrons/cm^2 on the postirradiation stress-corrosion behavior of type 316 and 20 wt.% chromium–25 wt.% nickel–1 wt.% niobium stainless steels in boiling 42% $MgCl_2$ has been reported by Harwell.[9] No effects were found with the 20-25 alloy, which did not crack after 130 hr of exposure at stresses to 55,000 psi in the irradiated and unirradiated conditions. The irradiation increased the susceptibility to stress-corrosion cracking of the type 316 stainless steel at low stress (13,000 psi levels) and caused all samples to fail in less than 1.5 hr regardless of stress loading in the range of 5000 to 23,000 psi. It was concluded that the irradiation damaged the oxide film, thereby affecting the initiation (rather than the propagation) of the cracks.

The intergranular corrosion behavior of unsensitized type 304 stainless steels in nitric acid–potassium dichromate was correlated with microstructure, alloy chemistry, and heat-treatment in studies conducted at Vallecitos Atomic Laboratory.[10] It was found that: (1) the corrosion rate increased with increasing grain size, (2) high-temperature annealing reduced the corrosion rate, (3) increasing the carbon content in the alloy reduced the corrosion rate, and (4) sensitized specimens rich in carbon were more corrosion resistant than solution-treated alloys of low carbon content. The results of the study were discussed in terms of solute segregation at austenite grain boundaries.

An iron-base fuel-element cladding alloy with excellent resistance to stress-corrosion cracking was developed by Westinghouse Electric Corp.[11] The alloy contains 16 wt.% chromium–20 wt.% nickel–0.015 wt.% (max.) carbon–0.010 wt.% (max.) nitrogen. Tests have shown that samples from commercial heats of this alloy did not crack after 300 days' exposure at 40,000-psi load in boiling $MgCl_2$. Type 304 stainless steel failed after 0.7 day, and type 310 stainless steel failed after 25 days, in similar tests. (W. E. Berry)

Corrosion of Base Metals

The compatibility of Hastelloy X-280, Inconel 600, and Haynes 25 alloy with expected contaminants in the helium coolant of the Advanced Test Reactor (ATR) was studied at Battelle–Northwest.[12] Hastelloy X-280 and Inconel 600 withstood oxidizing atmospheres for a period of several hours at 2192°F, but Haynes 25 alloy oxidized catastrophically at oxygen pressures greater than 0.3 torr. It was believed that low levels of oxygen in the coolant could prevent evaporation or carburization of the metals. Nitrogen at 2192°F and 100 torrs had no effect other than to inhibit evaporation.

The oxidation behavior of 10 high-temperature alloys in helium–water vapor was also studied at Battelle–Northwest.[13] After 300-hr exposure at 815 and 930°C, Hastelloy N, Hastelloy X-280, Inconel 625, Inconel 600, and Haynes 25 were found to possess optimum corrosion resistance, although the latter two alloys exhibited some intergranular attack at the higher temperature. At 1038°C, Hastelloy C, Hastelloy N, Hastelloy X-280, and Haynes 25 exhibited the best oxidation resistance, with tightly adherent oxide films and little or no intergranular penetration or internal oxidation.

A comprehensive study of the corrosion of nickel-base alloys in flowing superheated steam at 1050 and 1150°F was made by Vallecitos.[14] Hastelloy X, Incoloy 825, Inconel 625, and Incoloy 800 had low initial and long-time linear corrosion rates and formed a tenacious oxide. Inconel 600 was adequately resistant to 1050°F steam but produced a nonadherent film that was lost to the system at 1150°F. Type 304 stainless steel had significant corrosion rates and formed thick oxide films that eventually spalled. (W. E. Berry)

Corrosion of Other Alloys

Erratic corrosion of titanium in saline waters at 100 to 200°C with penetration rates in excess of 200 mils/year was observed at Oak Ridge.[15]

It was found that crevices favored initiation of the attack, which appeared to occur more frequently at contact areas between plastic and titanium than between titanium and itself. The corrosion process was often self-sustaining and continued beyond the confines of the crevice. Attack also appeared to initiate at microcrevices or surface imperfections such as laps, fissures, or inclusions. Attack was not observed at *p*H greater than 8.7. Of nine commercial alloys tested, only a titanium–0.15 wt.% palladium alloy exhibited increased resistance (but not immunity) to the attack.

The cavitation of type 316 stainless steel and aluminum, niobium, molybdenum, and tantalum alloys was studied by Pratt & Whitney Aircraft[16] in deaerated water at 95 to 105°F and static pressures of 9.5 to 10.5 psig. Test coupons were inserted in disks 9.5 in. in diameter by 0.175 in. thick, which contained 0.25-in.-diameter holes to induce cavitation. Disk speeds were 6000 to 6200 rpm. The most resistant alloys were tantalum–8 wt.% tungsten–2 wt.% hafnium, tantalum–10 wt.% tungsten, and niobium–18 wt.% tungsten–2 wt.% hafnium. The cavitation-damage resistance could not be defined in terms of any single property of the alloy. (W. E. Berry)

Corrosion and Oxidation of Refractory Metals

General Electric is evaluating sheathing materials to protect tungsten vs. tungsten–25 wt.% rhenium thermocouples in high-temperature carbonaceous environments.[17] Previous studies have shown that HfO_2 is the best available material for electrical insulation at temperatures above the melting point of BeO. However, the good electrical insulating characteristics of HfO_2 can be rapidly destroyed if it is carburized. In their search for a suitable sheathing material, the workers exposed various refractory metals and alloys to a temperature of 2450°C while in contact with graphite. Small rods of HfO_2 were hermetically sealed inside refractory-metal capsules that in turn were inserted into graphite. The external surface of the graphite was protected by a hydrogen atmosphere. If the surface of the HfO_2 rods inside the capsule became electrically conducting after the exposure, the sheathing was considered to be an inadequate barrier to carbon diffusion. Tantalum was found to be the only material capable of preventing carburization of the encapsulated HfO_2. The effectiveness of tantalum was verified by preparation of a thermocouple probe insulated with HfO_2 and sheathed with tantalum. The probe was placed in a graphite block and heated to 2450°C. The fact that the thermocouple output was stable over the 1-hr period at temperature indicated that carburization of the HfO_2 had not occurred.

The effect[18] of nitrogen on the oxidation of tantalum was studied at 600, 820, and 925°C. In all cases the oxygen partial pressure was close to 360 torrs; nitrogen partial pressures in the range of 0 to 250 torrs were investigated. Nitrogen was found to reduce the oxidation rate to less than linear at all three temperatures. (J. J. English)

Protective Coatings for Refractory Metals

An experimental study of the factors controlling the effectiveness of high-temperature (2000°C) protective coatings for tungsten is the subject of a recent report prepared by General Telephone and Electronics Laboratories, Inc.[19] The report contains (1) a comprehensive analysis of diffusion in refractory oxides, (2) a thermodynamic treatment of the vaporization processes in complex oxides, (3) an examination of reactions between tungsten and possible coating materials, and (4) a structural analysis of oxides and interdiffusion products. According to the authors, the results of the program indicate that the greatest problem in attempting to formulate a protective coating is the limited choice of oxides that restrict ionic migration at 2000°C (3630°F) sufficiently to be protective. Of the simple oxides, only Al_2O_3 and MgO have anion and cation diffusion rates low enough to be used as 10-mil-thick coatings at this temperature for 1 hr. Even these two oxides possess limitations: Al_2O_3 melts at 2050°C (3720°F), and MgO vaporizes at a rate of 10 mils/hr at 1760°C (3200°F) in a vacuum or at 2055°C under 0.2-atm oxygen pressure.

Aeronutronic Applied Research Laboratories has published the third report of a series on the mechanisms of protection and failure of intermetallic type coatings.[20] Four areas of investigation are discussed:

1. The kinetics of the growth rates of intermediate phases in the systems $Ta–TaSi_2$ and $Nb–NbSi_2$

2. The low-pressure high-temperature oxidation behavior of the following silicides: WSi_2, $TiSi_2$, $CrSi_2$, and $ReSi_2$

3. Thermal dilation, measured by X-ray and dilatometer techniques, of the following silicides: $MoSi_2$, $NbSi_2$, $TaSi_2$, WSi_2, $ReSi_2$, $MnSi_2$, $TiSi_2$, $NiSi_2$, $CrSi_2$, Mo_5Si_3, Nb_5Si_3, Ta_5Si_3, W_5Si_3, and Ti_5Si_3

4. A mathematical analysis of the thermal stresses that occur in silicide coatings on refractory metals

Marquardt Corp. has conducted an extensive evaluation of hafnium–tantalum alloy coatings for protecting the refractory metals from oxidation at very high temperatures.[21] The program results indicate that the alloys hafnium–20 wt.% tantalum, hafnium–27 wt.% tantalum, and hafnium–20 wt.% tantalum–2 wt.% molybdenum have significant potential for use as coatings at temperatures up to 4000°C. Relatively thick coatings, up to 30 mils, are required at these temperatures. The thicknesses depend on the time, temperature, and oxygen pressure. For example, a 28-mil-thick coating of hafnium–27 wt.% tantalum cladding on tantalum–10 wt.% tungsten was oxidized in an oxyacetylene flame at 3500°F (uncorrected optical temperature) for 40 min. An oxide scale about 37 mils thick formed, and 22 to 23 mils of cladding were consumed. Most significantly, it was noted that, although the remainder of the cladding was contaminated, no increase in the hardness of the tantalum–10 wt.% tungsten alloy was measured. The Marquardt studies indicated that the rate of conversion of these hafnium–tantalum alloys to oxide tends to decrease with decreasing oxygen pressure. Consequently, for applications involving low oxygen partial pressures, such as reentry and near-stoichiometric combustion thrust chambers, the required coating thickness would probably be less. The claddings, which have been successfully applied by roll bonding and plasma-arc-spraying techniques, deform readily with the substrate at elevated temperatures.

A slurry type coating for refractory metals, designated as a "fused slurry silicide," has been developed and evaluated at Sylcor Division, Sylvania Electric Products Inc.[22] The silicide slurry, comprising a mixture of blended elemental or prealloyed powders suspended in lacquer, is deposited on the substrate by either spraying or dipping. The coated substrate is then air dried and subsequently fired in vacuum for 1 hr at 2500°F. Numerous coating compositions of the type silicon–20 wt.% chromium or silicon–20 wt.% titanium modified with chromium, titanium, vanadium, aluminum, molybdenum, tungsten, boron, iron, and manganese were evaluated in (1) cyclic oxidation tests at 2500 to 2800°F at atmospheric and low pressures, (2) low-temperature and step-down oxidation tests, and (3) torch tests up to 3200°F. More than 30 compositions were found to protect the niobium alloy D-43 for greater than ten 1-hr cycles at 2500, 2600, and 2700°F. One of the more extensively evaluated compositions, silicon–20 wt.% chromium–5 wt.% titanium, had cyclic oxidation life in atmospheric air in excess of 150 hr at 1600 and 2000°F, about 50 hr at 2300 and 2600°F, and in excess of 10 hr at 2700°F. The effect of this coating on the mechanical properties of D-43 was minor.

The Air Force has awarded a series of contracts to various investigators to evaluate different coating processes for applying the promising chromium–titanium–silicon coating system to niobium alloys. The coating processes being investigated include: the fluidized bed by Boeing Co.,[23] chemical vapor deposition by Texas Instruments, Inc.,[24] electrophoretic deposition by Vitro Laboratories,[25] and fused-salt deposition by Solar Division of International Harvester Co.[26]

Pratt & Whitney has developed a slurry-applied coating for protecting niobium alloys from oxidation at elevated temperatures.[27] The coating system, designated PWK-5, is based on a niobium silicide barrier layer interposed between the base metal and a refractory aluminide, tin-containing envelope. Mean lifetimes (1 cycle/day) of PWK-5 coated niobium–1 wt.% zirconium exposed in air at 650 and 1100°C exceeded 6000 and 800 hr, respectively. Penetration of the tin through the silicide barrier layer was the principal factor in limiting coating life at 1100°C.

The Pfaudler Co. conducted a study of the methods and procedures that are applicable to the scale-up of pack-cementation coating processes, such as the PFR-6 coating for molybdenum alloys.[28] Suitable equipment was designed, procured, and checked out which would be capable of coating parts as large as 36 by 48 by 72 in. The performance of the resulting coatings on TZM molybdenum alloy was evaluated in oxidation tests at temperatures up to 3000°F, stress-rupture tests, and tensile tests.

(J. J. English)

Corrosion by Liquid Metals and Fused Salts

SNAP-50/SPUR MATERIALS

Several late-1965 reports[29-32] issued by Pratt & Whitney summarized their liquid-metals research oriented toward the SNAP-50/SPUR power plant (lithium reactor coolant, potassium Rankine-cycle working fluid, and eutectic NaK condenser coolant). The summary report on coolants and working fluids[29] includes a detailed discussion of the corrosion mechanism and thresholds of corrosion for refractory metals and alloys, as well as specifications designed to eliminate failures by alkali-metal corrosion. The solubility data on molybdenum and niobium in 1095°C potassium as a function of oxygen content of the potassium are shown in Fig. IV-1, and some existing data[30] on the solubilities of

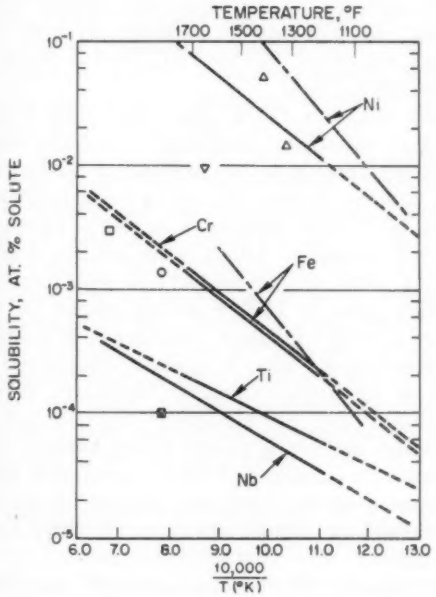

Fig. IV-1 Solubility of some metals in lithium.[30] ——–, United Nuclear data; ——, Pratt & Whitney—CANEL data; — — —, extrapolation; □, ○, Δ, ∇, ×, Soviet data (Bychkov et al.) for molybdenum, titanium, nickel, iron, and niobium, respectively.

a number of metals in lithium are summarized in Fig. IV-2.

Screening tests were conducted to narrow the choice of candidate bearing materials for the SNAP-50/SPUR lithium and NaK systems.[32]

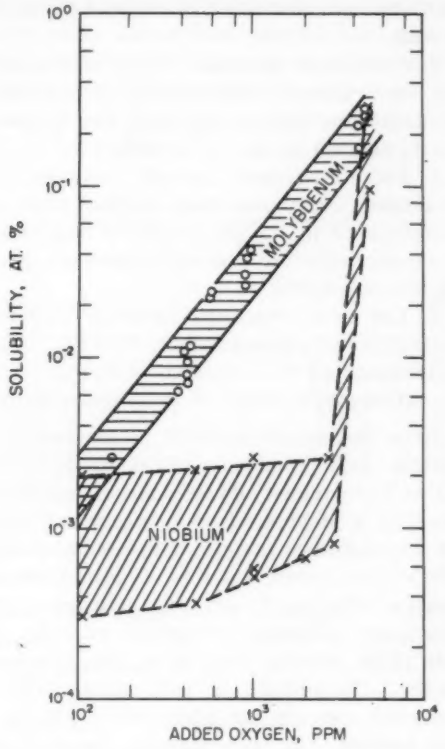

Fig. IV-2 Oxygen dependence of apparent equilibrium solubility of molybdenum and niobium in 1095°C potassium.[30]

Corrosion by 1100°F lithium for periods of 7000 hr was studied in tilting-capsule tests. Wear behavior was examined with a rotating-disk static-shoe device in lithium and NaK to 1000°F. The results are summarized as follows:

1. Molybdenum-bonded tungsten carbides, titanium carbides, and niobium carbides showed excellent compatibility with lithium at 1100°F.
2. Cobalt-bonded tungsten carbides are compatible with 1100°F lithium at binder concentrations of 3 to 5 wt.% but undergo significant solution corrosion at binder concentrations of 8 to 25 wt.%.
3. Nickel-bonded tungsten and titanium carbides containing 4.5 to 25 wt.% binder undergo severe solution attack of the nickel by 1100°F lithium.
4. Carbon loss from carbides of titanium and niobium in 1100°F lithium is negligible and that from tungsten carbides is slight.
5. Molybdenum- and cobalt-bonded carbides show excellent wear resistance in lithium and

NaK, but nickel-bonded carbides hold up only in NaK.

6. Carburized niobium–1 wt.% zirconium alloy wear behavior depends on the processing technique and coating thickness and, at best, is nearly as good as that of cermets.

7. Plasma-sprayed cermet coatings show promising wear behavior in NaK, but good performance in lithium seems to require substantially improved control of adhesion, porosity, and impurities.

8. The most promising couple for full-scale bearing tests is Kennametal K-7178 (WC–7 wt.% molybdenum–2 wt.% niobium–0.3 wt.% titanium) vs. carburized niobium–1 wt.% zirconium alloy.

Since the SNAP-50/SPUR power-conversion system may employ a TZM (molybdenum–0.5 wt.% titanium–0.08 wt.% zirconium) turbine wheel in a niobium–1 wt.% zirconium casing, the compatibility of this combination of alloys with wet potassium vapor is of special interest. General Electric[33] ran two niobium–1 wt.% zirconium refluxing-potassium capsule tests with TZM tubular inserts in the condensing region. The results of both tests (2500 and 5000 hr) indicate excellent compatibility for this system. The only changes observed were some staining of the walls in the vapor region, minute weight losses (1.3 mg/cm^2, maximum) from inserts in the condensing zone, and some surface decarburization and recrystallization of the TZM.

CORROSION BY LITHIUM

Previous studies by various investigators have shown that molten lithium corrodes niobium and niobium–zirconium alloys intergranularly and on the {1 1 0} crystallographic planes. In certain heat-treated conditions, however, niobium–zirconium alloys are not attacked by the alkali metal even though the alloys contain relatively large concentrations of oxygen. Pratt & Whitney studied the internal friction behavior of oxygenated niobium–1 wt.% zirconium to determine the physical situation of oxygen in the alloy that causes the heat-treatments to increase the corrosion resistance of the alloy. Their studies showed that lithium corrodes the alloy only when oxygen is in interstitial solid solution.[34] When the alloy is heat-treated near 2200°F, precipitation of oxygen as ZrO_2 occurs, and corrosion stabilization is thereby achieved.

Screening tests were run on tubular specimens of the following refractory alloys (wt.%):

PWC-11 (Nb–1 Zr–0.1 C)
PWC-33 (Nb–3 Zr–0.3 C)
T-111 (Ta–8 W–2 Hf)
FS-85 (Nb–28 Ta–10 W–1 Zr)
W–25 Re

for 200 and 1000 hr in the surge tank of a niobium–1 wt.% zirconium forced-circulation lithium loop.[35] Specimens were subjected to 2200°F lithium at 0.45 and 0.88 ft/sec over both their OD and ID surfaces. No lithium attack was observed in any of the specimens. Depletion of both carbide phase and zirconium, attributed to the lithium, was noted in PWC-11 and PWC-33 specimens. Single-phase surface regions were also found in T-111 and FS-85 alloys, but these could not be attributed to lithium because control specimens heated in argon showed the same effect. Thermally induced grain-boundary precipitation of sigma phase occurred in the tungsten–25 wt.% rhenium alloy. Although all except the T-111 alloy were softened by the argon and lithium exposures, no decrease in rupture strength was found, except for an expected 10 to 15% decrease in the PWC-11.

Oak Ridge workers conducted tests to see whether vanadium additions to niobium would have the same type of corrosion-inhibiting effect against molten lithium as zirconium additions do.[36] They exposed a series of niobium–40 wt.% vanadium alloys, homogenized (2 hr at 2375°F) with oxygen contents ranging from 500 to 4500 ppm, to 1500°F molten lithium for 100 hr in separate niobium containers. The attack on these alloys was, in general, just as bad as that on unalloyed niobium. Therefore it was concluded that the vanadium addition had no corrosion-arresting value. Under similar conditions, the niobium–1 wt.% zirconium alloy containing up to 3300 ppm oxygen would be unattacked by lithium when appropriately heat-treated.

At Argonne National Laboratory,[37] the alloys molybdenum–0.5 wt.% titanium and TZM (molybdenum–0.5 wt.% titanium–0.08 wt.% zirconium) were exposed to pure lithium at 1200°C for 210 hr in molybdenum capsules under about 38 torrs of helium pressure. The capsule itself showed slight evidence of general dissolution, but no corrosion was detected in either alloy insert. The molybdenum–titanium insert was partially recrystallized, but the TZM was unchanged.

In similar tests with tantalum capsules containing tantalum inserts, the effect of a small

piece (0.36 g) of metallic thorium in the lithium was studied. After 210 hr at 1200°C, it was shown that the thorium greatly accelerated the attack of the tantalum by the lithium. The gross attack was both intergranular and transgranular, and the thorium was partially disintegrated.

CORROSION IN POTASSIUM–STAINLESS-STEEL–REFRACTORY-METAL SYSTEMS

Two type 321 and two type 316 stainless-steel capsules, each containing two niobium–1 wt.% zirconium alloy test coupons, were exposed by General Electric[38] to 1400°F potassium for 1000 hr. Posttest studies of the inserts showed that the 321 stainless steel has a significant advantage over type 316 stainless steel in refractory-metal–stainless-steel–potassium systems in inhibiting the transfer of carbon and nitrogen to the refractory metal.

The results of thermal-convection potassium-loop studies by United Nuclear Corp. along the same lines[39] suggest that transfer of carbon and nitrogen from the stainless-steel loop walls to niobium–1 wt.% zirconium inserts may not cause serious embrittlement of the refractory alloy. Even after 5000 hr (longest test, with $T_{max.}$ = 1600°F and ΔT = 400°F), the niobium–1 wt.% zirconium inserts were saturated at low carbon and nitrogen levels and remained ductile. Apparently a thin (< 1 mil) carbonitride surface layer inhibits inward diffusion of carbon and nitrogen and slows the formation of embrittling carbides and nitrides. Carbon and nitrogen tend to migrate from hot regions of type 316 stainless steel (but not from type 321 stainless steel) to lower temperature regions, but this transfer produces no serious degradation of the strength of the stainless steel.

CORROSION BY SODIUM AND NaK

As pointed out in the last review, workers at Argonne National Laboratory, in evaluating vanadium alloys as cladding materials for sodium-cooled fast reactor fuels, found that their corrosion behavior is extremely sensitive to oxygen level in the sodium. They have continued their testing of vanadium-base alloys to see how various alloying additions and heat-treatments affect corrosion by sodium containing the degree of oxygen contamination (30 to 45 ppm) expected in a practical reactor system. Binary additions of 10 to 20 wt.% of aluminum, chromium, or titanium to vanadium were found to be beneficial.[40] Alloys in the annealed conditions are slightly superior corrosionwise to the same alloys cold worked. Also, alloys[41] with chromium as the major constituent show up to an order-of-magnitude improvement over vanadium–20 wt.% titanium. These effects[41] are illustrated in Table IV-1.

Table IV-1 CORROSION OF VANADIUM ALLOYS AFTER ONE WEEK IN 650°C SODIUM CONTAINING UP TO 30 PPM OXYGEN[41]

Alloy, wt.%	Heat-treatment*	Weight loss, mg/cm²	Surface loss, μ
V–20 Ti (control)	A	20.9	23
V–15 Ti–7.5 Mo	A	21.5	24
V–15 Ti–7.5 Mo	B	25.6	37
V–40 Ti–10 Mo	A	8.9	10
V–40 Ti–10 Mo	B	9.0	14
V–20 Cr–5 Al	A	20.7	8
V–25 Cr–5 Al	A	15.8	3
V–30 Cr–5 Al	A	6.0	–2
V–20 Cr–10 Al	A	1.8	3

*A = annealed at 900°C; B = 50% cold worked.

Workers at Atomics International[42] measured the diametral growth of 10-mil-wall, internally pressurized welded and drawn, type 304 stainless-steel tubing containing 950 to 1300°F sodium and a carbon source in the form of hyperstoichiometric UC slugs. The following observations were made:

1. Strain proceeded exponentially with time when the tubes were pressurized from 0 to 500 psi in 90 days and linearly with time when the same pressure increase was extended over two years. The diametral increase at failure was relatively constant, regardless of the temperature or mode of stressing.

2. Massive carburization of the tubing walls took place, particularly near the ends of the UC slugs. The areas of highest carbon content exhibited the greatest strain.

3. At these testing temperatures, sensitization of the steel took place, allowing the sodium to leach away the complex chromium carbides formed at every grain boundary; this action thus effectively reduced the cross-sectional area, increased the stress, and accelerated creep.

In connection with a program to predict the release and transport of matter and energy from primary-coolant-sodium fires, a study was made of the relative corrosion rates of type 304 stainless steel and 1020 carbon steel in environments that could be found in sodium fires.[42] It was found that 1600°F Na_2O–sodium

is much less corrosive than 1000 F Na_2O_2 and that the mild steel is significantly more resistant to attack by Na_2O_2 than stainless. The aggressiveness of Na_2O_2 (0.016 in. of stainless steel dissolved in 24 hr at 1000°F) may explain the eroded conditions sometimes found on the outside of sodium containers with small leaks.

CORROSION BY LEAD AND BY MOLTEN FLUORIDES

Type 304 stainless-steel corrosion tabs examined after 15,000 hr of exposure in a type 304 stainless-steel thermal-convection loop to the molten-salt fuel mixture $LiF-BeF_2-ZrF_4-UF_4$ (peak temperature, 1250°F; ΔT, 180°F) showed only about .2 mils of intergranular attack.[5,43] This material is being reconsidered for molten-salt reactor construction because of its cost advantage over Hastelloy N (INOR-8) and in view of the lower coolant temperatures of interest and improvements in salt processing that reduce corrosion.

Lead is being considered as a direct coolant for fused-salt systems. To test its compatibility, Oak Ridge ran a series of thermal-convection loops with the materials and conditions shown in Table IV-2. All the steel loops developed dense deposits of iron and chromium dendritic crystals in the cold regions. General surface roughening was noted, with a tendency toward intergranular attack. No effect was seen in the niobium alloy.

URANIUM FUELS

In the search for materials for containing molten uranium, 1-in.-diameter slugs of various carbides and nitrides were partially submerged for 24 hr in a 1400°C uranium bath under argon.[44] Hafnium carbide, niobium nitride, and zirconium diboride are the most promising materials investigated. Niobium carbide was wetted and attacked. Tantalum carbide was wetted and suffered severe intergranular corrosion.

In a separate study the wetting characteristics of uranium ceramic fuels by liquid sodium were measured with the use of the sessile-drop technique. The results, shown in Table IV-3, indicate uniformly poor wetting of all fuels at the temperatures studied and are all within the limits observed by Bradhurst and Buchanan for UO_2 and sodium of varying oxygen content. (E. M. Simons)

Table IV-3 SESSILE-DROP CONTACT ANGLES FOR MOLTEN SODIUM AND URANIUM CERAMICS[44]

Ceramic	Temp., °C	Measured contact angle, deg
UO_2	210	130 ± 2
UP	260	130 ± 2
US	240	150 ± 4
UC	250	144 ± 1
UN	255	157 ± 8
UO_2 (O-saturated Na)*	250	130
UO_2 (low-O Na)*	250	160

*D. H. Bradhurst and A. S. Buchanan, *Australian J. Chem.*, 14: 397 (1961).

Metal-Water Reactions

Argonne[37] has reported additional studies of metal–water reactions performed in the Transient Reactor Test Facility (TREAT). The cur-

Table IV-2 THERMAL-CONVECTION LOOPS WITH LEAD[5,43]

Loop material	Max. temp., °F	Temp. drop, °F	Time run, hr	Depth of attack, mils		Remarks
				Max.	Av.	
Croloy 2¼*	1022	221	27,765	None	None	25 ppm Mg, Zr inhibitor added
Croloy 2¼	1210	300	266	0.001		Graphite, salt, Nb–1 Zr placed in surge tank to test compatibility
Type 304 stainless steel	1215	300	1,346	0.002		Graphite, salt, Nb–1 Zr placed in surge tank to test compatibility
Croloy 2¼	1100	200	5,156	0.008	0.0055	
Carbon steel	1100	200	5,064	0.010	0.007	
Nb–1 wt.% Zr	1400	400	5,280	0.00	0.00	
Croloy 2¼	1200	230	1,848	0.0045	0.003	Zr specimen in hot leg

*Loop run at Brookhaven National Laboratory; included for comparison.

rent tests have utilized nine-pin clusters of UO_2-core fuel, clad with either Zircaloy-2 or type 304 stainless steel. The pins were 0.42 in. in diameter by $5\frac{5}{8}$ in. long. The total weight of UO_2 core material in each of the experiments was about 750 g. In an experiment the fuel-pin cluster, submerged in water and contained in an autoclave, was subjected to a transient burst of neutrons in TREAT. The fission heat generated in the enriched core of the fuel caused meltdown of the test pins. After the transient, the hydrogen evolved was measured by means of a mass spectrometer, and from this result the extent of reaction of cladding metal with water was computed. Sieve-screen analyses were also made on the residues from the fragmented fuels, and the mean particle size was calculated from the particle-size distribution.

In these studies two of the experiments utilized Zircaloy-clad specimens; the other two utilized stainless-steel-clad specimens. No explosive pressure rises were observed for either type of cladding material.

These scaled-up experiments utilized approximately 150 times as much core fuel material as did previous single-pin experiments. In Figs. IV-3 and IV-4, the extent of metal–water reaction in the present experiments is compared with the results of earlier experiments with single small pins. The extent of reaction with stainless steel is slightly higher for the fuel-pin clusters than for single pins, whereas the extent of reaction with Zircaloy is slightly lower. However, these differences are within the probability limits of reproducibility of the in-pile transient tests. The comparison indicates that there is no marked change in the extent of metal–water reaction on fuel meltdown when a nine-pin cluster is used instead of a single pin, lending additional confidence in the application of these results to the behavior of actual reactor cores. (A. W. Lemmon, Jr.)

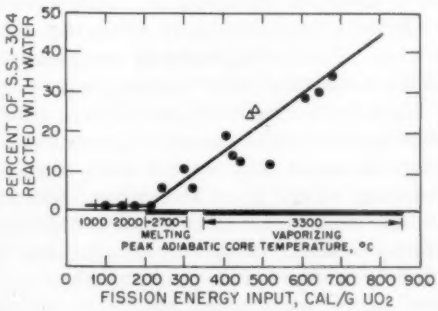

Fig. IV-3 Results of meltdown experiments in TREAT with UO_2-core, type 304 stainless-steel-clad fuel pins submerged in water.[37] Δ, nine-pin cluster; •, single pin.

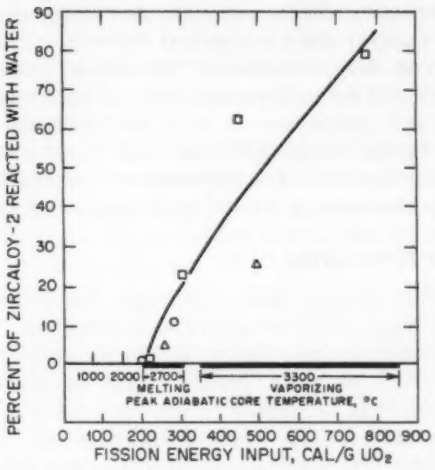

Fig. IV-4 Results of meltdown experiments in TREAT with UO_2-core, Zircaloy-2-clad fuel pins submerged in water.[37] Δ, nine-pin cluster; □, single pin (30°C H_2O, 20 psia); ○, single pin (285°C H_2O, 1000 psia).

Radiation Effects in Nonfuel Materials

Mild and Alloy Steels

Three different types of mild steels (En-2, aluminum grain-size controlled, and silicon killed) were irradiated at 100 to 350°C with different relative fast-neutron dose rates (1:4:100) to look for differences in radiation hardening.[45] As expected, the yield and ultimate strengths were increased and ductility was decreased by the exposures. These changes were found to be independent of neutron flux. The property changes were found to be less at higher irradiation temperatures, but the differences in behavior of the different steels were more pronounced at the elevated temperatures. The aluminum grain-size-controlled mild steel was the most resistant to radiation-induced property changes, whereas the En-2 steel was the least resistant. It is suggested that the variations in the hardening of the

respective steels are due primarily to differences in their interstitial contents.

The brittle-to-ductile transition temperature of a maraging steel (iron–12 wt.% nickel–5 wt.% chromium–3 wt.% molybdenum) was increased from −160°C to −112°C as a result of irradiation.[46] The specimens received a fast-flux exposure of 3×10^{19} neutrons/cm^2 at 60°C.

Stainless Steel

The British have repeatedly demonstrated the importance of boron content with regard to high-temperature (650 to 800°C) ductility of irradiated stainless steel.[47–51] The decrease in ductility is attributed to the $^{10}B(n,\alpha)^7Li$ reaction that occurs with thermal neutrons. It is thought that the transmuted helium and lithium atoms migrate to grain boundaries at high temperatures, where they form bubbles and cause intergranular fracture.

Pfeil and Barton established that the decrease in ductility at 750°C in irradiated stainless steel was proportional to the concentration of transmuted lithium and helium atoms in the sample.[47] To do this they irradiated samples of titanium-stabilized iron–20 wt.% chromium–20 wt.% nickel at 40°C. These samples contained varying amounts of ^{10}B and ^{11}B and were irradiated to varying thermal-neutron dosages. The results showed that the ductility decrease was dependent on the concentrations of transmuted helium and lithium.

Further tests were performed on irradiated niobium-stabilized iron–20 wt.% chromium–25 wt.% nickel and type 316 stainless steel.[48] The strength of the austenitic stainless steel was increased and elongation was decreased at test temperatures below 500°C. The magnitudes of the effects increased with increasing fast-neutron dose. At about 650 to 700°C, the ductility loss was due to thermal neutrons rather than fast neutrons. Annealing at 1170°C failed to restore the ductility.

In another test, thermal-neutron doses as low as 8×10^{18} neutrons/cm^2 were sufficient to cause a ductility decrease in specimens irradiated at 40°C and tested at 750°C.[49] Annealing at 500°C resulted in complete recovery of the low-temperature-radiation-induced property changes. This recovery phenomenon is believed to occur when point-defect clusters are annihilated by annealing. In specimens irradiated at 500°C, the ductility decrease at 750°C was similar to that experienced by specimens irradiated at 40°C. However, when tested below the irradiation temperature, these specimens showed no ductility decrease when compared with unirradiated specimens. It was concluded that helium or lithium was the cause of the ductility decrease at high temperature because helium diffusion would cause bubble formation at grain boundaries.

Higgins and Roberts[50] bombarded samples of niobium-stabilized 20 wt.% chromium–25 wt.% nickel austenitic stainless steel with alpha particles and lithium ions. Specimens that were tested at 750°C showed a slight increase in yield strength, no change in ultimate strength, and a significant decrease in ductility. About 100 times more lithium than helium is required to produce an equivalent ductility decrease.

Electron-microscopic examination was performed[51] on unstrained regions of niobium-stabilized 20 wt.% chromium–25 wt.% nickel austenitic stainless steel that had been irradiated to a thermal-neutron dose of 3.5×10^{20} neutrons/cm^2 at 750°C. These specimens had shown substantial ductility decreases when tested at 750 and 850°C, but no ductility decreases had been observed at 575°C. Electron microscopy of the specimens revealed 50- to 150-A-diameter gas bubbles that were unevenly dispersed at grain boundaries. The amount of gas observed in the bubbles would account for about 1% of the calculated helium production. More fine, intergranular precipitates were also found in the irradiated specimen, and these might be attributed to radiation-induced precipitation. Annealing of the irradiated material at 1200°C resulted in some of the gas bubbles growing to 2000 A in diameter.

Workers at Oak Ridge have found that additions of titanium, up to 0.2 wt.%, improve the high-temperature ductility of irradiated stainless steel.[5] This is explained by the theory that titanium is a strong boride former, and thereby fine titanium boride precipitates are formed throughout the matrix. These precipitates anchor the helium atoms and prevent them from agglomerating at the grain boundaries. Additions above 0.2 wt.% result in decreased high-temperature ductility, which may be caused by the excessive titanium boride precipitates.

Specimens[52] from types 406, 316, and 347 stainless steels were irradiated to an accumulated fast flux of 2.5×10^{19} neutrons/cm^2 at 700°C. These specimens underwent slight increases in yield and ultimate strengths when

tested at room temperature and 700°C. The ductility of types 406 and 347 stainless steel was somewhat reduced, whereas type 316 specimens did not undergo ductility decreases at either room temperature or 700°C.

The in-pile creep rate[53] of type 304 stainless steel at 550°C and 30,000 psi was 3.3×10^{-6}/hr, whereas the out-of-pile creep rate at comparable conditions was 2.5×10^{-6}/hr.

The change in mechanical and structural properties of 13 kinds of stainless steels of the chromium–nickel type, exposed to an integrated fast flux of 1.6×10^{19} neutrons/cm^2, was investigated.[54] The dose was held at a constant value, and the chemical composition varied in the chromium and nickel contents. The usual strengthening effect was observed, i.e., yield point, strength, and hardness increased, and plasticity decreased. The rate of strengthening was found to be independent of the chromium and nickel contents; however, it depended on the physical condition (amount of working and type of heat-treatment) of the steel before the irradiation. Ferromagnetic induction measurements indicated that irradiation did not decrease the corrosion resistance of austenitic steels.

Nickel-Base Alloys

Hastelloy X-280, Hastelloy R-235, Inconel 600, and Inconel 702 were irradiated[52] at 650°C to integrated fast-flux exposures of 2.5×10^{19} and 1.2×10^{20} neutrons/cm^2. These materials were tested at room temperature and at 700°C.

The solution-hardenable alloys, Hastelloy X-280 and Inconel 600, underwent only minor changes in mechanical properties as a result of irradiation, when tested at room temperature. However, both alloys, especially Hastelloy X-280, underwent considerable ductility decreases when tested at 700°C.

The room-temperature strength properties of the age-hardenable alloy, Hastelloy R-235, did not change significantly with irradiation, although considerable reduction in elongation was noted at 700°C.

Inconel 702, which is an age-hardenable alloy, did not undergo irradiation-induced changes when tested at room temperature. Out-of-pile heating of control specimens at 650°C resulted in considerable decrease in ductility and strength at 700°C. Irradiation by fast neutrons caused further substantial decreases in strength and elongation, as measured in 700°C tensile tests.

Inconel 625 tensile specimens[55] that had been irradiated at 50 to 740°C to fast-neutron exposures of 5.3×10^{19} to 8.3×10^{20} neutrons/cm^2 were tested at room temperature, at 300°C, and at 650°C.

Specimens that were irradiated at 50 and 280°C and tested at room temperature underwent some increases in yield strength, but their elongations did not change. Specimens that were irradiated at 580 and 740°C and tested at room temperature increased in yield and ultimate strengths and decreased in elongation. Heating control specimens at 580 and 740°C for equivalent lengths of time without irradiation resulted in ductility decreases equivalent to those undergone by the specimens irradiated at 740°C.

Specimens irradiated at 280°C and tested at 650°C did not show any changes in mechanical properties, except for a decrease in ultimate strength which is attributed to aging. Specimens that were irradiated at 740°C and tested at 300 and 650°C showed decreases in ultimate and yield strengths, accompanied by a decrease in elongation.

Postirradiation stress-rupture tests were performed on two heats of INOR-8, with one of the heats being especially low in boron.[43] For both heats the time to rupture for a given stress level decreased with increasing thermal-neutron dose (Table IV-4). The low-boron heat underwent more elongation before rupture than did the heat higher in boron content.

In-pile creep-rupture studies have been performed on INOR-8 at 650°C and a thermal flux of 6×10^{13} neutrons/(cm^2)(sec). The exposures appear to reduce the time to rupture as can be seen in Fig. IV-5. However, at lower stresses the creep resistance of the irradiated specimens approached that of unirradiated material.[43]

At 550°C the ultimate tensile strength of irradiated low-boron (3 ppm) Nimonic PE16 alloy was reduced with decreasing strain rate, whereas the yield strength was not affected by strain rate.[56] The elongation was reduced by irradiation (1.5×10^{20} thermal neutrons/cm^2 and 5×10^{19} fast neutrons/cm^2 at 45°C), with the magnitude of the decrease increasing with decreasing strain rate. At 650°C the ultimate tensile strength, yield strength, and elongation were all decreased with decreasing strain rate. The magnitude of the elongation decrease was considerably more than in the specimens tested at 550°C. As evident in Fig. IV-6, the elongation at 650 and 700°C was found to decrease propor-

Table IV-4 STRESS-RUPTURE TIMES AND DUCTILITIES* OF IRRADIATED INOR-8 TESTED[43] AT 650°C

Stress, 1000 psi	Times, hr, and ductilities, %, for specified thermal-neutron dose, neutrons/cm²					
	0	5×10^{16}	1.3×10^{18}	9×10^{18}	5×10^{19}	5×10^{20}
			Low-Boron Alloy			
52.6		70.6 (2.8)	57.4 (3.0)	30.4 (4.6)	21.1 (4.3)	19.9 (4.7)
32.4		1070 (37)	1525.7 (6.3)	1425 (5.6)	849.6 (5.1)	515 (3.4)
			Normal-Boron Alloy			
52.57	52 (10)	21.2 (2.6)	11.9 (2.0)	5.1 (3.4)	0.43 (0.85)	0.9 (0.64)
39.80	~270	424.7 (9.2)	147.0 (2.8)	80.2 (2.4)	23.5 (0.2)	5.3 (0.3)
32.35	~800	686.7 (6.7)	647.0 (6.3)	232 (2.5)	5.2 (1.8)	8.0 (0.42)
21.54	~2500			1603 (2.7)	521.8 (1.5)	312 (0.79)

*Elongations at fracture are in parentheses.

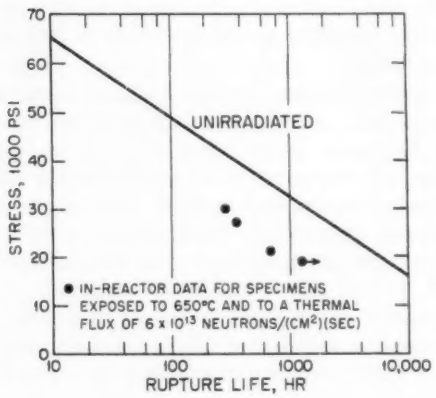
STRESS, 1000 PSI
RUPTURE LIFE, HR
UNIRRADIATED
● IN-REACTOR DATA FOR SPECIMENS EXPOSED TO 650°C AND TO A THERMAL FLUX OF 6 x 10¹³ NEUTRONS/(CM²)(SEC)

Fig. IV-5 Influence of irradiation[43] on creep-rupture properties of INOR-8.

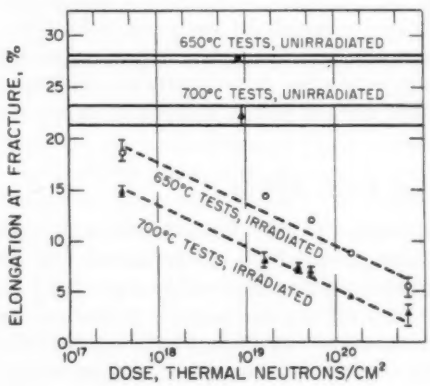

Fig. IV-6 The effect[56] of thermal-neutron dose on the total elongation to fracture of Nimonic PE16 in tests at a strain rate of 2×10^{-4}/sec.

tionally with log of thermal flux. Specimens that had been irradiated to 6×10^{20} thermal neutrons/cm² and 2×10^{20} fast neutrons/cm² at 650°C underwent larger elongation decreases when tested at 650 to 760°C than did specimens irradiated to the same dose at 45°C.

Zirconium Alloys

Westinghouse workers[57] have prepared a thorough summary of the mechanical properties of irradiated Zircaloy-2 and -4. Tensile properties of irradiated Zircaloy-4 are shown in Table IV-5.

In-pile creep tests[47] of 20% cold-worked zirconium–2.5 wt.% niobium at 300°C were stopped after about 3000 hr. The in-pile creep rate was comparable to the out-of-pile creep rate under the same conditions. This performance is superior to that of Zircaloy-2 (which shows a 10-fold higher creep rate in-pile than out-of-pile) and of annealed zirconium–2.5 wt.% niobium. The improvement might be attributed to the differences in radiation-damage mobility. Previous research has shown that the annealing temperature required to remove radiation damage is lower for Zircaloy-2 than for zirconium–2.5 wt.% niobium.

Table IV-5 EFFECT OF IRRADIATION ON TENSILE PROPERTIES[57] OF ZIRCALOY-4

Condition	Irradiation temp., °F	Test temp., °F	Exposure, 10^{21} fast neutrons/cm^2	Yield strength (0.2% offset), 1000 psi	Ultimate tensile strength, 1000 psi	Elongation		Reduction in area, %
						Uniform, %	Total, %	
		RT	0	48.9	70.2	11.2	17.9	
	545	RT	0.56	76.4	93	0.88	4.3	
	545	RT	0.56	80.9	96.3	0.75	2.5	
	545	RT	0.82		94			
	545	RT	0.82	78.6	90.1	0.55	1.1	
	545	RT	0.85		99.3			
	545	RT	0.85	85.7	97.2	1.63	2.4	
		650	0	26.1	35.6	2.1	7.9	
	545	650	0.21	36.6	46.1	1.0	3.8	
	545	650	0.44	57.1	57.1	0.19	1.9	
	545	650	0.44	52	52	0.18	1.8	
	545	650	0.72	53	53	0.14	1.8	
	545	650	0.90	52.4	53	0.38	1.0	
	545	650	0.90	56.3	58.5	0.44	2.3	
	545	650	0.72	55.4	55.4	0.15	1.8	
Annealed		RT	0	48.1	73.3	15.0	22.9	41.5
Annealed	200	RT	1.0	79.6	90	3.7	11.4	36.6
Annealed	200	RT	1.4	80.6	90	3.6	11.4	32.3
Annealed		300	0	35.1	56.5	13.0	23.9	42.1
Annealed	200	300	1.0	67.1	70.8	2.6	12.0	39.1
Annealed	200	300	1.4	69	72.2	2.2	11.6	39.9
Annealed	200	300	2.5	74.6	76	1.1	9.3	37.2
Annealed		550	0	21.2	40.6	15.7	27.0	48.0
Annealed	200	550	1.0	49.2	49.2	0.6	13.7	50.9
Annealed	200	550	1.4	48.8	49.1	0.6	12.9	45.1
Annealed	200	550	2.5	59	59	0.2	10.0	42.4
As extruded		300	0	53.8	73.7	9.3	21.4	50.5
As extruded	200	300	1.0	82.1	87.4	1.5	11.2	49.2
As extruded	200	300	1.4	85.8	88	0.6	9.4	49.7
As extruded	200	300	5.0	93.8	95	0.7	8.8	46.3

Miscellaneous Materials

Annealed and age-hardened aluminum alloy 6061 did not undergo significant changes in mechanical properties when irradiated to an integrated dose of 10^{20} thermal neutrons/cm^2 and 10^{19} fast (>2.9 Mev) neutrons/cm^2. The irradiation temperature ranged from 110 to 490°C. However, when 20% cold-worked material was irradiated at 43°C to integrated doses of 7.4×10^{19} thermal neutrons/cm^2 and 2.9×10^{18} fast (>2.9 Mev) neutrons/cm^2, considerable changes in mechanical properties took place. The yield strength was increased 10%, ultimate strength was increased 4.5%, and total elongation was reduced 20%. Annealing 30 min at 200°C resulted in complete recovery of those properties.

Irradiation to a dose of 9.25×10^{20} neutrons/cm^2 increased the ductile-to-brittle transition temperature of iron–chromium–aluminum–yttrium specimens containing more than 10 wt.% chromium.[17] No increase was noted for specimens containing less than 10 wt.% chromium. Radiation-induced hardness was reduced to almost preirradiation levels after ½-hr anneals at 250 and 300°C.

Irradiation of uncoated silica fibers at 200°C to an accumulated fast exposure of 10^{20} neutrons/cm^2 resulted in complete disintegration of 10- and 40-μ-diameter fibers.[46] Aluminum-coated 56-μ-diameter fibers suffered a 40% reduction of strength.

Bush discussed the general picture of radiation damage to reactor materials used as fuel cladding or as structural components. His report[58] includes information on: mechanisms of radiation damage; description of radiation effects in stainless steels, aluminum and magnesium alloys, beryllium, zirconium alloys, nickel-base alloys, refractory metals and alloys, and other metals; and problems, programs, and future trends.

Basic Studies of Irradiation Effects

The effects of fast-neutron irradiation on copper–0.9 wt.% cobalt alloys at 42 to 210°C were measured by magnetic techniques.[59] The radioinduced precipitation was much greater,

even though the particle size was smaller, than precipitation induced by annealing at the same temperatures.

Equations have been developed which describe the production and annealing of interstitial atoms and vacant lattice sites in niobium metal which is in the presence of a steady-state energy-dependent neutron flux.[60] The rate of accumulation of neutron-induced interstitial atoms and vacant lattice sites in niobium metal is equal to the rate of production minus the rate of recovery. The recovery rate is composed of two factors — temperature annealing and radioinduced annealing. The production rate and radioinduced annealing rate are dependent on the energy-dependent neutron flux, the defect concentration, neutron parameters, and metal parameters. The temperature annealing rate is dependent on the temperature, type of defect, defect concentration, and metal parameters.

A simple analytical possibility for the determination of the saturation concentration and the entry volume for the spontaneous recombination was given on the basis of the work of Lueck and Sizmann on the saturation type growth of the defect concentration in the irradiation of solids.[61] It was considered that, according to the defect structure, two cases can occur: in the case of the statistical production of isolated point defects, the entry volume is dependent on the defect concentration produced; in the case of defect cascades, a constant effective value for the entry volume is obtained.

The temperature and strain-rate dependence of the flow stress were measured from 4.2 to 373 °K in neutron-irradiated copper single crystals as a function of neutron dose and solute additions.[62] Between 77 and 373 °K, solutes have very little effect on the flow stress and its temperature dependence. At 4.2 °K, a large amount of solute, 7 to 14 at.%, lowers the flow stress of pure copper crystals. From these measurements an activation energy and activation volume were calculated. Both the activation energy and activation volume are independent of solute and are analyzed on the basis of a stress dependence rather than a temperature dependence.

Polycrystalline copper[63] was irradiated above room temperature with neutron doses up to 6.3×10^{20} neutrons/cm^2 (>0.1 Mev), then cold rolled to cross-section reductions up to 97%, and subsequently annealed at 200 °C. Recrystallization occurred much sooner in the irradiated material than in unirradiated material, with the same amount of cross-section reduction. The acceleration of recrystallization can be explained by an increase in the mean mobility of the atoms in the irradiated material, due to the destruction of large and relatively stable dilute zones.

The recovery of the coercive field strength and initial susceptibility of nickel single crystals above room temperature occurs in three stages.[64] These can be interpreted as being due to the migration of interstitial atoms, of vacancies, and to self-diffusion. After neutron irradiation at 80 °C, a recovery stage is found in the temperature range 100 to 300 °C. The activation energy of 0.5 ± 0.06 ev in the first part of this stage is interpreted as the difference between the migration and binding energy of divacancies. Comparison with a direct measurement of the migration energy of divacancies yields a divacancy binding energy of 0.3 ev. The last part of the recovery stage is attributed to the migration of single vacancies (migration energy 1.46 ± 0.09 ev). The migration energy of interstitial atoms is determined from measurements of the recovery of the electrical resistivity after electron irradiation, giving 1.03 ± 0.04 ev, in agreement with previous measurements.

The effects of neutron irradiation, at both ambient and elevated temperatures, on the structure of molybdenum were studied and compared and contrasted with previous observations on copper and nickel.[65] The defect structures produced by neutron irradiation at doses up to 10^{20} neutrons/cm^2, at temperatures from ambient to 600 °C, are being studied using transmission electron microscopy. For low doses, 10^{18} neutrons/cm^2 at 600 °C, large prismatic dislocation loops (average diameter 1100 A) were observed on planes approximately parallel to $\{1\,1\,1\}$ and having the normal slip vector $\frac{1}{2}\langle 1\,1\,1\rangle$. Diffraction contrast experiments carried out on these loops proved conclusively that these were formed by the collapse of interstitial aggregates. By comparison, ambient-temperature irradiation to this dose level produced a structure with a high density of spots, which were not readily resolvable as loops. Specimens were also irradiated to 10^{20} neutrons/cm^2 at ambient temperature and were found to contain a higher density of the unresolved damage. The mechanisms of the formation of the loops and their interaction with glide dis-

locations are discussed. Dislocation loops[66] were formed in molybdenum, containing 450 ppm carbon, by irradiation at 40 °C to an integrated exposure of 10^{20} neutrons/cm^2. The dislocation loops that were formed were studied by transmission electron microscopy before and after annealing 2 hr at 750 °C. It was concluded that dislocation loops in irradiated molybdenum can have different burgess vectors and that these loops can interact with each other to form nodes during annealing.

Dislocation loops were observed[46] by transmission electron microscopy in Zircaloy-2 in-pile creep specimens that had been irradiated to 300 °C to a fast-neutron dose of 10^{20} neutrons/cm^2. These dislocation loops had diameters of 150 to 180 A and had a distribution of 10^{15} loops/cm^3.

A U. S. patent[67] was issued which describes property improvements induced in an alloy by gamma rays having an energy greater than 0.1 Mev. The suitable alloy is one for which there is a theoretically producible equilibrium degree of order for any particular temperature, for which there is an atomic freeze-in temperature below which heat alone imparted to the alloy will not produce the equilibrium degree of order, and for which there is a vacancy freezing-in temperature below which no treatment will produce the equilibrium degree of order. (F. R. Shober)

Selected Mechanical Properties of Cladding and Structural Materials

Iron- and Nickel-Base Alloys

A Defense Metals Information Center report, discussing the use of fracture toughness as a basis for selection of materials, has been issued.[68] The report includes estimates of limiting design stresses, as well as failure analyses, assuming the presence of small flaws. Current methods of measuring plane-stress and plane-strain fracture-toughness parameters are presented. The specimens include center-cracked, edge-cracked, single-edge-cracked, surface-cracked, and notched round bars, which are subjected to tensile loading, and notched round bars for bend tests. These different types of specimens permit evaluating sheet, plate, bar stock, and forgings, as well as materials from failed structures. Application of fracture-toughness parameters to the design of high-strength structures is reviewed for both static and fatigue loadings.

The creep-rupture properties of Hastelloy X in vacuum at elevated temperatures are reported by Battelle–Northwest.[69] Stress-rupture data are presented in Fig. IV-7 for 1950 and 2100 °F and compared with literature values at lower temperatures. Figure IV-8 is a plot of stress vs. minimum creep rate. Grain growth occurred at 2100 °F for times greater than 20 hr, which caused a marked reduction from expected values of both ductility and time to rupture.

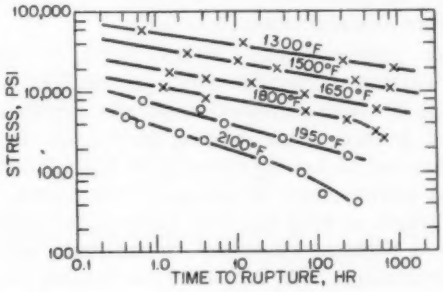

Fig. IV-7 Stress–rupture data[69] for Hastelloy X. ×, Donachie and Shepheard; ○, Battelle–Northwest data.

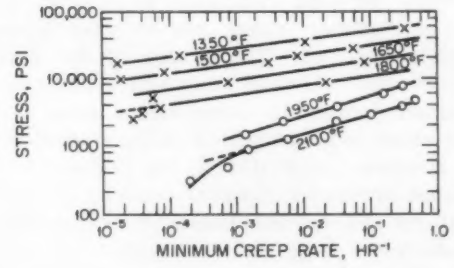

Fig. IV-8 Stress vs. minimum creep rate[69] for Hastelloy X. ×, Donachie and Shepheard; ○, Battelle–Northwest data.

According to tube-burst test results by Battelle–Northwest,[52] type 406 stainless-steel weld-drawn tubes have a higher average strength than either austenitic stainless tubes or Incoloy 800 and Zircaloy-2 tubes of comparable dimensions. The Zircaloy-2 tubes suffered a rapid

drop-off in strength between room temperature and 220°C, with a less rapid loss between 220 and 400°C.

Norwegian investigators report on a study[70] to correlate the calculated and measured mechanical properties of thin-walled stainless-steel tubing. The classical formulas for inner yield or burst pressure gave results that are in good agreement with experimental values. The collapse pressure or the minimum tube dimensions could be predicted by the use of the formula based on elastic-collapse theory when the wall thickness was below 7% of the inner radius of the tube ($t/R_0 < 0.07$). When t/R_0 was greater than 0.11, the formula based on inelastic-collapse theory was appropriate. In the region between 0.07 and 0.11, the collapse pressure could be predicted by a modified formula (tangent modulus criterion).

The instantaneous collapse (<0.2 hr) and creep-buckling characteristics (up to 5000 hr) of type 304 stainless-steel tubes, under external radial pressure and varying axial load, were determined at temperatures up to 1200°F in an argon environment at Atomics International.[71] The length of each tube was essentially infinite from a buckling standpoint. In addition, tubes in combination with fuel-element bundles corresponding to those proposed for a large sodium-graphite reactor were investigated to determine the extent to which the fuel-element bundle increased the resistance to collapse of the process tube. Also examined were ways to increase the tube resistance to collapse, the use of stiffener rings, and existing creep-buckling theories. The results of the study indicated that: (1) axial loads over a wide range in either tension or compression have very little effect on instantaneous collapse pressure; (2) accurate prediction of the instantaneous collapse pressures should be possible for temperatures and wall thicknesses other than those at which the tests were conducted; (3) considerable scatter in test results might occur in the determination of the time to collapse, during creep-buckling tests, because of variations in the magnitude and distribution of the out-of-roundness and thickness parameters along the length of the tube; (4) resistance to collapse of a tube may be enhanced by a factor of 2½ by installing compact "slip-on" stiffener rings; and (5) analytical predictions for time to collapse are not reliable and may be inaccurate by one or more orders of magnitude.

Refractory Metals

Lawrence Radiation Laboratory[72] reports the results of creep-rupture tests[6] on TZC (molybdenum–1.39 wt.% titanium–0.34 wt.% zirconium–0.30 wt.% carbon) at 2400 and 2600°F. The data are summarized in Table IV-6.

The tensile properties of molybdenum–0.5 wt.% titanium–0.08 wt.% zirconium (TZM), vanadium–10 wt.% titanium, and vanadium–20 wt.% titanium alloys are compared with those of niobium–1 wt.% zirconium alloy over the temperature range from room temperature[73] to 800°C. Above 650°C the molybdenum alloys exhibit higher strength than the other alloys tested. As might be expected, they exhibited the lowest elongation. These results are shown in Fig. IV-9.

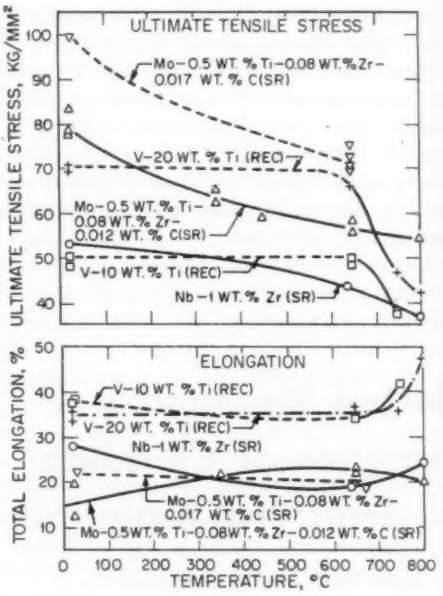
ULTIMATE TENSILE STRESS
ULTIMATE TENSILE STRESS, KG/MM²
Mo–0.5 WT. % Ti–0.08 WT.% Zr–0.017 WT. % C(SR)
V–20 WT. % Ti (REC)
Mo–0.5 WT. % Ti–0.08 WT. % Zr–0.012 WT. % C(SR)
V–10 WT. % Ti (REC)
Nb–1 WT. % Zr (SR)
ELONGATION
TOTAL ELONGATION, %
V–10 WT. % Ti (REC)
V–20 WT. % Ti (REC)
Nb–1 WT. % Zr (SR)
Mo–0.5 WT. % Ti–0.08 WT. % Zr–0.017 WT. % C (SR)
Mo–0.5 WT. % Ti–0.08 WT. % Zr–0.012 WT. % C (SR)
TEMPERATURE, °C

Fig. IV-9 Ultimate tensile stress and total elongation vs. temperature.[73]

The static Young's moduli of vacuum-arc-cast tungsten rod, powder-metallurgy-consolidated tungsten sheet, and powder-metallurgy-consolidated tungsten–25 wt.% rhenium sheet were measured[73] in vacuum over the temperature range 800 to 2000°C at a strain rate of 2.2×10^{-4}/sec. All these were wrought materials in the stress-relieved condition. The results are given in Tables IV-7 and IV-8.

Table IV-6 TZC (0.3 WT.% CARBON) MOLYBDENUM ALLOY CREEP-RUPTURE-TEST DATA[72]

At 2400°F				
Stress, psi	30,000	20,000	12,500	5,000
Rupture time, hr	11.75	125	744	282+
Rupture strain, %	20.7	35.9	38.9	1.14+
Reduction of area, %	76.9	90.4	93.9	
Minimum creep rate, %/hr	0.75	0.070	0.013	0.0015
Time to 1% strain, hr	0.8	1.5	12	228
Time to 3% strain, hr	3.4	27	155	
Time to 5% strain, hr	5.8	49.5	281	
Transition time, hr	5.5	45	245	
Transition strain, %	4.8	4.6	4.3	
Diameter, in.	0.1125	0.1781	0.1782	0.1125
Gauge length, in.	1.00	1.75	1.75	1.70
Original hardness, VHN (30-kg load)		305	295	
Final hardness, VHN (30-kg load)		280	265	
At 2600°F				
Stress, psi	15,000	10,000	8,000	5,000
Rupture time, hr	15.5	178.0	227	908.0
Rupture strain, %	26.1	21.2	29.6	36.4
Reduction of area, %	83.2	44.1	97.4	77.3
Minimum creep rate, %/hr	0.66	0.053	0.038	0.0085
Time to 1.0% strain, hr	0.8	2.5	5.0	3.0*
Time to 3.0% strain, hr	3.4	42.0	57	165.0
Time to 5.0% strain, hr	6.0	77.5	98	380.0
Transition time, hr	8.0	79.0	100	430.0
Transition strain, %	5.8	5.1	5.1	5.2
Original diameter, in.	0.1780	0.1780	0.1785	0.1782
Original gauge length, in.	1.75	1.75	1.75	1.75
Original hardness, VHN (30-kg load)	301	298	308	307
Final hardness, VHN (30-kg load)	268	266	227	211

*The initial portion of the creep curve from which this value was taken appears to be in error.

Table IV-7 STATIC YOUNG'S MODULUS FOR UNALLOYED TUNGSTEN[73]

Temp., °C	Literature dynamic Young's modulus, 10^3 kg/mm²	Literature static Young's modulus, 10^3 kg/mm²	Static Young's modulus for V.A.C., wrought W rod*		Static Young's modulus for P.M., wrought W sheet†	
			E	σ	E	σ
			10^3 kg/mm²	10^3 kg/mm²	10^3 kg/mm²	10^3 kg/mm²
RT	39–42					
RT		33–36				
800	36–38		37‡	21.4		
800		24–34	32§	35.6	34 ± 2§	8.5
1000	36–37		35‡	21.4		
1000		24–26	27§	28.5	33 ± 3§	6.5
1200	35–36		34‡	11.4		
1200		22–25	24§	17.5	31 ± 1§	6.4
1400	34–35		35‡	11.4		
1400		18–23	19§	17.1	23 ± 1§	6.0
1600	33–34					
1600		14–21	13§	5.5	16 ± 2§	5.0
1800	32–33					
1800		8–18	12§	4.3	14 ± 2§	3.5
2000	30–31					
2000		3–17	10§	3.6	14 ± 1§	2.8
2200	26–30					
2200		13				

*A 0.635-cm-diameter reduced section; V.A.C. = vacuum arc cast.
†A 0.15-cm-thick sheet; 0.635-cm-wide reduced section; P.M. = powder-metallurgy consolidated.
‡Unrelaxed modulus.
§Relaxed modulus.

Table IV-8 STATIC YOUNG'S MODULUS FOR RHENIUM AND TUNGSTEN–25 WT.% RHENIUM SHEETS[73]

Temp., °C	Dynamic Young's modulus for unalloyed Re, 10^3 kg/mm²	Static Young's modulus for P.M., wrought W–25 Re sheet*	
		E,† 10^3 kg/mm²	E,‡ 10^3 kg/mm²
RT	47		
800	42	35 ± 2	
1000	40	33 ± 2	42 ± 4
1200	37	30 ± 1	37 ± 5
1400		22 ± 2	32 ± 3
1600		18 ± 2	25 ± 3
1800		13 ± 1	21 ± 2
2000		11 ± 1	17 ± 1
2200		10 ± 1	12 ± 1

*A 0.076-cm-thick sheet; 0.635-cm-wide reduced section.

†Measurements on heatup; specimen recrystallized during heatup.

‡Measurements on cooldown; specimen in recrystallized condition.

Below the recrystallization temperature range (approximately 1200 to 1600°C, depending upon prior material history and the applied stress), the measured static modulus is in close agreement with the literature values for dynamic modulus given in Table IV-7. However, above this temperature range, the measured static modulus is in closer agreement with the literature values for static modulus. This difference in the measured static modulus above and below the recrystallization-temperature range is attributed to a lowering of the yield point, through recrystallization, to a strain level below the resolution capability of the mechanical extensometer. Therefore the relaxed static modulus is observed above this temperature range, and the unrelaxed modulus is observed below this temperature range.

The slope of the stress–strain curve for vacuum-arc-cast (V. A. C.) tungsten rod appears to be stress dependent, so that both the unrelaxed and relaxed static moduli are observed below the recrystallization-temperature range. This is indicated in the modulus values for tungsten rod shown in Table IV-8. The powder-metallurgy-consolidated (P. M.) tungsten sheet did not exhibit a stress dependence.

The measured static modulus of the tungsten–25 wt.% rhenium alloy lies between that for unalloyed tungsten and that for unalloyed rhenium at all temperatures below the recrystallization-temperature range. However, the measured static modulus of this alloy sheet after recrystallization at 2360°C is observed to be higher when obtained by a regressing temperature technique than when the measured modulus is obtained on heatup. This behavior is consistent with observations reported for single crystals, which do not show the same degree of relaxation of Young's modulus, and therefore suggests a possible grain-size dependence. The larger-grained recrystallized material will have less grain-boundary area and might therefore be expected to exhibit less relaxation. Young's modulus data for unalloyed rhenium and tungsten–25 wt.% rhenium above the recrystallization-temperature range are not available in the literature for comparison.

The P. M. tungsten–25 wt.% rhenium sheet did not exhibit a stress dependence such as was observed for V. A. C. tungsten rod.

The General Electric creep-rupture characteristics[74] of arc-cast tungsten over the temperature range 1600 to 3000°F are summarized in Table IV-9. Similar data for molybdenum are summarized in Table IV-10, with data for tungsten–rhenium and tungsten–rhenium–molybdenum alloys given in Table IV-11.

The deformation behavior and fracture modes of tungsten single crystals were studied as a function of orientation by the British.[75] The orientation of the crystals was varied systematically around the edge of the unit stereographic triangle, and tensile tests were carried out at 77 and 295°K. The stress–strain curves showed considerable variation with orientation, and only crystals of orientation close to [1 1 0] showed discontinuous yield behavior. Deformation occurred purely by slip, but the proportional limit did not obey a critical-resolved-shear-stress criterion. The tensile behavior was rationalized in terms of the number of operative slip vectors. Specimens of orientation [1 0 0] were tested over a temperature range from 20 to 465°K. The proportional limit increased rapidly at temperatures below 250°K. The specimens always necked before fracture, even at 20°K, indicating that tungsten single crystals are not inherently brittle.

Miscellaneous Materials

A literature search was conducted by Westinghouse personnel[57] to find available properties of Zircaloy tubing of importance to the design of fuel elements. In addition, laboratory tests were conducted to obtain properties not available in the literature. The report is an excellent compilation of existing data on Zircaloy-2 and Zircaloy-4 tubing.

Table IV-9 CREEP-RUPTURE RESULTS FOR ARC-CAST TUNGSTEN, TESTED AT 1600 TO 3000°C IN HYDROGEN*[74]

Test conditions		Time to indicated elongation, hr								Rupture elongation, %	Linear creep rate, min^{-1}
Temp., °C	Stress, kg/mm^2	0.2%	0.5%	1%	2%	3%	5%	10%	Rupture		
1600	3.37	0.08	0.80	2.90	11.6	21.9	45.5	76.8	137†		1.4×10^{-6}
1600	3.37		0.35	2.10	8.90	18.2	40.2	64.0	160	89	1.5×10^{-6}
1600	4.22		0.08	0.15	1.40	3.35	9.70	16.0	30.9	76	5.1×10^{-6}
1600	4.92		0.01	0.13	0.70	1.67	4.20	7.85	14.7	65	1.3×10^{-4}
1600	5.62		0.01	0.07	0.32	0.71	1.83	3.75	6.45	73	2.9×10^{-4}
1800	2.11	0.05	0.75	3.10	11.5	21.7	46.0	92.2	150	62	1.4×10^{-6}
1800	2.81		0.03	0.37	2.10	4.45	9.90	14.7	28.4	73	6.1×10^{-6}
1800	3.37		0.03	0.13	0.58	1.25	2.85	4.85	7.60	60	1.9×10^{-4}
2000	1.05	0.12	1.70	6.30	16.5	25.2	45.3	101	256	65	1.5×10^{-6}
2000	1.41		0.80	2.50	6.10	8.25	11.0	16.2	63.1	94	4.6×10^{-6}
2000	1.41‡		0.17	0.65	2.80	6.10	14.4	35.1	100	92	3.9×10^{-6}
2000	1.76			0.25	1.40	2.93	4.95	6.35	17.8	60	9.8×10^{-6}
2000	2.11			0.08	0.50	1.15	2.63	3.85	6.70	70	2.3×10^{-4}
2000	2.11‡				0.01	0.06	0.28	1.73	6.50	60	5.4×10^{-4}
2200	0.70	0.12	1.33	5.00	14.5	25.0	46.5	95.0	237	125	1.5×10^{-6}
2200	0.70‡	0.01	0.29	1.73	6.33	12.2	25.0	57.5	182	91	2.6×10^{-6}
2200	0.84	0.01	0.41	1.90	6.45	11.8	22.3	48.0	119	86	3.1×10^{-6}
2200	1.05		0.05	0.35	1.58	3.30	6.60	14.8	40.7	106	9.6×10^{-6}
2200	1.26			0.10	0.52	1.18	2.60		3.35†		2.3×10^{-4}
2200	1.41			0.02	0.20	0.51	1.30	3.30	7.72	74	4.0×10^{-4}
2200	1.41‡				0.05	0.18	0.63	2.00	6.77	95	6.3×10^{-4}
2200	2.11‡					0.01	0.05	0.25	0.91	76	4.4×10^{-3}
2400	0.46	0.05	0.50	2.12	6.00	9.80	18.5	40.0	146	102	3.9×10^{-6}
2400	0.56		0.17	0.80	2.70	5.00	9.75	21.3	61.4	120	7.0×10^{-6}
2400	0.70		0.02	0.18	0.78	1.52	3.18	7.40	17.5	83	2.0×10^{-4}
2400	0.84		0.004	0.05	0.28	0.60	1.40	3.42	9.25	73	4.0×10^{-4}
2400	1.05			0.01	0.08	0.20	0.50	1.30	3.09	86	1.0×10^{-3}
2600	0.28	0.12	0.71	2.30	6.30	10.5	19.2	41.0	123	84	3.8×10^{-6}
2600	0.35	0.03	0.17	0.64	1.97	3.45	6.60	14.0	43.4	87	1.1×10^{-4}
2600	0.46		0.04	0.20	0.71	1.32	2.62	5.60	15.0	104	2.6×10^{-4}
2600§	0.56			0.02	0.12	0.28	0.67	1.62	4.77¶	64	8.5×10^{-4}
2600	0.84				0.004	0.02	0.08	0.25	0.78	78	5.0×10^{-3}
2800	0.18	0.33	1.48	4.00	12.0	22.0	45.0	79.0	144	40	1.5×10^{-6}
2800	0.21	0.06	0.33	1.18	3.40	6.30	13.4	28.8	51.9	46	4.9×10^{-6}
2800	0.28		0.03	0.12	0.55	1.14	2.50	5.60	14.0	74	2.4×10^{-4}
2800	0.35			0.01	0.10	0.28	0.68	1.61	4.30	64	8.3×10^{-4}
3000	0.21		0.01	0.03	0.10	0.22	0.61	1.82	2.80	22	6.7×10^{-4}

*Annealed for 2 hr at test temperature in H_2 prior to test.
†Test terminated, no rupture.
‡Annealed for 1 hr at 2400°C in H_2 prior to test.
§Tested in argon.
¶Specimen rotated at 4.1 hr, affecting rupture time.

The tensile properties[76] of a zirconium diboride–molybdenum disilicide material were investigated by Southern Research Institute. The values of tensile strength, initial elastic modulus, and total strain to fracture were determined for both a hot-pressed and a pressed-and-sintered material at several temperature levels from 70 to 3650°F. The tensile strengths were in agreement with the flexural strengths at up to 2000°F, but then a rapid loss in tensile strength was detected and attributed to silica, probably in the grain boundaries.

The tensile properties of ATJ and pyrolytic graphite were investigated within the 5000 to 6500°F temperature range.[76] The results indicated quite high strengths and a large influence of strain rate on tensile strength at the temperature levels of 6000 and 6500°F.

Techniques[76] were developed to allow the determination of Poisson's ratio and shear properties for brittle materials within the temperature range of 70 to 5000°F. For Poisson's ratio determinations, a lateral-strain-measuring system was developed to record accurately the small lateral strains of brittle materials loaded in tension or compression. For shear-property determinations a single shear specimen was developed that permits the determination of both the shear modulus and the shear strength. (J. A. DeMastry)

Table IV-10 CREEP DATA FOR ARC-CAST MOLYBDENUM* FROM 1600 TO 2200°C OBTAINED WITH THE OPTRON[74]

Specimen No. for M(6) material	Test temp., °C	Stress, kg/mm²	Test time, hr	Test atmosphere	Room-temperature elongation, %	Elongation per optron, %	Optron elongation error, %	Second-stage creep rate, min^{-1}	Total train second-stage creep rate, min^{-1}	ϵ vs. t^m	$\log(\epsilon^- \epsilon_0)$ vs. $\log t$	ϵ_0	†	Duration of first-stage creep, min
36	2200	0.32	4.28	Ar	51.8	Rupture		1.0×10^{-3}	1.2×10^{-3}	‡	‡	‡	‡	13
17	2200	0.39	2.03	Ar	48.7	Rupture		2.3×10^{-3}	2.6×10^{-3}	0.65	0.65	0.0005	0.0076	8
45§	2200	0.32	0.88	Ar	6.20	6.96	+12.0	1.1×10^{-3}		0.65	0.60	0.0009	0.0049	18
1–3	2200	0.32	0.63	Ar	4.60	4.55	–1.0	9.9×10^{-4}		0.60	0.62	0.0008	0.0048	13
1–1	2200	0.32	0.62	H_2	3.60	3.54	–1.7	7.5×10^{-4}	9.5×10^{-4}	0.65	0.65	0.0005	0.0030	12
44	2200	0.30	0.58	H_2	†	2.60		5.2×10^{-4}		0.65	0.65	0.0013	0.0024	19
1–2	2200	0.32	0.63	H_2	3.62	3.63	+0.3	7.8×10^{-4}	9.8×10^{-4}	0.65	0.64	0.0013	0.0030	13
2–1	2200	0.39	0.32	H_2	4.83	4.75	–1.7	1.9×10^{-3}	2.8×10^{-3}	0.65	0.64	0.0028	0.0062	9
2–2	2200	0.20	1.20	H_2	0.98	0.92	–5.0	Not run to second stage		0.80	0.80	0.00055	0.00028	>72
2–8	2200	0.25	4.75	H_2	8.18	8.25	+0.9	2.5×10^{-4}		0.75	0.75	0.0017	0.0010	85
2–11	2000	0.70	0.77	H_2	†	9.60		1.7×10^{-3}		0.60	0.57	0.0025	0.0069	8
2–9	2000	0.50	3.70	H_2	9.50	9.11	–4.1	3.7×10^{-4}	4.8×10^{-4}	0.75	0.79	0.0014	0.0013	70
2–4	1800	1.20	0.65	He	8.42	8.40	+0.2	1.8×10^{-3}	2.6×10^{-3}	0.70	0.71	0.0030	0.0056	13
2–3	2000	0.32	20.83	He	9.55	9.70	–1.5	7.0×10^{-4}	8.3×10^{-4}	0.60	0.60	0.0000	0.00064	110
2–7	2200	0.25	3.75	He	8.8	9.3	+4.9	3.6×10^{-4}	4.4×10^{-4}	0.77		0.00085	0.0013	64
2–15	1800	1.2	0.77	He	†	9.2		1.5×10^{-3}	2.2×10^{-3}	0.69		0.0052	0.0048	11
2–14	1800	0.84	4.66	He	7.8	7.6	–3.3	2.4×10^{-4}	3.3×10^{-4}	0.79		0.0011	0.00084	120
2–17	2200	0.32	1	He	7.0	7.6	+8.9	9.8×10^{-4}	1.3×10^{-3}	0.7		0.003	0.0036	19
2–20§	1600	2.1	2.1	He	†	5.6		1.3×10^{-3}	1.6×10^{-3}	0.62		0.0074	0.0056	12
2–6	1600	1.62	4.58	H_2	8.7	8.6	–1	2.7×10^{-4}	3.8×10^{-4}	0.70		0.0007	0.0014	65
2–18	1600	1.2	22.1	H_2	9.4	9.04	–4	5.8×10^{-5}	8.8×10^{-5}	0.615		0.0013	0.00076	120
2–13	1800	0.53	24.8	H_2	7.3	7	–4	4.2×10^{-4}	5.1×10^{-4}	0.47		0.00016	0.00099	80
2–19	2200	0.14	44.5	H_2	†	10.9		2.7×10^{-4}	3.6×10^{-4}					

*All samples annealed for 2 hr at test temperature before test.
†Target wire broken on removal of sample from furnace.
‡Tracker unlocked on sample loading—sample removed; first-stage data not obtained.
§Cyclic temperature control.

Table IV-11 CREEP-RUPTURE RESULTS* FOR TUNGSTEN–RHENIUM–MOLYBDENUM ALLOYS TESTED AT 2200°C AND 0.56 KG/MM² IN HYDROGEN†[74]

Alloy‡	Time to indicated elongation, hr							Elongation at rupture, %	Linear creep rate, min^{-1}	DPH§ hardness	
	0.5%	1%	2%	3%	5%	10%	Rupture			Before	After
W–26 Re	0.6	1.3	2.8	4.3	7.0	13.8	30.6	45	1.1×10^{-4}	550	440
W–27 Re	0.4	1.0	2.1	3.3	5.6	10.9	24.5	42	1.4×10^{-4}	495	465
W–28 Re	0.4	1.0	2.3	3.5	6.0	11.2	23.9	42	1.4×10^{-4}	570	475
W–29 Re	0.6	1.4	2.8	4.3	7.0	12.7	21.8	32	1.1×10^{-4}	630	400
W–26 Re–10 Mo	1.0	2.0	4.0	6.1	10.0	18.0	32.0	32	8.1×10^{-5}	490	410
W–27 Re–10 Mo	0.6	1.2	2.6	3.8	6.2	11.0	20.5	38	1.3×10^{-4}	525	425
W–28 Re–10 Mo	0.6	1.1	2.2	3.4	5.4	9.5	16.6	40	1.5×10^{-4}	590	450
W–29 Re–10 Mo	0.5	1.2	2.4	3.6	5.8	10.1	16.6	32	1.3×10^{-4}	610	450
W–26 Re–20 Mo	0.9	1.9	3.8	5.6	9.0	15.4	23.0	23	8.8×10^{-5}	450	415
W–27 Re–20 Mo	1.6	3.3	6.6	10.0	15.8	24.8	29.0	15	4.8×10^{-5}	480	410
W–28 Re–20 Mo	0.4	0.9	1.8	2.7	4.2	7.4	12.5	33	1.8×10^{-4}	500	410
W–29 Re–20 Mo	0.3	0.7	1.5	2.3	3.8	6.8	12.6	35	2.1×10^{-4}	525	410

*A 0.05-cm sheet, 0.6 × 2.54-cm gauge section.
†Annealed 2 hr at 2200°C in H_2 before test.
‡At.%.
§A 5-kg load.

Selected Metallurgical Aspects of Cladding and Structural Materials

Light Metals

The ductility of magnesium during creep is limited by the formation of cavities at the grain boundaries.[77] Application of a hydrostatic pressure of the same magnitude as the tensile creep stress eliminates the cavity formation. As expected, the formation of cavities is accompanied by a density decrease. The rate of density change is too large to be explained by growth of a constant number of cavities through vacancy condensation. Therefore the number of cavities must increase with increasing strain. At stresses lower than those at which cracking occurs, creep cavities are most probably nucleated heterogeneously at second-phase particles.[78] The mechanism for nucleation of these cavities is believed to be grain-boundary sliding.

In SAP alloy the following deformation kinetics take place:[79]

1. From temperatures of −196°C to ambient, the deformation is controlled by thermally activated intersection of dislocations.
2. From ambient temperature to about 350°C, the process of cross slip and processes controlled by self-diffusion become important.
3. Above 350°C the deformation is controlled by the pinning action of the Al_2O_3 particles and the interaction of attractive dislocations between the particles.

In developing alpha-phase titanium alloys for application at 1200°F, Pratt & Whitney[80] investigated a number of solid solution–dispersion strengthening combinations. The most promising alloys had the following composition range: titanium–5 to 7 wt.% aluminum–1.5 to 4.0 wt.% zirconium–0.2 to 0.4 wt.% carbon. The best combination of strength and ductility was obtained when the material was worked below the beta transformation temperature and then heat-treated to produce fine carbide dispersions. The stress-rupture properties of these alloys at 30,000 psi and 1200°F were comparable to those of austenitic stainless steels.

Zirconium and Its Alloys

The Italians found that both work hardening and recovery phenomena in zirconium proceed by two stages.[81] During the first stage in work hardening, all the physical properties observed (electrical resistivity, line breadth, and dislocation density) changed. In the second stage, only the electrical resistivity varied. This showed that, as deformation increases, the defects that are introduced are mostly point defects. The first step in recovery is attributed to migration and mutual annihilation of vacancies and dislocations. The second step is part of the recrystallization process and is attributed to self-diffusion.

Workers at Oak Ridge[82a] were able to grow large single crystals of alpha zirconium by traversing a beta-phase zone with an electron-beam heater at rates of 1 cm/hr. Temperature gradients of at least several hundred degrees

centigrade are required between the heated zone and the material adjacent to it. The damping capacity[83] of zirconium metal can be considerably increased by prestraining the metal at 77°K. This prestraining forms 1121 twins, with the maximum dampening capacity taking place after a prestrain of about 1%.

The British found that hydriding of zirconium sheet to 250 ppm hydrogen resulted in increases in yield strength and decreases in elongation at fracture.[84] The decrease in elongation was much more severe for thin-walled specimens (from 20 to 3%) than for the thick-walled specimens (from 20 to 12%). The reason for this difference is associated with the ratio of length of hydride platelets to wall thickness of tube. Since the zirconium hydride particle sizes were the same for all wall thicknesses and their distribution was random, the hydride would be likely to occupy a larger fraction of the cross-sectional area in thin-walled specimens.

A stress of 20,000 psi parallel to the basal poles causes a reorientation of hydride platelets.[85,86] Platelets that were parallel to the stress were reoriented to a perpendicular position. The higher the hydrogen content, the greater was the total number of hydride platelets reoriented, but the smaller was the fraction of the platelets that were reoriented. This may be explained by the presence of preferred sites for precipitation in stressed specimens. These sites are filled at low hydrogen levels, and higher hydrogen levels force less favorable sites to be filled. The embrittlement of zirconium and zirconium alloys is caused by precipitation of hydrogen as Zr_2H_3 platelets.[87] Cracks are originated in these brittle platelets, and these cracks propagate to the matrix, causing failure.

A thorough compilation of physical and mechanical properties of Zircaloy-2 and Zircaloy-4 has been made by Westinghouse.[57]

Heating of zirconium-alloy specimens at temperatures as low as 80°C resulted in a segregation of hydrogen in the grain boundaries of zirconium and Zircaloy-2 and at phase boundaries in zirconium–2.5 wt.% niobium, according to the Canadians.[88] This effect was most pronounced in specimens with small grains, whereas in larger grains the hydrogen segregated along the slip planes. It is also suspected that plastic deformation enhances hydride nucleation by increasing the dislocation density.

The following trends have been observed in tests on the reorientation of Zr_2H_3 during stress in the zirconium–2.5 wt.% niobium alloy.[89]

1. Cold-worked material is less susceptible to hydride reorientation than heat-treated material.
2. Increased temperature during stressing increases reorientation of hydrides.
3. Hydride reorientation does not appear to be dependent on time at stress and temperature.

Nickel Alloys and Steels

Workers at Atomics International have made a thorough compilation of physical, electrical, thermal, chemical, and mechanical properties of alloys that are considered as cladding materials for SNAP hydride reactors. The alloys covered are: Hastelloy N, Hastelloy X, Hastelloy R-235, René 41, TD nickel, and TZM. The irradiation effects on mechanical properties are also included.[90] The Defense Metals Information Center has issued a report covering the metallurgy and mechanical properties of ThO_2-strengthened nickel.[91]

It was found that carburization of stressed type 304 stainless steel at 1205°F doubled the rupture life, so long as severe thermal cycling did not cause cracking of the carburized material.[92] Failures were caused in the less creep-resistant small grains that resulted from welding.

A British patent for a manganese–molybdenum steel with improved mechanical properties for boilers and reactor pressure vessels was issued.[93] The steel contains 2 wt.% manganese and 0.3 to 1.0 wt.% molybdenum, 0.15 wt.% aluminum in solid solution, and 0.006 to 0.010 wt.% precipitated aluminum nitride. The best properties are obtained when the steel is rapidly cooled from 1050°C and then tempered at 150°C above the A_1 transformation point.

Refractory Metals

Evaporation losses of refractory alloys T-111, FS-80, FS-85, B-66, C-1294, and D-43 were determined for various times at temperatures of 1200 to 1500°C and pressures of 7×10^{-7} to 6×10^{-10} torr.[94] The evaporation losses were due to alloying constituents with high vapor pressures at these temperatures, such as vanadium, zirconium, and hafnium. Most of the

losses occurred from the surfaces, except for interstitial losses of carbon, nitrogen, oxygen, and hydrogen which occurred from throughout the specimens and were pressure dependent.

The surface recession rates of various metals in vacuum and in 1 atm helium at a velocity of 100 ft/sec were determined at various temperatures of interest.[95] The results, shown in Figs. IV-10 and IV-11, indicate that vaporization will not be a problem for tungsten, rhenium, and tantalum below about 4000°F in vacuum or in 1 atm of helium flowing at 100 ft/sec. For molybdenum, vaporization becomes troublesome at about 2900°F in vacuum and at 3300°F in helium under forced convection.

Fansteel Metallurgical Corporation was issued U. S. patents on high-strength oxidation-resistant alloys of niobium, tantalum, molybdenum, and tungsten containing additions of zirconium and titanium.[96,97] A 0.001 to 0.1 wt.% content of both oxygen and carbon is desirable in the alloys.

It was found that sintering in hydrogen improves the strength, density, modulus of elasticity, and purity of plasma-arc-sprayed molybdenum bodies.[98] A microstructure similar to that of recrystallized molybdenum sheet was obtained. Thermal-conductivity measurements by General Electric[99] on molybdenum at high temperatures indicate somewhat lower values than have been reported previously. The new values, along with previous values, are shown in Fig. IV-12.

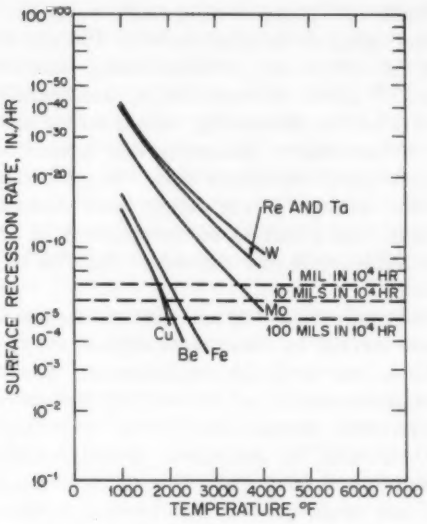

Fig. IV-11 Surface recession rates of various metals with helium at 100 ft/sec and 1-atm pressure blowing across the surfaces.[95]

For the best strength characteristics, 0.020 to 0.030 wt.% carbon is desirable in TZM alloy.[100] Recrystallization temperature was not affected by the allowable amount of cold work or by annealing and rolling temperatures. The ductile-to-brittle transition temperature was affected by almost all fabrication variables. Sheet specimens were cycled in bending in the plastic yielding range at toom temperature[101] to improve the ductility of TZM and molybdenum–0.5 wt.% titanium. The smooth-bend and tensile ductilities were not improved. However, the notch-bend ductility was considerably improved by the strain softening.

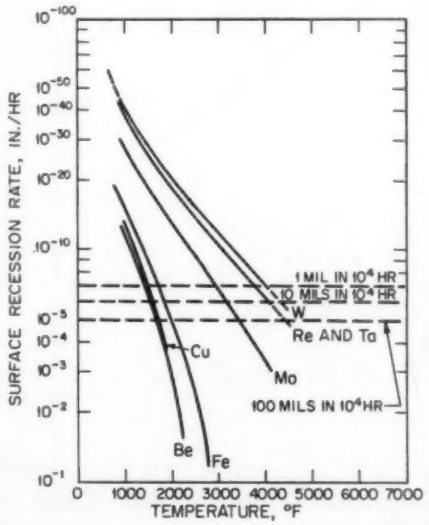

Fig. IV-10 Surface recession rates of various metals in vacuum.[95]

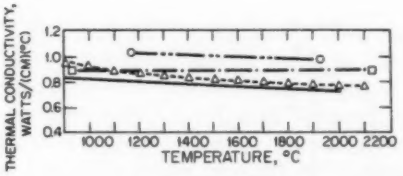

Fig. IV-12 Thermal conductivity vs. temperature for molybdenum.[99] ——,*GE-NMPO;* Δ--Δ--Δ, *Lebedev;* ○ ——--○, *Rudkin et al.;* □ —·□, *Wheeler.*

Tests at room temperature revealed that strain aging of tantalum between 100 and 200°C had no effect on work-hardening characteristics.[102] Also, the strain aging was found to be unaffected by the cooling rate from the annealing temperature, indicating that quench aging has no effect on strain aging. No precipitation occurs during strain aging, and dislocation pinning was found to be independent of nitrogen and carbon and dependent only on oxygen atoms.

The properties[103] of arc-melted tungsten were characterized by chemical analysis, recrystallization and grain-growth behavior, low-temperature ductility at 200 to 750°F, and high-temperature tensile and creep properties at 2500 to 4140°F. Increased metallic-impurity content decreased the rates of recrystallization and grain growth. Yield strength, ultimate tensile strength, work-hardening coefficient, and creep strength were found to increase with decreasing grain size. The grain size in turn decreased with increasing impurity contents. The higher-purity tungsten was produced by field freezing during zone refining.[82b] Workers at Oak Ridge have determined the thermal conductivity[5] of tungsten to 2600°C, and those values are shown in Fig. IV-13 where they are compared with previously published results. Russian workers have established the relation between hardness and tensile strength in the range 1000 to 2710°C for tungsten.[104] This relation is shown in Fig. IV-14.

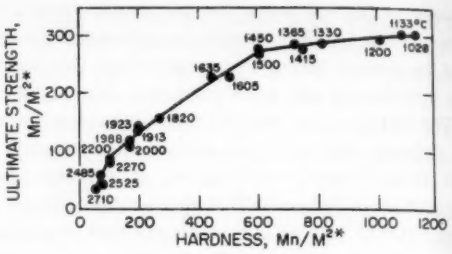

*Fig. IV-14 Relation between hardness and ultimate strength of tungsten at various temperatures.[104] *Mn/M² presumably stands for meganewtons per square meter. In that case, 1 Mn/M² = 145 psi. It is not clear what kind of hardness indenter was used.*

A tungsten–0.3 wt.% nickel–0.2 wt.% copper alloy exhibited properties[105] similar to those of wrought recrystallized powder-metallurgy and arc-cast tungsten at temperatures of 3000 to 4000°F. However, the ternary alloy could be sintered at temperatures as low as 2200°F. Additions of copper and nickel above 0.5 wt.% resulted in large decreases in strength at 2500°F.

Workers at Oak Ridge[5] found that the solubility of nitrogen in niobium is reduced about 10-fold by the addition of 1 wt.% zirconium at 1200°C. Also, the equilibrium nitrogen content

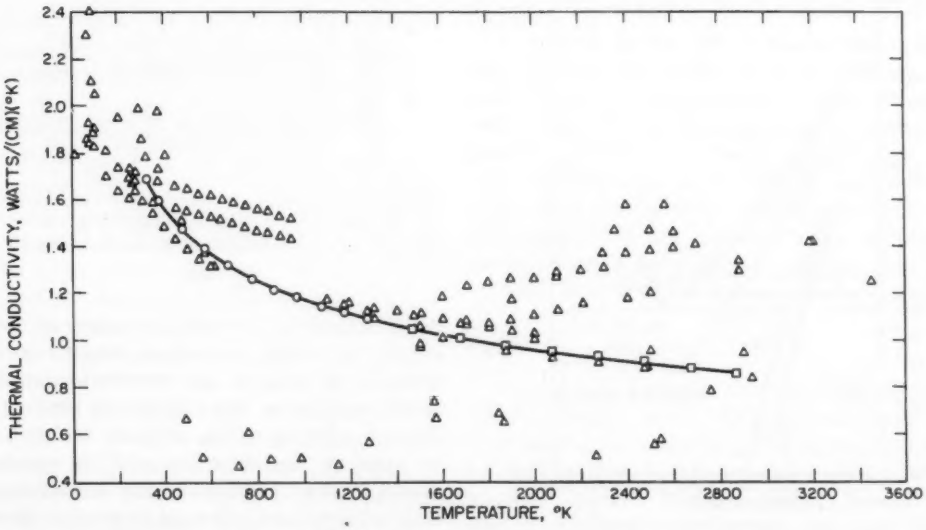

Fig. IV-13 Thermal conductivity of tungsten.[5] ○, ORNL measured; □, ORNL extrapolated; △, other investigators.

in niobium–1 wt.% zirconium was established as a function of temperature and pressure.

Solid-solution additions of most metals to niobium result in increases in strength and decreases in ductility.[106] Chromium, rhenium, zirconium, and iridium were found to have the largest effects. The modulus of elasticity was increased at both room temperature and at elevated temperatures by solid-solution additions of tantalum, tungsten, rhenium, molybdenum, and iridium to niobium. However, the coefficient of thermal expansion decreased with alloying by the above metals, indicating an increase in the forces of interatomic attraction. In niobium alloys that form a second phase on alloying, boron was found to have a larger effect on mechanical properties than either silicon or lanthanum.

The electrical[107] resistivity of niobium–1 wt.% zirconium was determined in the temperature range of 200 to 1446°C, as shown in Fig. IV-15. The electrical resistivity was found to follow the equation: Electrical resistivity, μohm-cm = $16.337 + 4.224 \times 10^{-2}T - 4.922 \times 10^{-6}T^2 - 3.941 \times 10^{-10}T^3$ (T is the temperature, °C). The recrystallization temperature of niobium–zirconium alloys was decreased by increases in the degree of cold work, impurity level, and zirconium content.[108]

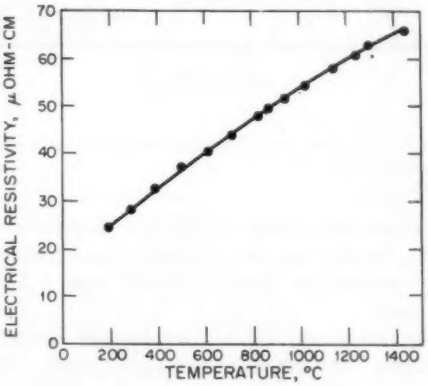

Fig. IV-15 Electrical[107] resistivity of niobium–1 wt.% zirconium.

Evaluation[109] of D-43 (niobium–10 wt.% tungsten–1 wt.% zirconium–0.1 wt.% carbon) indicated that the alloy has potential as a structural material in reentry vehicles, with operating temperatures approaching 3000°F. The alloy was found to have superior elevated-temperature strength over other niobium alloys owing to special heat-treatment and strain-hardening processing procedures. The alloy has good formability and good weldability, with the welds having good strength but marginal ductility. The ductile-to-brittle bend-transition temperature of stress-relieved D-43 was −200°F. Disil protective coating provided less oxidation protection for D-43 than for other niobium alloys at 2700 to 3000°F.

It was found that the annealing temperature of D-43 is very important in determining its ductility.[5] Annealing at 1500°C instead of 1800°C results in elongation of 32% as compared to 20%. If the alloy is cooled slowly from 1800°C, further loss of elongation to 8% takes place owing to aging of the Nb_2C particles. Annealing times of 1 hr at 1425°C or 100 hr at 1095°C are required to recover the ductility loss caused by slow cooling. Annealing of D-43 alloy that has been fast cooled from 1815°C results in an initial decrease in ductility, followed by a period of increasing elongation. The ductility minimum occurs sooner at higher annealing temperatures.

The oxidative weight gains[110] of PWC-11 (niobium–1 wt.% zirconium–0.08 wt.% carbon) and niobium–1 wt.% zirconium were 2.6×10^{-4} mg/(cm²)(hr) and 4.8×10^{-4} mg/(cm²)(hr), respectively, at 2000°F in a vacuum of 3×10^{-8} torr. The durations of the exposures were about 1000 hr.

A British patent[111] was granted for strengthening niobium by additions of 1000 to 2000 ppm of oxygen, plus 1 to 4 wt.% zirconium. A water quench from 875°C, followed by aging at 475 to 525°C for 2 hr, hardens the alloy and converts it to beta phase, in addition to dispersing the oxygen finely throughout the structure.

A U. S. patent[112] was granted for a cold-workable niobium alloy whose composition is 10 wt.% tungsten, 2.5 wt.% zirconium, 0.01 wt.% carbon (max.), and less than 0.04 wt.% O_2, H_2, and N_2. The alloy can be cold rolled into thin sheets that have an excellent combination of ductility, fabricability, weldability, and strength at temperatures of −325 to 3000°F. The alloy can be machined by conventional methods and can be cold rolled into foils as thin as 0.5 mil.

The presence of 1 wt.% zirconium in niobium–40 wt.% vanadium alloys containing 350 to 380 ppm oxygen was found to cause aging

by limiting the oxygen solubility in niobium.[36] Annealing for 1 hr at 925°C produced a hardness increase in the alloy containing zirconium; however, after 20 hr, overaging resulted in a hardness less than that in the niobium–40 wt.% vanadium alloy.

Evaporation studies on a niobium–39 wt.% vanadium–1 wt.% titanium alloy at 1100°C for 672 hr in 2.8×10^{-9} torr showed that a minor weight loss took place. This weight loss was traced to vanadium and titanium evaporation.

Considerable ternary-phase-diagram work with refractory metals has been recently carried out. The 1092 and 1538°C isotherms of the niobium corner of the niobium–zirconium–carbon system were determined by use of X-ray diffraction and chemical analysis.[113] The following areas were found in the 1538°C isotherm:

1. Niobium–zirconium bcc solid solution containing 1.3 wt.% zirconium and 200 ppm carbon (β)
2. A $(Nb,Zr)C_{1-x}$ fcc phase containing 44.7 wt.% zirconium and 7.64 wt.% carbon (γ)
3. A $(Nb,Zr)_2C$ hcp phase containing 5.15 wt.% zirconium and 6.15 wt.% carbon (δ)

The gamma phase represents a continuous series of solid solutions between NbC_{1-x} and ZrC_{1-x}. Figures IV-16 and IV-17 show the 1538°C and the preliminary 1092°C isotherms, respectively.

The molybdenum–niobium–silicon isotherm was determined by the Soviets[114] for 800°C and is shown in Fig. IV-18. No ternary compounds were found in the system. The maximum

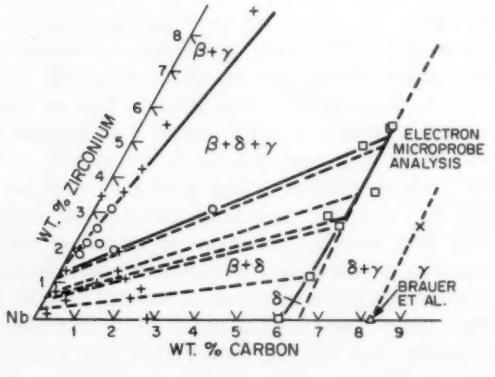

Fig. IV-16 The 1538°C isotherm of the niobium-rich region of the niobium–zirconium–carbon system.[113] ×, one phase; +, two phase; ○, three phase; □, extracted phase.

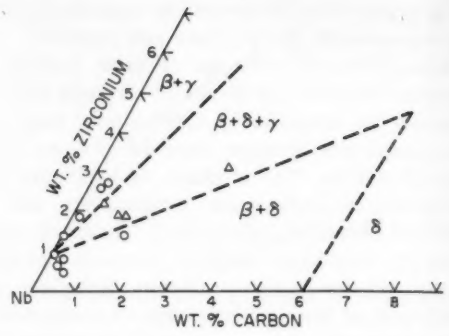

Fig. IV-17 Preliminary 1092°C isotherm of the niobium–zirconium–carbon system.[113] ○, two phase; Δ, three phase.

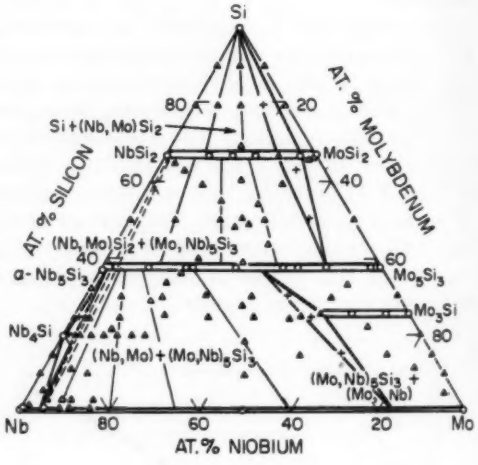

Fig. IV-18 The molybdenum–niobium–silicon isotherm at 800°C.[114]

hardness was found in the low modification of alpha Nb_5Si_3, and the maximum heat resistance was shown by $MoSi_2$ alloyed with 0.5 wt.% niobium.

The Russians[115] have determined isothermal sections of the tungsten–zirconium–carbon system at room temperature, 1500°C, and 1950°C. The isotherm at 1500°C is shown in Fig. IV-19. The system is characterized by the absence of ternary phases. The solubility of WC in zirconium was found to be 34 and 40 mole % at 1500 and 1950°C, respectively.

Tentative constitutional diagrams for tungsten–molybdenum–osmium at 1600, 2000, and 2375°C were determined by Westinghouse, using thermal, metallographic, and X-ray diffraction

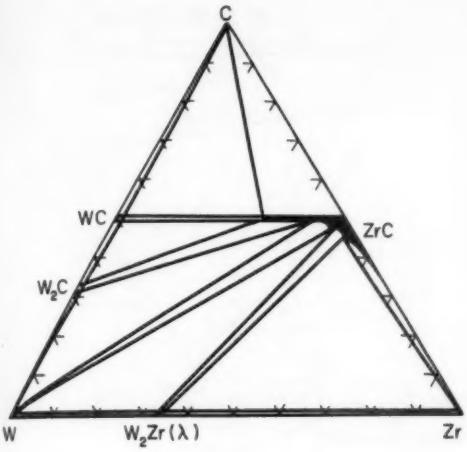

Fig. IV-19 Isothermal section of system zirconium–tungsten–carbon at 1500°C.[115]

techniques.[116] These isotherms are shown in Fig. IV-20.

The tungsten–molybdenum–zirconium system isotherms were determined[117] at 1000, 1500, and 1800°C. These isotherms are shown in Fig. IV-21. The mutual solid solubility of tungsten, molybdenum, and zirconium was found to increase with increasing temperature. No ternary alloys were found in the system.

The ternary systems of tantalum–vanadium–molybdenum and tantalum–vanadium–niobium were studied by physical chemical analysis at various temperatures.[118] The systems show mutual solid solubility, except for TaV_2. Isotherms of the systems are shown in Figs. IV-22 and IV-23.

The ternary system tantalum–rhenium–hafnium has been investigated.[119] Isotherms were determined for 1600, 1700, and 2400°C, and these are presented in Fig. IV-24. No ternary intermetallic phases were found.

Miscellaneous

Isothermal sections[120] of the cobalt–tungsten–oxygen phase diagram were determined at 1000, 1400, and 1700°C. The only ternary phase in the system was $CoWO_4$, which melted congruently at 1280°C. At 1400°C, only the tungsten + WO_2 + W_6Co_7 phase assemblage contained no liquid. At 1700°C, tungsten was the only solid phase with a large range of compositions melting to two immiscible liquids, one metallic and the other oxide.

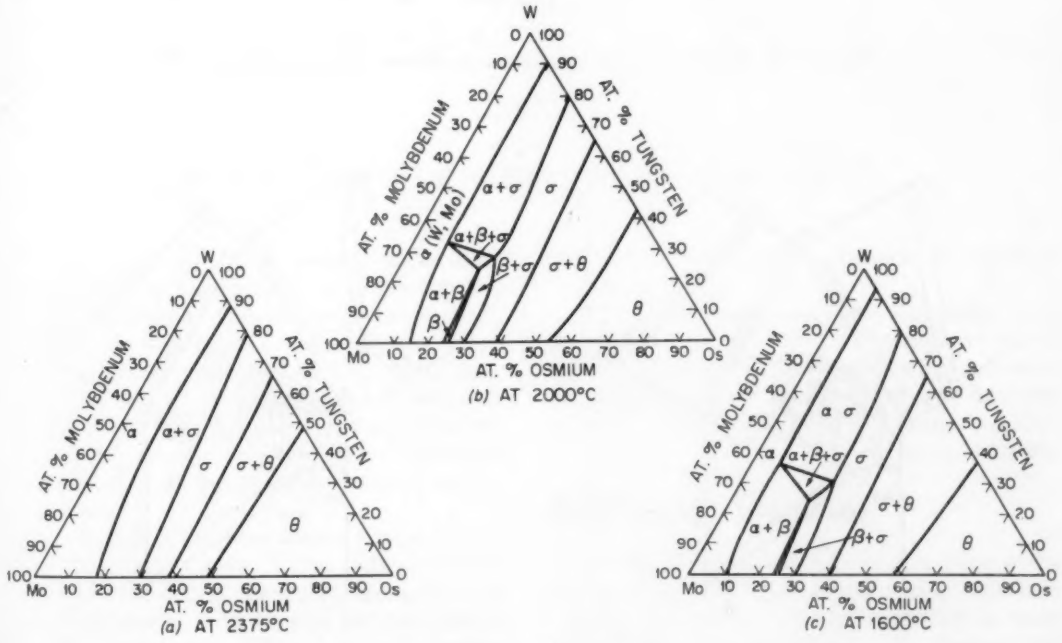

Fig. IV-20 Isotherms of the tungsten–molybdenum–osmium system.[116]

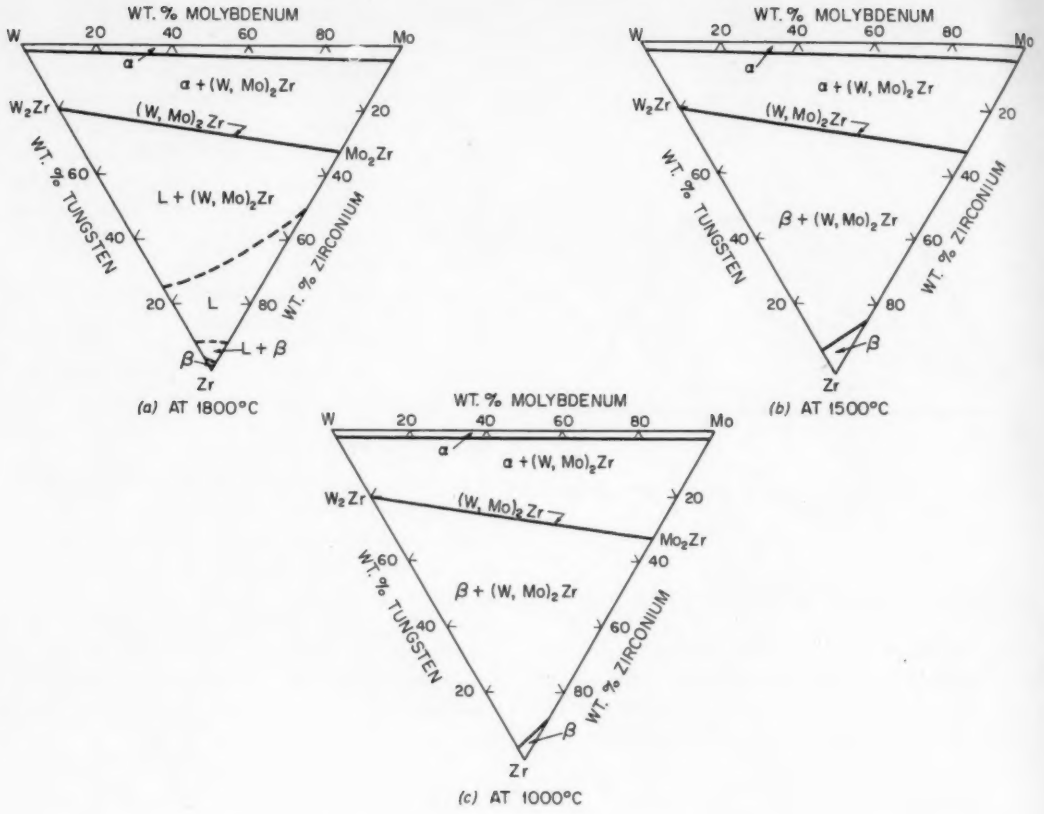

Fig. IV-21 Isotherms of the tungsten–molybdenum–zirconium system.[117]

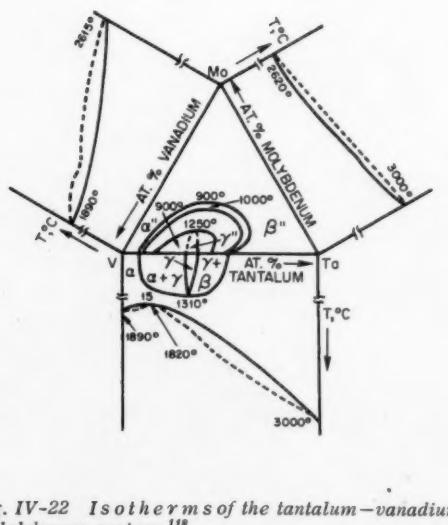

Fig. IV-22 Isotherms of the tantalum–vanadium–molybdenum system.[118]

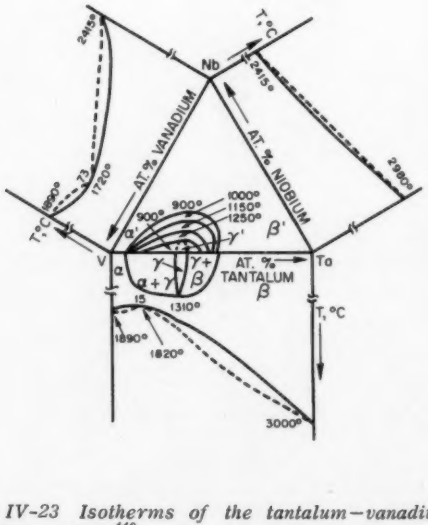

Fig. IV-23 Isotherms of the tantalum–vanadium–niobium system.[118]

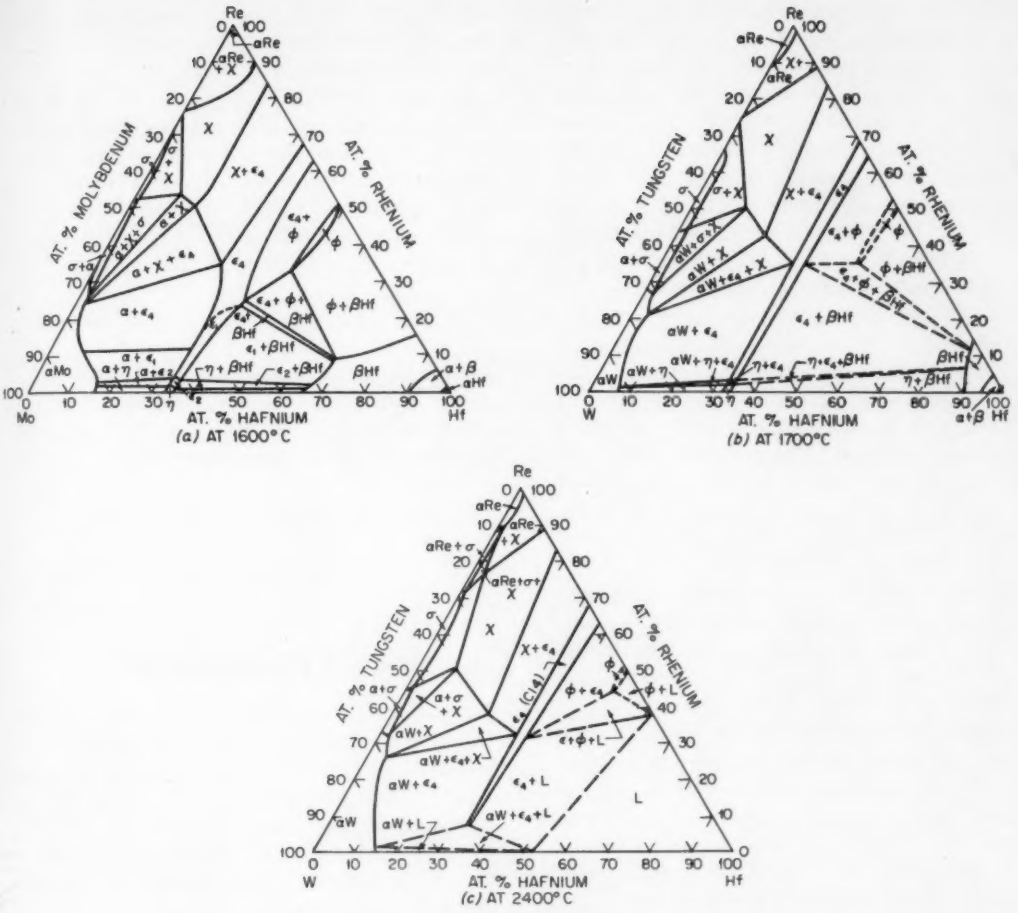

Fig. IV-24 Isotherms of the tungsten–rhenium–hafnium system.[119]

It was found that silicon content above 0.49 wt.% reduced the elongation[121] of L-605 (cobalt–20 wt.% chromium–15 wt.% tungsten–10 wt.% nickel–1 wt.% iron–0.1 wt.% carbon) alloy after aging 1000 hr at 1600°F. Varying the iron content from 0.16 to 3.24 wt.% had no effect on the ductility. Microstructure showed that the increase of silicon resulted in the formation of precipitates at the grain boundaries and in the matrix.

A U. S. patent has been issued for oxidation-resistant cobalt alloys.[122] The alloys contain 54 to 61 wt.% cobalt, 21 wt.% chromium, and 10 wt.% tungsten, 7 to 12 wt.% niobium, tantalum, or molybdenum, 0.3 to 1.25 wt.% carbon, and 0.9 to 1.3 wt.% yttrium. The alloy is oxidation resistant up to 2300°F and maintains high strength up to 1800°F and moderate strength up to 2000°F.

The yttrium–aluminum–carbon phase diagram from 55 to 100 at.% yttrium at 950°C was determined.[123] The significant findings were the low aluminum solubility in Y_3C and the presence of the ternary carbide phase, Y_3AlC.

(M. Kangilaski)

Diffusion Studies

An extensive compilation by Oak Ridge of all known data on radioactive-tracer diffusion studies in metals is being published in table form.[124,125] The bibliography is divided into four parts: (1) self-diffusion in pure metals; (2) impurity diffusion in pure metals; (3) self-

diffusion and impurity diffusion in alloys; and (4) grain-boundary diffusion in metallic systems. Values of frequency factors and activation energies were compiled from the literature reported between 1938 and 1964. The first two parts of the bibliography are currently available.

A study of binary interdiffusion in body-centered-cubic transition metal systems has been made.[126] The use of Darken's analysis for binary diffusion in several systems resulted in negative values for intrinsic diffusion coefficients of the slower moving component. This is attributed to the existence of a finite chemical potential gradient due to vacancies. Enhanced diffusion in regions of sharp concentration gradients is also attributed to a gradient of chemical potential. The systems studied include niobium–vanadium, niobium–molybdenum, niobium–titanium, niobium–zirconium, molybdenum–titanium, molybdenum–zirconium, and titanium–platinum.

Additional contributions on diffusion studies of reactor materials come from foreign reports, including a German study of diffusion in the copper–zirconium system.[127] The investigation was made at four different temperatures. Six intermetallic phases were observed after 1000 hr. The results were corroborated by microhardness and by concentration determinations made by electron-microprobe analyses. The authors describe the observed phases as $ZrCu_5$, $ZrCu_4$, $ZrCu_3$, ZrCu, and Zr_2Cu. The Kirkendall effect was observed in all diffusion couples.

The diffusion of ^{14}C in beta zirconium has been reported in Russian literature[128] in the temperature range of 900 to 1200 °C. The diffusion coefficient and activation energy were compared with data on carbon diffusion in other body-centered cubic metals and with magnitudes calculated on the basis of the Wert–Zener theory. The activation energy and frequency factor for ^{14}C diffusion in zirconium were reported to be 26,700 cal/mole and 0.0048 cm^2/sec, respectively. The authors note that these diffusion values for carbon and nitrogen in zirconium are similar to those for zirconium self-diffusion.

A translation of another Russian report describes the diffusion of carbon and molybdenum in chromium.[129] Several different techniques were used to study the diffusion processes. The Russians studied the molybdenum–chromium system by plating molybdenum containing the isotope ^{99}Mo onto polished chromium plate and heating in an argon atmosphere. They prepared the carbon–chromium system by heating the chromium in a carburizing atmosphere containing $Ba^{14}CO_3$ and charcoal. A second method for studying the carbon–chromium system involved the use of a decarburizing atmosphere of hydrogen after a mixture of chromium and carbon containing ^{14}C was blended and melted. The authors describe the diffusion of molybdenum in chromium by the equation

$$D = 2.7 \times 10^{-3} \exp(-58{,}000/RT) \text{ cm}^2/\text{sec}$$

Interpretation of diffusion data in the chromium–carbon system was complicated by carbide formations in the chromium. Nevertheless, the authors give an expression of

$$D = 8.3 \times 10^{-3} \exp(-28{,}000/RT) \text{ cm}^2/\text{sec}$$

to describe the diffusion of carbon in chromium.

(A. N. Ashurst)

Ceramic Technology

A survey of the art of preparing ceramic fibers and whiskers has been prepared by General Electric.[130] The report shows the types of such material available, sources, and property data. This compilation should be very useful to persons considering applications of these materials. It is hoped that similar surveys covering techniques for the incorporation of these materials into useful structures, and property data on the composites, will be forthcoming.

Shaffer has patented an easily applied oxidation-resistant coating.[131] The coating is applied to the formed shape prior to sintering. The coating consists of a mixture of (1) hafnium or zirconium boride, (2) molybdenum, zirconium, tungsten, or tantalum silicide, or a mixture of molybdenum and tantalum silicides, or boron nitride, and (3) silicon carbide or silicon metal and a temporary binder.

The oxidation resistance of dense SiC bodies can be improved by the addition of 2 to 10 wt.% tungsten, chromium, iron, hafnium, tantalum, titanium, zirconium, or molybdenum, or mixtures of these, according to a second patent of The Carborundum Company.[132] These may be added as the metal or as a compound. It is claimed that the improved bodies are oxidation resistant up to 1850 °C.

In equilibrium studies of Nb_2O_5 with a 1:1 (molar) mixture of $Nb_2O_5-WO_3$ at 1300 to 1400°C, Roth and Wadsley identified five compounds in what previously had been reported as a region of solid solution.[133] Each of the phases was characterized and some of the structures described.

Investigators at Los Alamos Scientific Laboratory found the thermal-expansion coefficient of near-stoichiometric TaC from 25 to 3000°C to be 8.4×10^{-6}/°C.[134] Expansion was found to be nearly linear through this range. The results are in good agreement with earlier measurements in the range below 2000°C. No previous work is known in the 2000 to 3000°C range. (H. D. Sheets)

References

1. W. F. Bourgeois and J. N. Chirigos, Development of Zirconium-Base Alloys, USAEC Report WAPD-TM-546, Westinghouse Electric Corp., Bettis Atomic Power Laboratory, November 1965.
2. K. C. Thomas and R. J. Allio, The Failure of Stressed Zircaloy in Aqueous Chloride Solutions, *Nucl. Appl.*, 1(3): 252-258 (June 1965).
3. R. K. Betts, Evaluation of the Zircaloys for Use in the 630A Reactor, USAEC Report GEMP-346, General Electric Company, Nuclear Materials and Propulsion Operation, Feb. 26, 1965.
4. H. C. Bowen, Corrosion Evaluation of High-Silicon Aluminum Alloys, USAEC Report BNWL-125, Pacific Northwest Laboratory, September 1965.
5. S. Peterson (Comp. and Ed.), Metals and Ceramics Division Annual Progress Report for Period Ending June 30, 1965, USAEC Report ORNL-3870, Oak Ridge National Laboratory, November 1965.
6. A. B. Johnson, Jr., Nickel-Plated Aluminum in Deionized Water, *p*H 10 NH_4OH and LiOH at 330°C, USAEC Report BNWL-98, Pacific Northwest Laboratory, September 1965.
7. M. Warzee, J. Hennaut, J. Waty, M. Maurice, C. Sonnen, and P. Berge, Effect of Surface Treatment on the Corrosion of Stainless Steels in High-Temperature Water and Steam, *J. Electrochem. Soc.*, 112(7): 670-674 (July 1965).
8. P. Haymann, C. Waldburger, and J. J. Trillat, Oxidation of Iron Surfaces Under Ion Bombardment, *Mem. Sci. Rev. Met.*, 62: 135-139 (May 19, 1965).
9. M. J. Davies, D. A. Landsman, and W. E. Seddon, Stress Corrosion of Irradiated Stainless Steels, British Report AERE-R-5014, August 1965.
10. J. S. Armijo, Intergranular Corrosion of Nonsensitized Austenitic Stainless Steels: II. Metallurgical Variables, Report APED-4670, General Electric Company, Atomic Power Equipment Department, January 1965.
11. K. C. Thomas and R. J. Allio, Stress Corrosion in Alloys for Fuel Element Cladding—Stainless Steel and Zircaloy, USAEC Report WCAP-3269-50, Westinghouse Electric Corp., Atomic Power Division, September 1965.
12. L. A. Charlot and R. E. Westerman, High-Temperature Corrosion of Candidate ATR Structural Materials, USAEC Report BNWL-100, Pacific Northwest Laboratory, September 1965.
13. T. T. Claudson and R. E. Westerman, An Evaluation of the Corrosion Resistance of Several High-Temperature Alloys for Nuclear Applications, USAEC Report BNWL-155, Pacific Northwest Laboratory, November 1965.
14. G. P. Wozadlo and W. L. Pearl, General Corrosion of Stainless Steels and Nickel Base Alloys Exposed Isothermally in Superheated Steam, *Corrosion*, 21(11): 355-369 (November 1965).
15. E. G. Bohlmann and F. A. Posey, Aluminum and Titanium Corrosion in Saline Waters at Elevated Temperatures, USAEC Report ORNL-P-1430, Oak Ridge National Laboratory, July 20, 1965.
16. L. K. Knudsen, Cavitation Damage Tests with Rotating Disk in Water, USAEC Report TIM-894, Pratt & Whitney Aircraft—CANEL, Division of United Aircraft Corp., July 1965.
17. General Electric Company, Nuclear Materials and Propulsion Operation, High Temperature Materials Program Progress Report No. 53, Part A, USAEC Report GEMP-53A, Nov. 26, 1965.
18. J. Stringer, The Effect of Nitrogen on the Oxidation of Tantalum at High Temperatures, *J. Electrochem. Soc.*, 112(11): 1083-1091 (1965).
19. J. Brett, L. L. Seigle, J. Berkowitz-Mattuck, B. Lement, D. I. Phalen, D. A. Vaughn, N. A. Richard, A. E. Austin, and C. M. Schwartz, Experimental Study of Factors Controlling the Effectiveness of High-Temperature Protective Coatings for Tungsten, Report AFML-TR-64-392, General Telephone and Electronics Laboratories, Inc., and subcontractors, November 1964.
20. R. W. Bartlett, Investigation of Mechanisms for Oxidation Protection and Failure of Intermetallic Coatings for Refractory Metals, Report ASD-TDR-63-753 (Part III), Aeronutronic Applied Research Laboratories, September 1965.
21. K. Marnoch, Research on High-Temperature Oxidation-Resistant Hafnium-Tantalum Systems, Report AD-461565, Marquardt Corp., July 1965.
22. S. Priceman and L. Sama, Development of Slurry Coatings for Tantalum, Columbium, and Molybdenum Alloys, Report AFML-TR-65-204, Sylcor Division, Sylvania Electric Products Inc., September 1965.
23. A. Pietromonaco, Fluidized-Bed Techniques for Coating Refractory Metals, Interim Report, March 8–June 8, 1965, Report IR-8-184 (II), The Boeing Co.
24. G. F. Wakefield, Refractory Metal Coatings by Chemical Vapor Deposition, Interim Report, August 15–November 15, 1965, Report IR-8-264 (II), Texas Instruments, Inc.
25. M. H. Ortner and K. A. Gebler, Electrophoretic Deposition of Refractory Metal Coatings, Interim Report, June 28–September 30, 1965, Report IR-8-344 (I), Vitro Laboratories.
26. A. R. Stetson, J. D. Steinman, and V. S. Moore, Refractory Metal Coatings by the Fused Salt Process, Interim Report, July 1–September 30, 1965, Report IR-8-346 (I), Solar, Division of International Harvester Co.

27. L. A. Friedrich, N. S. Bornstein, and E. C. Hirakis, Refractory Metal Protective Coatings for Long-Term Applications, USAEC Report PWAC-499, Pratt & Whitney Aircraft—CANEL, Division of United Aircraft Corp., September 1965.
28. G. J. Dormer, B. S. Payne, and E. G. Pike, Final Report on Manufacturing Methods for High Temperature Coating of Large Molybdenum Parts, Report AFML-TR-65-282, The Pfaudler Co., August 1965.
29. Pratt & Whitney Aircraft—CANEL, Division of United Aircraft Corp., SNAP 50/SPUR Final Summary Report, Coolants and Working Fluids, USAEC Report PWAC-491, November 1965.
30. R. E. Cleary, S. S. Blecherman, and J. E. Corliss, Solubility of Refractory Metals in Lithium and Potassium, USAEC Report TIM-850, Pratt & Whitney Aircraft—CANEL, Division of United Aircraft Corp., November 1965.
31. S. S. Blecherman and J. Hodel, The Compatibility of Structural and Turbo-Machinery Alloys in Boiling Potassium, USAEC Report PWAC-501, Pratt & Whitney Aircraft—CANEL, Division of United Aircraft Corp., October 1965.
32. M. J. Wallace, Summary Report of Potential Liquid Metal Bearing Materials for SNAP 50/SPUR Pumps, USAEC Report PWAC-468, Pratt & Whitney Aircraft—CANEL, Division of United Aircraft Corp., November 1965.
33. E. E. Hoffman (Ed.), Potassium Corrosion Test Loop Development, Quarterly Progress Report 8, April 15–July 15, 1965, Report NASA-CR-54843, General Electric Company, Space Power and Propulsion Section, Nov. 23, 1965.
34. G. F. Schenck, Application of Internal Friction Methods to Corrosion Study in Columbium Alloys, USAEC Report CNLM-6344, Pratt & Whitney Aircraft—CANEL, Division of United Aircraft Corp., July 30, 1965.
35. P. A. Bourdon, S. S. Bleckerman, and G. F. Schenck, Columbium-1 Zirconium Alloy Forced Convection Lithium Slave Loop Test LCCDB-1, USAEC Report TIM-898, Pratt & Whitney Aircraft—CANEL, Division of United Aircraft Corp., October 1965.
36. T. K. Roche (Comp.), Evaluation of Niobium-Vanadium Alloys for Application in High-Temperature Reactor Systems, USAEC Report ORNL-TM-1131, Oak Ridge National Laboratory, October 1965.
37. Argonne National Laboratory, Reactor Development Program Progress Report, September 1965, USAEC Report ANL-7105, Oct. 20, 1965.
38. R. W. Harrison, Studies of Alkali Metal Corrosion on Materials for Advanced Space Power Systems, Quarterly Progress Report No. 3, December 26, 1964–March 26, 1965, Report NASA-CR-54390 (N65-27271), General Electric Company, Space Power and Propulsion Section.
39. K. Goldmann, N. Hyman, S. Kostman, and J. McKee, Carbon and Nitrogen Transfer in a Type 316 Stainless Steel Cb-1% Zr, Liquid Potassium System, in *Remote Systems Technology*, Conference Proceedings, Washington, 1965, American Nuclear Society, Hinsdale, Ill., 1965.
40. Argonne National Laboratory, Reactor Development Program Progress Report, October 1965, USAEC Report ANL-7115, Nov. 23, 1965.
41. Argonne National Laboratory, Reactor Development Program Progress Report, November 1965, USAEC Report ANL-7122, Dec. 27, 1965.
42. Atomics International, Annual Technical Progress Report, AEC Unclassified Programs, Fiscal Year 1965, USAEC Report NAA-SR-11450, Nov. 10, 1965.
43. Oak Ridge National Laboratory, Molten-Salt Reactor Program Semiannual Progress Report for the Period Ending August 31, 1965, USAEC Report ORNL-3872, December 1965.
44. Argonne National Laboratory, Chemical Engineering Division Semiannual Report, July–December, 1964, USAEC Report ANL-6925, May 1965.
45. P. J. Barton, D. R. Harries, and I. L. Mogford, Effects of Neutron Dose Rate and Irradiation Temperature on Radiation Hardening in Mild Steels, *J. Iron Steel Inst. (London)*, 203: 507-510 (May 1965).
46. Atomic Energy of Canada Limited, unpublished, 1965.
47. P. C. L. Pfeil and P. J. Barton, The Effect of Impregnation with ^{10}B and ^{11}B on the Elevated-Temperature Tensile Properties of an Irradiated Austenitic Steel, British Report AERE-R-5027, August 1965.
48. G. H. Broomfield, D. R. Harries, and A. C. Roberts, Neutron Irradiation Effects in Austenitic Stainless Steels and a Nimonic Alloy, *J. Iron Steel Inst. (London)*, 203: 502-506 (May 1965).
49. R. S. Barnes, Embrittlement of Stainless Steel and Nickel-Based Alloys at High Temperature Induced by Neutron Radiation, *Nature*, 206: 1307-1310 (June 26, 1965).
50. P. R. B. Higgins and A. C. Roberts, Reduction in Ductility of Austenitic Stainless Steel After Irradiation, *Nature*, 206: 1249-1250 (June 19, 1965).
51. R. Sumerling, Electron Metallography of Irradiated 20Cr-25Ni-Nb Tensile Specimens, British Report TRG-Report-1056, Aug. 5, 1965.
52. T. T. Claudson and H. J. Pessl, Evaluation of Iron- and Nickel-Base Alloys for Medium- and High-Temperature Reactor Applications: Part II, USAEC Report BNWL-154, Pacific Northwest Laboratory, November 1965.
53. Pacific Northwest Laboratory, Metallurgy Research Section, Quarterly Progress Report, July–September, 1965, USAEC Report BNWL-166, Oct. 15, 1965.
54. J. Cervasek and J. Kutka, Effect of Neutron Radiation on Certain Mechanical and Structural Properties of Austenitic Chrome Nickel Steel, Report FTD-TT-65-125 [translated from *Jaderna Energie*, 9: 342-346 (1963)].
55. T. T. Claudson, Effects of Neutron Irradiation Upon the Mechanical Properties of Inconel 625, USAEC Report BNWL-153, Pacific Northwest Laboratory, October 1965.
56. G. H. Broomfield, The Effects of Strain Rate, Neutron Dose and Irradiation Temperature on the Tensile Properties of Nimonic PE16, British Report AERE-R-4982, July 1965.
57. D. B. Scott, Physical and Mechanical Properties of Zircaloy-2 and -4, USAEC Report WCAP-3269-41, Westinghouse Electric Corp., Atomic Power Division, May 1965.
58. S. H. Bush, Irradiation Effects in Cladding and Structural Materials, *Monograph Series on Metallurgy in Nuclear Technology*, 1965.
59. A. Blaise, Irradiation of Cu-Co Alloys, USAEC

Report ORNL-tr-667 (French), translated by G. L. Boisvert, Oak Ridge National Laboratory, 1964.

60. N. B. Kristianson, Computed Effect of Neutron Irradiation on the Concentrations of Interstitials and Vacancies in Niobium, Ph. D. Thesis, Iowa State University, 1964.
61. M. Balarin and O. Hauser, Radiation Saturation and Defect Structure in Solids, *Phys. Status Solidi*, 10: 475-480 (Aug. 1, 1965).
62. T. J. Koppenaal, Neutron Irradiation Strengthening in Copper Single Crystals, *Phil. Mag.*, 11: 1257-1288 (June 1965).
63. W. Christ, K. Gechwendtner, and F. Haessner, Recrystallization of Neutron-Irradiated and Cold-Rolled Polycrystalline Copper, *Phys. Status Solidi*, 10(1): 337-344 (July 1965).
64. H. Mehrer, H. Kronmueller, and A. Sieger, The Recovery of Nickel Above Room Temperature, *Phys. Status Solidi*, 10: 725-738 (Aug. 1, 1965).
65. J. L. Brimhall, B. Mastel, and T. K. Bierlein, Loop Interactions During Annealing of Neutron-Irradiated Molybdenum, *J. Appl. Phys.*, 36: 2585 (August 1965) (USAEC Report BNWL-SA-36).
66. J. D. Meakin and A. Lawley, Direct Observation of Radiation Damage in Molybdenum, *Materials Science Research*, Vol. 2, pp. 69-90, Plenum Press, Inc., New York, 1965.
67. A. C. Damask, Method of Improving Properties of an Alloy by Radiation, U. S. Patent 3,193,678, Aug. 14, 1962.
68. J. E. Campbell, Current Methods of Fracture-Toughness Testing of High-Strength Alloys With Emphasis on Plane Strain, Report DMIC-207, Battelle Memorial Institute, Defense Metals Information Center, Aug. 31, 1964.
69. D. H. Nyman, High-Temperature Creep-Rupture Properties of Hastelloy X in Vacuum, USAEC Report BNWL-167, Pacific Northwest Laboratory, November 1965.
70. E. Brodahl and S. Aas, Correlation Between Calculated and Measured Mechanical Properties of Thin-Walled Fuel Element Canning Tubes of Stainless Steel, Norwegian Report KR-96, July 1965.
71. M. Lemcoe, Study of Instantaneous Collapse and Creep Buckling Characteristics of Large SGR Process Tubes, USAEC Report NAA-SR-11323, Atomics International, July 25, 1965.
72. H. F. Conrad and P. R. Landon, Melting, Fabrication, and Creep Testing of a 1.39% Ti-0.34% Zr-0.30% C Molybdenum Alloy, USAEC Report UCRL-14437, Lawrence Radiation Laboratory, Nov. 1, 1965.
73. Argonne National Laboratory, Metallurgy Division, Annual Progress Report for 1964, USAEC Report ANL-7000.
74. General Electric Company, Nuclear Materials and Propulsion Operation, High-Temperature Materials Program Progress Report No. 49, Part A, USAEC Report GEMP-49A, July 28, 1965.
75. P. Beardmore and D. Hull, Deformation and Fracture of Tungsten Single Crystals, *J. Less-Common Metals*, 9: 168-180 (1965).
76. Southern Research Institute, The True Stress-Strain Properties of Brittle Materials to Very High Temperatures, Final Report, 1963-1964, USAEC Report TID-21843, Oct. 30, 1964.
77. R. T. Ratcliffe and G. W. Greenwood, The Mechanism of Cavitation in Magnesium During Creep, *Phil. Mag.*, 12: 59-69 (July 1965).
78. J. E. Harris, Nucleation of Creep Cavities in Magnesium, *Trans. AIME*, 233: 1509-1516 (August 1965).
79. E. Ruedl and P. Guyot, Electron Microscopy of SAP Following Tensile Deformation or Quenching, Euratom Report EUR-2479.e, European Atomic Energy Community, August 1955.
80. E. J. Delgrosso, J. J. Kaminsky, and L. M. Raring, High Temperature Titanium Alloy Development, USAEC Report PWAC-472, Pratt & Whitney Aircraft—CANEL, Division of United Aircraft Corp., October 1965.
81. A. Desalvo, P. Gondi, G. F. Missiroli, and F. Zignani, Work Hardening and Recovery Phenomena in Zirconium, *Met. Ital.*, 57: 177-186 (May 1965).
82. Papers presented at First International Conference on Electron and Ion Beam Science and Technology, 1965.
    a. J. C. Wilson and M. L. Picklesimer, Variable-Gradient, Electron-Beam Heating Methods for Growing Single Crystals of Zirconium.
    b. D. R. Hay and E. Scala, Field-Aided Electron-Beam Zone Refining of Tungsten.
83. R. E. Reed-Hill, E. P. Dahlberg, and W. A. Sleppy, Jr., Some Anelastic Effects in Zirconium at Room Temperature Resulting from Prestrain at 77°K, *Trans. AIME*, 233: 1766-1771 (September 1965).
84. G. P. Walters, The Ductility of Hydrogenated Zirconium Sheet Specimens of Varying Thickness, British Report AERE-R-4981, July 1965.
85. P. L. Rittenhouse and M. L. Picklesimer, Precipitation of Hydrides in Zircaloy-2 as Affected by Preferred Orientation, Elastic Stress, and Hydrogen Content, USAEC Report ORNL-TM-1239, Oak Ridge National Laboratory, September 1965.
86. W. G. Jolley and W. I. Clark (Eds.), Papers and Proceedings of the Meeting on Application of X-ray Diffraction in the Atomic Energy Field, Richland, Washington, February 25-26, 1965, USAEC Report RL-REA-2595, Pacific Northwest Laboratory, October 1965.
87. W. H. Erickson and D. Hardie, The Role of Hydride Precipitate in the Fracture of Zirconium and Its Alloys, *J. Inst. Metals*, 93: 444-446 (August 1965).
88. C. Roy, Nucleation and Growth of Hydrides in Zirconium Alloys, Canadian Report AECL-2297, September 1965.
89. Atomic Energy of Canada Limited, unpublished, 1965.
90. G. F. Burdi, Properties of Cladding Materials for SNAP Hydride Reactors, USAEC Report NAA-SR-MEMO-11149, Atomics International, Mar. 22, 1965.
91. L. P. Rice, Metallurgy and Properties of Thoria-Strengthened Nickel, Report DMIC-MEMO-210, Battelle Memorial Institute, Defense Metals Information Center, Oct. 1, 1965.
92. D. H. Stone and A. D. Schwartz, Effect of Carburization on the Low Strain Rate Behavior of Type 304 Stainless Steel, USAEC Report NAA-SR-10487, Atomics International, Aug. 31, 1965.

93. Manganese-Molybdenum Ductile Steel, British Patent 997,292, July 7, 1965.
94. D. T. Bourgette, High-Temperature Chemical Stability of Refractory-Base Alloys in High Vacuum, USAEC Report ORNL-P-1394, Oak Ridge National Laboratory, June 1965.
95. G. E. Zima, Vaporization of Advanced Powerplant Metals Under Vacuum and Forced Convection Conditions, USAEC Report UCRL-14274, University of California, Lawrence Radiation Laboratory, June 24, 1965.
96. A. B. Michael, Columbium Alloy, U. S. Patent 3,188,205, to Fansteel Metallurgical Corporation, June 8, 1965.
97. A. B. Michael, Columbium Alloy, U. S. Patent 3,188,206, to Fansteel Metallurgical Corporation, June 8, 1965.
98. D. J. Sellers and M. Levy, A Study of the Effect of Heat Treatment on the Microstructures and Properties of Sprayed Molybdenum, Report AMRA-TR-64-50, Army Materials Research Agency, December 1964.
99. General Electric Company, Nuclear Materials and Propulsion Operation, High-Temperature Materials Program Progress Report No. 51, Part A, USAEC Report GEMP-51A, Sept. 30, 1965.
100. W. A. McNeish, Effects of Process Variables on the Properties of Molybdenum-TZM Alloy Sheet, *Mater. Sci. Res.*, 2: 135-148 (1965).
101. E. J. Ripling and S. Zager, The Use of Strain Softening to Improve the Properties of Refractory Metals, Report AD-618925, Materials Research Laboratory, Inc., March 1965.
102. C. L. Formby and W. S. Owen, The Strain Aging and Quench Aging of Tantalum, *J. Less-Common Metals*, 9: 25-34 (1965).
103. W. D. Klopp and P. L. Raffo, Effects of Purity and Structure on Recrystallization, Grain Growth, Ductility, Tensile, and Creep Properties of Arc-Melted Tungsten, Report N64-33085, National Aeronautics and Space Administration, Lewis Research Center, November 1964.
104. V. A. Borisenko, The Relationship Between Hardness and Strength Characteristics of Tungsten and Molybdenum Over a Wide Temperature Range, *Poroshkovaya Met., Akad. Nauk Ukr. SSR*, No. 2: 57-59 (February 1965).
105. R. D. McIntyre, Tungsten-Nickel-Copper Ternary Alloys for High-Temperature Applications, Report NASA-TN-D-3015 (N65-32648), National Aeronautics and Space Administration, Lewis Research Center, September 1965.
106. N. D. Tarasov, R. A. Ulyanov, and Y. D. Mikhaylov, The Effect of Alloying on the Physiomechanical Properties of Niobium, Report N65-27681 (NASA-TT-F-9374) [translated from *Fiz. Metal. i Metalloved.*, 18(15): 740-745 (1964)].
107. D. V. Rigney, S. M. Kapelner, and R. E. Cleary, The Electrical Resistivity of Lithium and Columbium-1 wt.% Zirconium Alloy to 1430°C, USAEC Report TIM-854, Pratt & Whitney Aircraft—CANEL, Division of United Aircraft Corp., September 1965.
108. C. E. Carlson and E. J. Delgrosso, Recovery and Recrystallization of Columbium and Several Columbium-Zirconium Alloys, USAEC Report PWAC-465, Pratt & Whitney Aircraft—CANEL, Division of United Aircraft Corp., September 1965.
109. R. G. Baggerly and R. T. Torgeson, Evaluation of D-43 Columbium Alloy (Cb-10 W-1 Zr-0.1C), Report N64-27085, Boeing Co., Feb. 3, 1964.
110. J. F. Hogan, E. A. Limoncelli, and H. Slotnick, Stability of Carbon Strengthened Columbium-Zirconium Alloys at Elevated Temperatures in Ultra-High Vacuum, USAEC Report TIM-955, Pratt & Whitney Aircraft—CANEL, Division of United Aircraft Corp., October 1965.
111. J. Winton and R. Murgatroyd, Improvements Relating to Zirconium Base Alloys, British Patent 997,761, July 7, 1965.
112. M. Schussler, Cold Workable Columbium Base Alloy, U. S. Patent 3,188,207, to Union Carbide Corporation, June 8, 1965.
113. J. A. Cornie, E. J. Delgrosso, and R. Granger, Phase Diagram of the Cb-Zr-C System at 1538 and 1092°C, USAEC Report PWAC-461, Pratt & Whitney Aircraft—CANEL, Division of United Aircraft Corp., October 1965.
114. E. M. Savitskii, Constitution Diagram and Properties of Nb-Mo-Si Alloys, *Izv. Akad. Nauk SSSR, Metal.*, No. 3: 159-166 (March–April 1965).
115. Yu. B. Kuz'ma, T. F. Fedorov, and E. A. Shvets, Phase Equilibrium in the Zr-W-C System, *Poroshkovaya Met., Akad. Nauk Ukr. SSR*, No. 2: 22-25 (February 1965).
116. A. Taylor and N. J. Doyle, The Constitution Diagram of the Tungsten-Molybdenum-Osmium System, *J. Less-Common Metals*, 9: 190-205 (1965).
117. A. M. Zakharov and E. M. Savitskii, Investigation of the Ternary W-Mo-Zr Phase Diagram, *Izv. Akad. Nauk SSSR, Metal.*, No. 1: 151-159 (1965).
118. A. P. Nefedov, E. M. Sokolovskaya, A. T. Grigor'ev, and I. G. Sokolova, Constitution Diagrams of the Ternary Systems V-Ta-Nb and V-Ta-Mo, *Izv. Akad. Nauk SSSR, Neorgan. Materialy*, 1: 715-720 (May 1965).
119. A. Taylor and N. J. Doyle, The Ternary Alloy System Tungsten-Rhenium-Hafnium, *Am. Soc. Metals, Trans. Quart.*, 58: 341-352 (1965).
120. B. Phillips, L. Y. Chang, and M. G. Scroger, Condensed-Phase Relations in the System Co-W-O at High Temperature (1000 to 1700°C), *Trans. Met. Soc. AIME*, 233: 1220-1226 (July 1965).
121. G. D. Sandrock, R. L. Asbrook, and J. C. Freche, Effect of Variations in Silicon and Iron Content on Embrittlement of Cobalt-Base Alloy (L-605), Report NASA-TN-D-2989, National Aeronautics and Space Administration, Lewis Research Center, September 1965.
122. D. E. Deutsch, High-Temperature Oxidation-Resistant Cobalt-Base Alloys, U. S. Patent 3,202,506, to USAEC, Aug. 24, 1965.
123. S. Rosen and P. G. Sprang, Phase Equilibria in Yttrium-Rich Ternary Alloys Containing Aluminum and Carbon, *Trans. Met. Soc. AIME*, 233: 1265-1269 (July 1965).
124. J. Askill (Comp.), A Bibliography on Tracer Diffusion in Metals. Part I. Self-Diffusion in Pure Metals, USAEC Report ORNL-3795, Part I, Oak Ridge National Laboratory, May 1965.
125. J. Askill (Comp.), A Bibliography on Tracer Diffusion in Metals. Part II. Impurity Diffusion in Pure Metals, USAEC Report ORNL-3795, Part II, Oak Ridge National Laboratory, November 1965.

126. C. S. Hartley, J. E. Steedly, Jr., and L. D. Parsons, Binary Interdiffusion in Body-Centered Cubic Transition Metal Systems, Report AD-457333, Air Force Materials Laboratory, September 1964.
127. G. Hillmann and W. Hoffman, Diffusion Measurements in the System Copper-Zirconium, *Z. Metallk.*, 56: 279-286 (May 1965).
128. L. V. Paulinov and V. N. Bykov, Carbon Diffusion into β-Zirconium (in Russian), *Fiz. Metal. i Metalloved.*, 19: 397-400 (March 1965).
129. P. L. Gruzin, S. V. Zemskii, and I. B. Rodina, Study of Diffusion of Carbon and Molybdenum in Chromium, British translation AERE-Trans-1032 [from *Met. i Metalloved. Chistykh Metal., Sb. Nauchn. Rabot*, No. 4: 243-250 (1963)].
130. L. R. McCreight, H. W. Rauch, Sr., and W. H. Sutton, A Survey of the Art of Ceramic and Graphite Fibers, Report AFML-TR-65-105, General Electric Company, Space Sciences Laboratory, May 1965.
131. P. T. B. Shaffer, Oxidation Resistant Ceramics and Methods of Manufacturing the Same, U. S. Patent 3,189,477, to The Carborundum Company, June 1965.
132. K. Taylor, Refractory Articles, U. S. Patent 3,189,472, to The Carborundum Company, June 15, 1965.
133. R. Roth and A. Wadsley, Multiple Phase Formation in the Binary System Nb_2O_5-WO_3, *Acta Cryst.*, 19(1): 26-47 (July 1, 1965).
134. C. Kempter and M. R. Nadler, Thermal Expansion of Tantalum Monocarbide to 3020°C, *J. Chem. Phys.*, 435: 1739-1742 (Sept. 1, 1965).

Section

V

Reactor Materials

Special Fabrication Techniques

Melting, Casting, and Hot and Cold Working

Techniques for processing into fuel elements the uranium–20 wt.% plutonium–2.5 wt.% molybdenum alloy have been investigated at Argonne.[1] Satisfactory fuel plates were obtained when the alloy was induction melted in yttria-washed graphite crucibles and poured into graphite molds. Various melt temperatures and mold temperatures were investigated, and it was noted that close control of both was required to obtain a satisfactory yield. The optimum melt and mold temperatures were 1275 and 545°C, respectively. Rolling studies on the alloy indicate that a temperature in excess of 600°C is required to inhibit cracking. Argonne workers also noted that uranium–15 wt.% plutonium alloys containing 10 wt.% of either titanium or zirconium were easy to cast.[2]

A niobium–39 wt.% vanadium–1 wt.% titanium alloy and numerous niobium–vanadium binary alloys were prepared and evaluated at Oak Ridge.[3] Prior to alloying, the vanadium and niobium were electron-beam melted in an effort to reduce their interstitials. Losses approximating 22% occurred in the vanadium, whereas losses on the order of 6% were noted in the niobium. The binary alloys were prepared by nonconsumable-electrode arc-melting techniques into 500- to 600-g disks, 4 in. in diameter by $\frac{3}{8}$ to $\frac{1}{2}$ in. thick. These alloys were homogenized for 2 hr at 1200°C and cold rolled. The alloys containing 20 to 70 wt.% vanadium reduced as much as 90% without annealing; the alloys containing 10 and 80 wt.% vanadium did not twin during rolling and cracked after approximately 10% reduction.

Climax Molybdenum vacuum-arc-melted a molybdenum-base ingot containing 1.39 wt.% titanium, 0.34 wt.% zirconium, and 0.30 wt.% carbon. The 4-in.-diameter by $30\frac{3}{4}$-in.-long ingot weighed 132 lb and exhibited a trace of microporosity throughout its structure. Two 3-in.-diameter by 6-in.-long extrusion blanks were extruded at 3100°F, with a 4 to 1 reduction ratio. The extrusions were smooth but exhibited severe nose bursts. After being straightened at 2400°F, the extruded material was swaged into rod at temperatures of 3000 to 2460°F by General Electric.[4]

The skull-reduction program currently in progress at Argonne[2,5] has progressed to the point where a process can be defined. This process consists of extraction of the noble fission products, reduction of the remaining uranium oxides in a magnesium–40 wt.% zinc solution, dissolution of the precipitated uranium in a zinc–14 wt.% magnesium solution, and casting into an ingot. The solvent metals are then evaporated to leave sponge uranium, which is melted into an ingot for recycling. Of particular interest to those concerned with melting and casting is the fact that a thixotropically cast beryllia crucible has proven superior to an isostatically pressed beryllia crucible for the retorting runs where the zinc and magnesium are removed from the uranium.

An Argonne translation[6] contains an excellent treatment of the theory of tube reductions. This theoretical treatment is substantiated in tests which showed that, in either the cold or hot die drawing of tubes, the change in wall thickness is primarily a function of the ratio of wall thickness to tube diameter and that, if this ratio is approximately 0.17, the tube can be reduced without increasing the wall thickness.

(N. E. Daniel)

Cladding

Canning

General conclusions at Oak Ridge[7] from recently completed studies indicate that the most important factor in producing a high bulk density of powder-packed fuels is a relatively high radial acceleration of the tube wall. A high longitudinal acceleration is also required, and this was found to be best produced by pneumatic vibrators. It appears that densification is achieved by a combination of the radial expansion and contraction of the tube wall which promotes settling, while agitation of the powder by the axial vibration orients the particles into a good geometrical fit. (V. D. Linse)

Nonelectrolytic Chemical Plating

The major interest in nonelectrolytic chemical plating continues to be in the development of the tungsten-vapor plating process and its modification for the preparation of tungsten alloys, protective coatings, formed parts, and for the welding or joining of refractory-metal components.

Workers at Oak Ridge[7,8] deposited uniformly thick tungsten sheet, 12 in. by 1.5 in. by 0.060 to 0.093 ± 0.003 in. in size, on the inside of a sintered molybdenum mandrel by hydrogen reduction of WF_6. The total variation in deposit thickness over the length of the mandrel was about 10% or less. The workers obtained uniform deposition by heating the mandrel with a tube furnace having a properly profiled temperature gradient and by preheating the feed gases to 350°C. A deposition rate of 3.2 mils/hr was obtained at a substrate temperature of 560 to 580°C and a system pressure of 5 torrs. The deposition efficiency was 76%.

A computer program is being written[8] in an attempt to relate experimental variables such as temperature, pressure, H_2/WF_6 ratio, gas velocity, and substrate geometry to deposit characteristics, especially to nodular growth. An initial, empirical study[7] of this problem has shown that nodular growth may be due to (1) the presence of complex oxyfluorides generated by oxidizing contaminants in the gas feed, (2) incomplete reduction of WF_6 due to local buildup of HF in turbulent-to-laminar flow transition regions, and (3) occlusion of randomly oriented tungsten particles produced homogeneously in the gas phase. With an H_2/WF_6 ratio of 15 at a system pressure of 5 torrs, nodular growth resulted[8] when air was added to the deposition atmosphere in amounts greater than a few parts per million (e.g., 0.03 vol.%) at a deposition temperature of 580°C, or when the deposition temperature was raised to slightly over 700°C with no contaminants present.

Mills, Lindgren, and Weinberg[9] evaluated 17 tubes of commercially available vapor-deposited tungsten. They concluded that (1) the chemical-impurity contents of the tubing obtained from six different sources are comparable, (2) the metallic impurities are at a low level in all samples and are related to the mandrel material, (3) there is a positive correlation between the residual fluorine content and the ductile-to-brittle transition temperature of vapor-deposited tungsten tubing, (4) the lowest fluorine content of the vapor-deposited tubing is comparable to that found in extruded tubing made by powder-metallurgy techniques (which still contains some fluorine), (5) columnar structures that are deposited in a highly oriented manner will exhibit less grain growth, at elevated temperatures, than those deposited in a less oriented manner, (6) grain growth in vapor-deposited tubing is not related primarily to the chemical-impurity content, (7) extensive grain growth occurs in extruded tubing under conditions that produce little grain growth in vapor-deposited tubing, (8) the ductile-to-brittle transition temperatures of extruded tungsten tubing and the best vapor-deposited tubing are comparable, and (9) no correlation was found between hardness and impurity content, microstructure, or ductile-to-brittle transition temperature. The columnar grain structure of vapor-deposited tungsten does not appear[7] to be detrimental to ductility.

The vapor deposition of tungsten metal has been investigated[7] as a method of joining tungsten components. Joint designs included flat plates and tube-end closures. Deposition onto an angle of 90° at the intersection of sheets resulted in cracked deposits. Workers modified the joint configuration by grinding one member to a radius of 0.5 in. tangent to the root of the weld to prevent cracking. End caps were joined to tubes to give a joint which was leaktight to helium by mass-spectrometer detection.

Landsberg, Campbell, and Block[10] applied coatings of tungsten or molybdenum to the surface of powdered magnesia, alumina, zirconia, zirconium carbide, and zirconium boride in a

fluidized-bed reactor. The coatings were applied by the vapor-phase reduction of the metal chlorides or by deposition of the metal oxide which was reduced subsequently with hydrogen. The oxide process appeared more favorable from the standpoint of materials handling, reactor corrosion, and by-product disposal. Also, coatings could be applied by the oxide process four times as fast as by the chloride reduction process.

High-density smooth-textured molybdenum deposits were obtained[7,8] on extended surfaces (copper substrates) by workers at Oak Ridge using hydrogen reduction of MoF_6. The deposition efficiency was not high unless the incoming gas mixture was preheated to 600°C, which also had the effect of improving deposit uniformity.

Unalloyed rhenium has also been deposited[7] at Oak Ridge by hydrogen reduction of ReF_6. The deposits consisted of nodular growths, mechanically interlocked crystals having considerable grown-in porosity, and some smooth coating. Deposits of high density and uniform thickness were obtained under conditions giving low deposition efficiency.

Work was continued[7,8] at Oak Ridge on the development of the process for depositing rhenium–tungsten alloys by hydrogen reduction of mixtures of WF_6 and ReF_6. Deposits containing 24 to 27 wt.% rhenium over the middle 4-in. section of a 6-in.-long deposit were obtained in a coating system by the use of a moving hot zone created by a 1-in.-long induction coil. The deposition efficiency was 100%.

Development of the process for forming UO_2 parts and coatings by chemical vapor deposition was continued at Oak Ridge.[7] The UO_2 is deposited by the reaction of UF_6 with hydrogen and oxygen, or steam, at elevated temperatures and reduced pressures. The UO_2 can be obtained as dense or dendritic deposits, or as a submicron-size powder, depending on the conditions used and method of mixing the reactants. The dense deposits had a density of 10.96 g/cm^3 and an oxygen-to-uranium ratio of 2.000 to 2.003.

Workers at Pfaudler[11] have applied titanium and silicide coatings to alloy D-43 (niobium–10 wt.% tungsten–1 wt.% zirconium) and alloy D-14 (niobium–5 wt.% zirconium) from a fused-salt bath by a batch process. Titanium, chromium, and silicide coatings have also been deposited in a continuous process. The study of silicide coatings applied by a slurry process has shown promising results.

Page, Moeller, and Sneesby have received a patent[12] on a process for forming molybdenum disilicide coatings on molybdenum or its alloys with titanium and titanium–zirconium. The molybdenum, or its alloy, is immersed for a period of 3 to 5 hr in a molten alkali metal, preferably molten sodium, containing 10 wt.% silicon, 5 wt.% tin, and 1 wt.% carbon, maintained at a temperature of 1000 to 2000°C under an inert-gas atmosphere.

The carburization of niobium–1 wt.% zirconium alloy was studied[13] at Pratt & Whitney in an effort to improve the antigalling characteristics of the alloy. Three carburization techniques were developed: (1) reaction with a slurry coating of oil–graphite mixture, (2) reaction with a methane–argon atmosphere, and (3) reaction with carbon in solution in molten lithium. The coating thickness could be varied within the range of 0.0001 to 0.0006 in., depending on the choice of technique and process conditions. The activation energy for NbC film growth was -72.7 ± 3 kcal/mole, and for Nb_2C film growth, -68.8 ± 3 kcal/mole.

A British patent[14] has been issued to the Norwegian Institutt for Atomenergi on a process for applying a protective surface layer to aluminum or aluminum alloys. The aluminum or aluminum-alloy body is given a coating of phosphorus-containing nickel alloy by chemical deposition (electroless nickel plating). The phosphorus is then extracted from the coating and the nickel alloyed with the substrate by treatment of the coated body with a fused-salt mixture containing KNO_3 and $NaNO_2$ in the weight ratio 0.9 to 1.1, or $NaNO_3$ and KNO_2 in the weight ratio 1.1 to 0.9, at a temperature between 450 and 600°C for a period of 0.5 to 100 hr.

(C. F. Powell)

Electroplating

Dense, coherent, and smooth electrodeposits of zirconium, zirconium diboride, zirconium–aluminum, and zirconium–titanium alloy were produced at Union Carbide[15] in 700 to 800°C mixtures of lithium, sodium, potassium, and zirconium fluorides at current densities of 10 to 30 ma/cm^2. Zirconium deposits with a thickness up to 0.1 mil had a columnar structure, the large columns characteristic of an annealed metal. With 12 wt.% potassium fluo-

borate added to the melt, a finer-grained diboride deposit was obtained. The zirconium–aluminum alloy produced with 1 wt.% aluminum oxide showed a banded structure. All electrodeposits were of high purity and contained only very small amounts of other metals. The fluoride-salt mixtures were better than bromide, chloride, or chloride–fluoride systems for depositing dense, sound metal or alloy.

Niobium, tantalum, tungsten, and molybdenum also have been electrodeposited in a dense, coherent form.[16] Workers produced refractory-metal shapes by plating niobium and other metals in high-temperature fluoride-salt mixtures on removable steel, copper, or copper-plated nickel mandrels. The thickness of the electroformed metal ranged up to 0.25 in. The density of each metal approached the theoretical value for the pure metal. Impurities totaled less than 5 ppm in tungsten and less than 50 ppm in the other refractory deposits. Electrodeposited coatings became impervious at thicknesses of 0.003 to 0.004 in. Tantalum-plated copper was successfully reduced 86%, which demonstrates good adhesion and ductility. The development should make it possible to produce complex shapes with good high-temperature characteristics appropriate for nuclear reactor components.

Electrodeposition of iridium in fused-salt baths also has been investigated at Union Carbide[17] with the objective of producing a protective coating for tantalum and niobium at high temperatures. Surface-preparation procedures for consistent reproduction of good adherence were not identified. Iridium-plated tantalum and niobium exhibited a brittle behavior in bend tests, unlike roll bonds of iridium and the refractory metals. The brittleness of the electroplated specimens might have been associated with precipitation of impurities at low temperatures. Yet, iridium-plated copper exhibited a ductile behavior. Electroplated coatings with a thickness of 2 to 3 mils on niobium failed in an oxymethane flame at 1450 °C because of pinholes in the coating. Electrodeposited tungsten did not appear to be a good diffusion barrier for roll-bonded iridium because it did not reduce the formation at 1350 °C of a niobium–iridium compound.

In Czechoslovakia,[18] electrodeposited copper protected uranium fuel elements during forging at 300 to 600 °C while the elements were reduced 60%. The copper was deposited in a conventional copper sulfate–sulfuric acid solution after the uranium was pickled in 50% nitric acid solution, treated in concentrated hydrochloric acid, reimmersed in the nitric acid solution, and anodically etched for 20 sec at a current density of 3 amp/sq ft. This anodic treatment in the copper (or other) plating baths is similar to a procedure commonly applied to steel before it is chromium plated, but the treatment has not heretofore been reported for etching uranium and promoting improved electroplate adhesion. Heat-treating (1 hr at 600 °F) promoted good diffusion bonding of the electroplated copper. The same preparation procedure and postplating heat-treatment was successful for plating electroless nickel, which was about equal to copper electroplate for protecting uranium at 300 to 600 °C but better than electroplated copper for protecting uranium from corrosion in boiling water. Nickel electroplating solutions containing boric acid were judged unsatisfactory because the deposited nickel contained up to 0.05 wt.% boron; so a solution buffered with magnesium sulfate and ammonium chloride and containing a wetting agent was preferred for nickel plating.

Rhenium with satisfactory properties was electroplated with good continuity up to a thickness of 2 μ on tungsten and molybdenum.[19] Thicker coatings were obtained when 2-μ-thick layers were deposited with intermediate heat-treatment (1000 °C for 10 to 20 min), because rhenium deposits thicker than 2 μ were highly stressed and brittle. Current interruption or addition of sulfur-containing stress-reducing agents was not effective in reducing stress or brittleness. This experience matches the results of earlier work in the United States. A new plating bath was proposed, however, which appeared to deposit rhenium with improved efficiency. The new bath, prepared with perrhenic and sulfuric acids and ammonium sulfate, has a throwing power about equal to that of the potassium perrhenate–sulfuric acid–ammonium sulfate bath or a conventional chromium-plating bath. A unique a-c treatment in sodium hydroxide was adopted to prepare molybdenum or tungsten for plating. After conventional anodic treatments in acid (such as 70% sulfuric acid), the rhenium coatings were discontinuous.

Nonuniformly quenched aluminum alloy is nonuniformly dissolved in solutions of sodium hydroxide during chemical milling because the smut layer is adherent over water-quenched

areas and nonadherent over air-quenched areas. The adherent smut reduces the dissolution rate. Learning that the smut contained large amounts of metallic copper and iron (deposited in powder form by a displacement reaction), Illinois Institute technologists investigated complexing agents, but without success.[20] One supplier of a proprietary chemical-milling solution evidently has identified an effective agent, because smutting was uniform and the dissolution rate was constant on both water- and air-quenched zones.

The porosity in thin nickel electrodeposits on uranium was decreased during research at Battelle–Northwest[21] by adoption of an anodic etching procedure in an $HCl-H_2SO_4$ mixture. An 11-μ-thick nickel plate over the $HCl-H_2SO_4$ anodically etched surfaces exhibited less porosity than 18-μ-thick nickel over uranium anodically etched in an $HCl-H_3PO_4$ mixture. Thus the thickness of nickel needed as a diffusion and corrosion barrier between uranium fuel and aluminum cladding can be reduced, and a reduction in the parasitic neutron capture will occur. The Hanford researchers also noted that the substitution of $NiBR_2$ for $NiSO_4$ in the Watts nickel-plating bath (or the nickel sulfamate bath) greatly reduced the reactivity of uranium and produced less corrosion product at the uranium–nickel interface. The anode efficiency was 100% in each case. Neither the superimposition of alternating current nor the adoption of ultrasonic agitation reduced the porosity in the nickel deposits. This fact was ascertained by measurement of the iron content of the precipitate formed on nickel-plated uranium surfaces when specimens were anodized in $K_4Fe(CN)_6 \cdot 3H_2O-KNO_3$ solution.

(W. H. Safranek)

Pressure Bonding

Hot isostatic pressing of powder materials by a technique involving the action of high-pressure oil or water on a directly heated sample via a sand medium has been described.[22] With this approach, it is required that the sand be inert, insulating, nonforming, and pressure transmitting. Initial experiments evaluated the effectiveness of different pressure-transmitting media on UO_2 compaction. Since the compaction behavior of UO_2 in conventional pressing is well known, a pressure value could be assigned to each sand material and compared with the system pressure. During the course of this work, MgO, Al_2O_3, natural flake graphite, BN, UO_2, SiC, and CrO_3 were examined. Of these, MgO provided the most satisfactory behavior. Bag materials were also studied and included polyvinyl chloride and thin metal containers of aluminum, copper, lead, and stainless steel. The process has demonstrated the practicability of fabricating 8-in.-diameter bars at 2000°C and 12-in.-diameter bars at 1200°C. Twenty-four specimens were pressed by this method without leakage problems. Extrapolating the current work to larger existing equipment indicates that 40-in.-diameter pressings at 2500°C and 30,000 psi should be possible. No mechanical problems are anticipated in such a scale-up.

The design and operation of gas-pressure-bonding autoclaves capable of pressures to 50,000 psi and temperatures to 5000°F have been discussed in a recent paper.[23] A major area of investigation involved the study of high-temperature and high-pressure gas phenomena. By use of an exploratory type analog, the convective behavior of fluids was examined and related to observed patterns in autoclave operation. The similarity noted permitted redesign of glass vessels to restrict fluid flow and reduce temperature variations as a model for subsequent autoclave furnace designs. It was concluded that end closures for the furnace would permit the greatest control and enhance furnace capacity. These designs are currently being evaluated in high-pressure autoclaves. (S. W. Porembka)

Welding and Brazing

Niobium

Much of the recent joining research on refractory metals has been concerned with niobium alloys. General Electric investigators are looking at the structural stability of welds.[24] The bend-transition temperatures for alloy C129Y have been established and found significantly superior to those of the alloys B-66 or D-43 welded under similar conditions. The data are recorded in Table V-1. Solution treatments above 1540°C reduced the ductility of C129Y alloy because of grain growth and/or grain-boundary precipitation. Nitrogen absorption in welds in this alloy is also detrimental.

The stability of welds in niobium alloys is being studied at Westinghouse Electric Corp.[25] Tantalum and other refractory-metal alloys are also included in this program for National

Table V-1 BEND-TRANSITION TEMPERATURES OF AS-WELDED ALLOYS[24]

Alloy	Type of weld	Welding speed, in./min	Weld-chamber atmosphere	Fusion-zone contamination	Bend-transition temperature, °C
C129Y	Base metal				−165
C129Y	TIG	8	Purified He		−150*
C129Y	TIG	24	Purified He		−140
C129Y	TIG	Manual two pass	Purified He		−37
C129Y	TIG	8	He + 1.6% N_2	300−400 ppm N_2	+9
C129Y	Electron beam	25	Vacuum		−120
B-66	TIG	8	Purified He		+43
B-66	TIG	24	Purified He		+2
B-66	TIG	Manual two pass	Purified He		+195
B-66	TIG	8	He + 1.4% N_2	300−400 ppm N_2	+145
B-66	Electron beam	28	Vacuum		+43
C-43	TIG	8	Purified He		+170
D-43	TIG	24	Purified He		+135
D-43	TIG	Manual two pass	Purified He		+285
D-43	TIG	8	He + 2.5% N_2	350−400 ppm N_2	+250
D-43	Electron beam	22	Vacuum		−34

*Estimated.

Aeronautics and Space Administration (NASA). Some of the work is similar to that being done by General Electric; e.g., they are examining the effects of contamination and postweld heat-treatments. Bend ductility is being used to show the effect of annealing, as illustrated in Figs. V-1 and V-2, for alloys whose compositions are included in Table V-2.

At Oak Ridge, engineers are studying the aging reactions that occur in refractory-metal alloys.[7] Their recent work has been on 0.5-in.-thick B-66 and D-43 niobium alloys and the T-111 tantalum alloy. No problems were encountered in making bend- and tensile-test specimens in a high-purity atmosphere. All welds were porosity-free and crack-free. Side

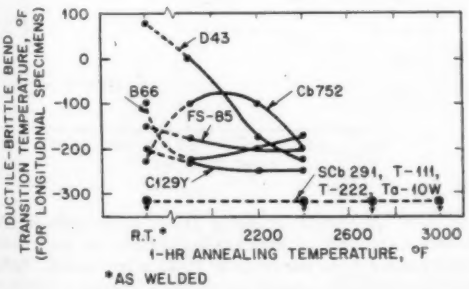

Fig. V-1 Effect of annealing on electron-beam weld-bend ductility.[25]

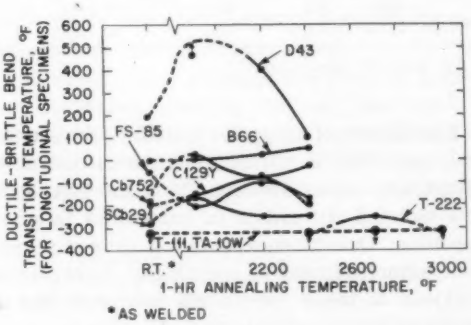

Fig. V-2 Effect of annealing on TIG weld-bend ductility.[25]

Table V-2 ALLOYS INCLUDED IN THE WELDABILITY AND THERMAL-STABILITY EVALUATIONS[25]

Alloy*	Nominal composition, wt.%
AS-55	Cb−5 W−1 Zr−0.2 Y−0.06 C
B-66	Cb−5 Mo−5 V−1 Zr
C129Y	Cb−10 W−10 Hf + Y
Cb-752	Cb−10 W−2.5 Zr
D-43	Cb−10 W−1 Zr−0.1 C
FS-85	Cb−27 Ta−10 W−1 Zr
SCb-291	Cb−10 W−10 Ta
D-43 + Y	Cb−10 W−1 Zr−0.1 C + Y
T-111	Ta−8 W−2 Hf
T-222	Ta−9.6 W−2.4 Hf−0.01 C
Ta−10 W	Ta−10 W
W−25 Re	W−25 Re
W	Unalloyed
Sylvania "A"	W−0.5 Hf−0.02 C

*All alloys are from arc-cast and/or electron-beam-melted material except Sylvania "A."

bend tests over a 2T radius gave these results, measured after fracture: D-43, 5°; B-66, 15°; and T-111, 65°. All failures were in the weld or its edge. An anneal at 1315°C for 2 hr improved the ductility of each alloy. The results of tensile tests are given in Table V-3.

Table V-3 RESULTS OF TRANSVERSE TENSILE TESTS FROM ½-IN.-THICK WELDED PLATES OF REFRACTORY ALLOYS[7]

Alloy	Test temp., °C	Elongation, %	Yield strength (0.2% offset), 1000 psi	Ultimate tensile strength, 1000 psi	Location of failure*
D-43	Room	5.0	60.8	81.0	B-W
	980	8.5	35.1	54.4	B
	1095	10.0	37.0	51.5	B
	1205	13.0	39.9	42.0	B
	1315	10.0	29.8	33.4	B-W
B-66	Room	11.5	76.3	99.4	W
	980	10.0	48.9	63.0	B
	1095	7.5	45.3	41.1	B
	1205	6.5	41.0	43.8	B-W
	1315	9.0	37.4	39.5	B
T-111	Room	5.0	82.7	90.5	W
	980	11.0	40.0	55.5	B-W
	1095	7.5	41.9	52.5	W
	1205	8.0	41.1	50.8	W
	1315	10.0	37.7	43.9	W

*W, weld; B, base metal.

The effects of aging the niobium alloys at 815, 980, and 1205°C on the bend ductility of sheet alloys are shown in Figs. V-3 and V-4. Aging was carried out either in vacuum or in quartz capsules. Quartz encapsulation caused permanent embrittlement of specimens. Laser-probe analysis of these specimens indicated that the surfaces were contaminated with silicon.

Oak Ridge investigators have also been examining the weldability of alloys in the niobium–vanadium binary system with and without small additions of other metals.[3]

Tungsten

A final report has been issued by Solar[26] on the weldability of the Materials Advisory Board, Refractory Metals Sheet Rolling Program's "pedigreed" tungsten sheets. The objectives of this study were quite broad and included examination of metallurgical uniformity, mechanical properties, formability, and joining. A number of joining methods were evaluated and tested to determine the properties of joints up to 3000°F. None of the usual problems encountered when tungsten is being welded were eliminated by the special preparation and handling

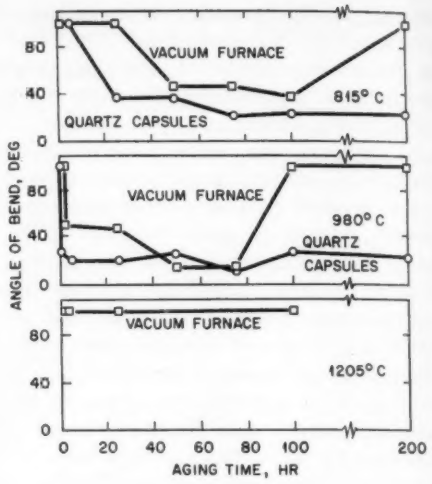

Fig. V-3 Influence of aging time and environment at various temperatures on the bend ductility of FS-85 alloy welds.[7]

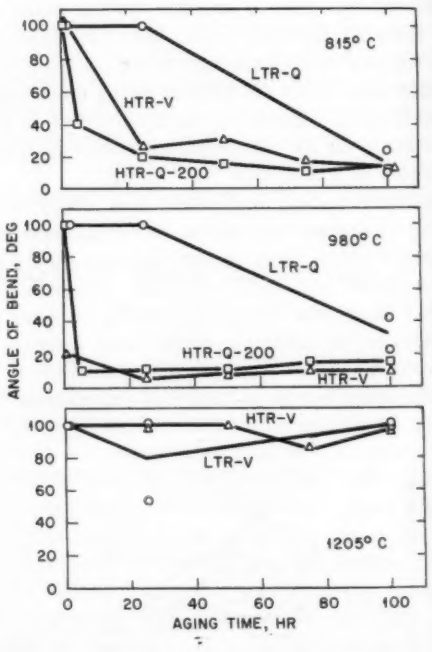

Fig. V-4 Influence of aging time, temperature, and environment and of processing history on the room-temperature bend ductility of D-43 alloy welds. Aging environments: Q, quartz capsule; V, vacuum furnace. Maximum processing temperatures: HTR, 1425°C; LTR, 1205°C. Specimens designated HTR-Q-200 were tested[7] at 93°C.

received by these sheets. Electron-beam welds, for example, in sheet thicknesses which ranged from 0.010 to 0.100 in., were just as brittle as those made in normal commercial tungsten.

Titanium

Significant advances in the welding of thick titanium plate for pressure vessels, etc., have been reported by the U. S. Naval Applied Science Laboratory. The plate used was the titanium–7 wt.% aluminum–2 wt.% niobium–1 wt.% tantalum alloy.[27] It was welded out-of-chamber. Welds produced by the short-circuit process showed fine porosity and cold shutting, but the properties were better than those made by the spray-transfer technique. Filler wires of the 7-2-1 type were stronger than the base plate, but the notch toughness was low. Filler wires of the 6-2-1 and 5-2-1 types gave notch-toughness results significantly better than those of the base plate, but at some sacrifice in strength. The procedures developed were then applied to the fabrication of a 7-ft diameter, 2.5-ft-long, 2.125-in.-thick cylinder from the above alloy and were found satisfactory.[28]

The Navy work and other recent studies on the welding of thick titanium plate are reviewed in a new Defense Metals Information Center publication, Memorandum No. 211, Nov. 24, 1965.

The replacement of dry boxes and inert-gas backup bars when titanium is being welded may result from the development of a nonreactive flux by Mitron Research.[29] The flux can be used as either a powder or a paste made with methyl alcohol. The alcohol is removed from the paste before welding by allowing it to dry in an oven or by ignition. After welding, the flux is removed by chipping and wire brushing. Water washing removes all traces of the flux. The impact properties of welds in the titanium–6 wt.% aluminum–4 wt.% vanadium alloy, with and without flux, are compared in Table V-4.

Nickel-Base Alloys

The Westinghouse-Aerospace Electrical Division has published several specifications for the TIG and electron-beam welding of several dissimilar-metal alloy combinations.[30] The material combinations included Inconel 600 to Inconel 600, to Haynes 25, to 316L stainless steel, and to 70-30 cupronickel. Haynes 25 to Haynes 25, to 316L stainless steel, and to 70-30 cupronickel joints are also included. Joint configurations include butt, tee, and corner.

The results of a comparative study at Southwest Research Institute indicate that Inconel 625 is better than Incoloy 800, on the basis of weldability and strength, for use in fabrication of heat exchangers.[31] Several joint designs were

Table V-4 TRANSVERSE, SUBSCALE, V-NOTCH IMPACT STRENGTH OF 0.050-IN.-SHEET TITANIUM–6 wt.% ALUMINUM–4 wt.% VANADIUM TIG WELDMENTS MADE WITH GAS AND PASTE FLUX BACKUP[29]

Weld backup	Notch position	Heat-treatment	Impact strength, in.-lb, at indicated temperature	
			Room	550°F
Base material			24.9	49.1
Gas	Weld	As welded	20.8	48.1
Flux	Weld	As welded	20.6	39.9
Gas	HAZ*	As welded	30.9	54.2
Flux	HAZ	As welded	27.9	59.7
Base material		Solutionized	33.0	46.4
Gas	Weld	Solutionized	23.9	36.0
Flux	Weld	Solutionized	25.7	34.8
Gas	HAZ	Solutionized	28.2	44.5
Flux	HAZ	Solutionized	26.9	42.3
Base material		Aged	26.8	61.0
Gas	Weld	Aged	19.0	34.1
Flux	Weld	Aged	20.5	35.9
Gas	HAZ	Aged	22.8	40.1
Flux	HAZ	Aged	25.8	44.3
Base material		Solutionized and aged	24.1	40.6
Gas	Weld	Solutionized and aged	13.0	24.3
Flux	Weld	Solutionized and aged	13.2	20.3
Gas	HAZ	Solutionized and aged	23.9	20.0
Flux	HAZ	Solutionized and aged	15.0	26.7

*Heat-affected zone.

also evaluated. The conventional tube-to-sheet joint design proved best. Tests of the standard joints in Inconel 625 gave the following fatigue strengths for a 1000-cycle life:

Type of joint	Temp., °C	Stress, psi
Tube-to-tube sheet	400	+60,000
Boiler cladding-to-tube sheet	315	+54,000
Tube-to-tube, lap	500	+38,000

A program at Oak Ridge to determine the properties of welds in INOR-8 has been concluded with the publication of the hot-ductility and stress-rupture properties.[7] The test specimens were machined from welds made under conditions of high restraint. The as-welded creep properties were equal to those of the wrought alloy at all temperatures. The elevated-temperature creep properties obtained are given in Table V-5. Hot-ductility tests by the Gleeble technique (synthetic heat-affected-zone specimens) gave a nil-ductility temperature of 1260°C for INOR-8. Microstructures of INOR-8 which were heated through the range 980 to 1260°C for Gleeble tests showed some grain-boundary liquation.

Dissimilar Materials Joining

An increasing volume of the metals-joining literature contains data on the making of dissimilar-metal and metal-to-ceramic joints. In the case of metals, this literature is concerned usually with brazing or diffusion bonding of metallurgically incompatible materials.

Oak Ridge investigators are examining the possibilities of replacing the gold–nickel–molybdenum brazing alloy normally used for brazing INOR-8 to graphite with a palladium–nickel alloy.[7] This is because palladium has a lower cross section than gold, and in addition its transmutation products are more desirable.

Pratt & Whitney reports that silver is the best brazing material for joining beryllium to the niobium–1 wt.% zirconium alloy or to type 316 stainless steel for extended service[32] around 600°C. The maximum useful temperature is 760°C owing to the formation of a brittle intermetallic compound. Curves were developed during this study to show the reaction-zone thickness vs. time at 540, 650, and 760°C for a large group of dissimilar-metal couples when they are in intimate contact.

Harwell engineers have overcome the problem of making a transition joint from Zircaloy to stainless steel.[33] They first TIG-welded niobium to the Zircaloy component and then brazed the niobium to the stainless steel. Standard high-temperature nickel-base brazing alloys were used. Others have accomplished essentially the same joint by roll bonding.

Joints between the niobium–1 wt.% zirconium alloy and alumina ceramics were made at Los Alamos by brazing.[34] The Al_2O_3 was metallized by standard processes, plated with nickel, and then brazed to the metal alloy with a 55 wt.% copper–45 wt.% nickel alloy. Uncoated Al_2O_3 + 0.5 wt.% Y_2O_3 was brazed to the niobium alloy with a 48 wt.% titanium–48 wt.% zirconium–4 wt.% beryllium brazing alloy. Both joint systems withstood limited cycling to 1000°C but failed below 1200°C.

Texas Instruments has published a state-of-the-art review on ceramic-to-metal joining.[35] The current status of the subject in relation to developments made in the last decade was evaluated. Mechanical and chemical methods are considered without regard to specific areas

Table V-5 RESULTS OF ELEVATED-TEMPERATURE CREEP TESTS ON INOR-8 TRANSVERSE WELD SPECIMENS[7]

Test temp. °F	Test temp. °C	Applied stress, 1000 psi	Average time to rupture, hr: As welded	Stress relieved*: H_2	Stress relieved*: Argon	Average elongation, %: As welded	Stress relieved*: H_2	Stress relieved*: Argon	Average minimum creep rate, hr^{-1}: As welded	Stress relieved*: H_2	Stress relieved*: Argon
1100	594	74	1.3	1.7		14.1	13.0		2.6×10^{-3}	1.3×10^{-2}	
1100	594	54	197.8	188.3		2.5	8.2		2.3×10^{-5}	1.0×10^{-5}	
1100	594	49	308.4	570.5		2.2	5.3		1.4×10^{-5}	3.2×10^{-5}	
1300	704	45	3.7	6.4	5.5	3.9	8.2	5.4	4.9×10^{-3}	7.4×10^{-3}	7.0×10^{-3}
1300	704	24	158.4	337.8	185.4	3.7	8.8	7.4	1.2×10^{-4}	1.6×10^{-4}	2.2×10^{-4}
1300	704	20	472.3	936.7	452.2	4.6	10.8	3.7	3.5×10^{-5}	6.6×10^{-5}	4.4×10^{-5}
1500	816	22	12.7	12.1		16.9	20.9		5.8×10^{-3}	7.0×10^{-3}	
1500	816	12	172.1	117.5		14.4	9.8		4.8×10^{-4}	4.4×10^{-4}	
1500	816	10	446.9	314.5		8.3	8.1		9.8×10^{-5}	2.0×10^{-4}	

*Stress relieved 2 hr at 1600°F in atmosphere specified.

of utility. All major facets are covered, including techniques, materials, equipment, test methods, and joining theory. The report includes 155 pertinent references.

A new process for joining nonweldable and dissimilar materials was recently reported by General Dynamics/Fort Worth.[36] The process is called Unidyne or high-energy-release-rate (HERR) bonding. Few details have been released, but an interatomic bond showing no signs of prior interfaces is obtained by the process. Bonds have been made in a wide range of materials. Stainless steel, aluminum, titanium, and beryllium are given as examples.

(R. M. Evans)

Nondestructive Testing

Ultrasonic Techniques

The British are doing work which appears to parallel that in the United States with respect to accomplishments with ultrasonics in the nondestructive testing of reactor components. Mann et al. at the UKAEA Reactor Fuel Element Laboratory at Springfields have developed an ultrasonic system using two water-immersed ultrasonic probes that can be oriented to produce circumferential and longitudinal waves and detect 0.001-in.-deep defects located in either the outer or inner surface of tubes ranging down to a bore diameter[37] of 0.020 in.

Argonne has found it very difficult to prepare a mixture of tungsten-loaded epoxies having the high acoustic impedance necessary to match PZT-4 elements used in transducers for nondestructive testing.[2] Consequently they have investigated the feasibility of using porous stainless steel as backing material in these probes.[5,38] Their measurements show that the longitudinal velocity varies linearly with the sample density. The velocity increases approximately 0.062×10^3 in./sec for each 1% increase in density, with an assumed velocity of 5.75×10^3 in./sec at 100% density. According to Argonne, a 90% dense type 316 stainless-steel disk would match the impedance of a disk of PZT-4 [acoustic impedance found to be 34×10^6 kg/(m^2)(sec)].

Worlton claims that transducers $^3/_{16}$ in. in diameter with beams focusing to 0.008 in. in diameter are in common use at Battelle–Northwest for inspecting thin-walled tubing.[39] He claims that using tiny highly focused transducers with diameters less than half of the wall thickness, as well as wide-band electronic circuitry, permits testing thin-walled tubing with the same confidence and readily interpreted results as are obtained on thicker sections. These probes, operating at a center frequency of 15 Mc and as wide a bandwidth as possible, can locate notches on the inner or outer surface with nearly equal amplitude when the incidence angle is high enough to eliminate longitudinal modes. This system is capable of detecting notches 0.001 in. deep. The amplitude response is not critically dependent on incident beam angle.

Referring to the testing of components for the reactor of the first Czechoslovakian Atomic Power Station, Radislav of the V. I. Lenin Works, Pilsen, Czechoslovakia,[40] states that 44% of the total production time for welded parts, sections, and reactor-vessel joints is allocated to defectoscopic examination. Inspection is repeated after every manufacturing operation that could possibly impair the integrity of the material. Techniques and applications appear to parallel those of the West. Ultrasonic inspection is, perhaps, most widely used. "The raw material is examined over its whole volume by the ultrasonic test in at least five different directions by means of rectangular and prismatic probes." Welded seams are also tested ultrasonically. The ultrasonic tests are backed by fluorescent penetrant, electromagnetic, and X-ray inspection wherever applicable. X-ray inspection is performed on weld sections up to 320 mm in thickness, but, at thicknesses greater than 320 mm, ultrasonics only can be applied.

The Czechoslovakians have developed automatic ultrasonic inspection equipment. In one of these systems, inspection of thicknesses to 620 mm is accomplished. The surface to be scanned is flat and horizontal. A mechanical contrivance moves the probe over the inspected surface while recording all flaws down to the smallest permissible size in the whole volume of the inspected product. The electronic system is "the ultrasonic defectoscope type UID-A2 developed by the State Thermodynamics Research Institute in Prague. The mechanical part consists of a moving and recording device developed and manufactured at the V. I. Lenin Works in the town of Pilsen."

Acoustic coupling is compensated for electronically — the time interval between two pulses is used "to regulate the power of the generator. The power of the first echo pulse (e.g. from the

bottom) is compared with a standard pulse, their difference is recorded in the memory, and this controls the generator at the next pulse.

"To compensate for distance (depth of flaw) the amplification of the amplifier is varied with time in the same relationship as applies to the variation of echo signal with depth of flaw.

"These two compensations result in a constant height of echo signals from flaws of a definite size within certain limits of the distance of the flaw from the surface of the probe."

Compensated echo signals exceeding the reject level actuate a recording device that records the projection of the flaw *upon the inspected surface.* The transducers travel along straight guides which advance each time the transducer arrives at the end of travel. A C-scan recording is also made of the test results, as well as a B-scan recording. Radislav claims they can record 2-mm-diameter defects to a depth of 300 mm and 3-mm-diameter defects to a depth of 500 mm. Water is used as couplant.

It is claimed that the equipment can also be used, with some alterations, for examining vertical surfaces, plane or cylindrical. The automatic system, with one operator, is six times faster, regardless of the number of flaws, than a team of two operators inspecting manually at maximum speed (i.e., if there are few flaws within the test piece).

Radislav also claims to be inspecting materials ultrasonically at 60 to 70°C with "slanting" probes made of "organic glass." The changes of velocity from 20 to 60°C can be neglected, but "consequences of dimensional changes due to differential thermal expansion can be avoided by proper construction of the probe." To eliminate errors due to the effect of temperature changes on attenuation in the organic glass, the Czechoslovakians have developed a probe in which the temperature is held constant at the elevated temperatures. Water at 60°C is circulated through copper tubing surrounding a metal casing for the probe. The temperature of the water is controlled by a thermistor embedded in the wedge of organic glass. (D. Ensminger)

NDT Techniques Other Than Ultrasonic

An eddy-current induction probe to measure levels of liquid metals and to detect the interface between metals and salts has been developed by investigators at Argonne.[41] The probe employs an elongated helical dual winding of Nichrome wire in a stainless-steel well (0.032-in. wall) in the liquid-metal bath. Induction from one winding into the liquid metal influences the voltage induced in the second winding. The coil, of simple design, apparently does not have to be moved to make a measurement. Good linearity was obtained for changes in depth of 6 in. in liquid cadmium with a 5-in.-long coil. Operating frequency was 50,000 cps. Calibration curves are given over the range of 400 to 700°C. The probe, its mode of operation, and the circuit diagram are presented in the cited reference.

In connection with their work on X-ray imaging with closed-circuit television, investigators at Oak Ridge[7] have devised a rather unusual penetrameter to assist in establishing "defect sensitivity" for various conditions. The penetrameter is aluminum, about 7.5 in. in diameter and 30 mils thick. Indentations range from 1 mil in diameter and 1 mil deep to 20 mils in diameter and 20 mils deep. The indentations of a given size are arranged in a circle that is concentric with the circles containing other indentation sizes, so that the depths of the indentations vary with the radius of the penetrameter. The circular pattern was chosen so that the specimen can be rotated while a telemonitor is watched. The motion makes the "defect" easier to see, and also the smallest indentation that can be seen is relatively easy to locate.

An instrument for measuring bowing in long tubes has been developed by investigators at Battelle–Northwest.[42] The instrument permits measurements when the outside of a bowed tube is not accessible and when the degree of bowing prohibits conventional line-of-sight optical measurements through the bore. The equipment employs a differential-transformer principle, in which the core of the transformer becomes displaced from center by means of a linkage as the measuring head of the device passes through the tube. The head contacts the inside diameter of the tube at three points. Readout values in the form of digital voltages are processed by computer to determine displacements. Equipment diagrams, analytical considerations, and details of the FORTRAN-II program are presented. (A. F. Leatherman)

References

1. A. B. Shuck, E. M. Pilarski, A. G. Hins, and G. Burton, Jr., Development of a Process for Manufacturing ZPR-III U–Pu–Mo Test Fuel Ele-

ments, USAEC Report ANL-6955, Argonne National Laboratory, March 1965.

2. Argonne National Laboratory, Reactor Development Program Progress Report, October 1965, USAEC Report ANL-7115, Nov. 23, 1965.
3. T. K. Roche (Ed.), Evaluation of Niobium–Vanadium Alloys for Application in High-Temperature Reactor Systems, USAEC Report ORNL-TM-1131, Oak Ridge National Laboratory, October 1965.
4. H. F. Conrad and P. R. Landon, Melting, Fabrication, and Creep Testing of a 1.39 Percent Ti + 0.34 Percent Zr + 0.30 Percent C Molybdenum Alloy, USAEC Report UCRL-14437, University of California, Lawrence Radiation Laboratory, Nov. 1, 1965.
5. Argonne National Laboratory, Reactor Development Program Progress Report, September 1965, USAEC Report ANL-7105, Oct. 20, 1965.
6. B. Pocta, Change in Wall Thickness of Tubes During Drawing, USAEC Report ANL-Trans-189 [translated from *Hutnicke Listy*, 10: 194-200 (May 1955)].
7. S. Peterson (Comp. and Ed.), Metals and Ceramics Division Annual Progress Report for Period Ending June 30, 1965, USAEC Report ORNL-3870, Oak Ridge National Laboratory, November 1965.
8. W. O. Harms (Comp.), High-Temperature Materials Program Quarterly Progress Report for Period Ending July 31, 1965, USAEC Report ORNL-TM-1300, Oak Ridge National Laboratory, December 1965. (Classified)
9. R. G. Mills, J. R. Lindgren, and A. F. Weinberg, Topical Report: An Evaluation of Vapor-Deposited Tungsten Tubing, Report NASA-CR-54277 (GA-5721), General Atomic Division, General Dynamics Corp., Oct. 19, 1964.
10. A. Landsberg, T. T. Campbell, and F. E. Block, Tungsten and Molybdenum Coated Nonmetallic Powder, *J. Metals*, 17: 850-855 (August 1965).
11. J. Zupan, E. G. Pike, and J. B. Whitney, Investigation of Practical Techniques for Coating Refractory Metals. Quarterly Progress Report No. 4, February 1–April 30, 1964, Report PF-64-8, The Pfaudler Co., May 15, 1964.
12. J. P. Page, R. D. Moeller, and G. V. Sneesby, Method of Forming Molybdenum Silicide Coating on Molybdenum, U. S. Patent No. 3,192,065 (to North American Aviation, Inc.), June 29, 1965.
13. N. S. Bornstein, E. C. Hirakis, and L. A. Friedrich, Carburization of Cb–1 Zr Alloy, USAEC Report TIM-927, Pratt & Whitney Aircraft Division, United Aircraft Corp., August 1965.
14. A Process for the Preparation of a Protective Surface Layer on Aluminum or Aluminum Alloys, British Patent No. 991,817, May 12, 1965.
15. G. W. Mellors and S. Senderoff, The Electrodeposition of Coherent Deposits of Refractory Metals, III. Zirconium, *J. Electrochem. Soc.*, 113(1): 60-66 (January 1966).
16. P. West, Refractory Metals Can Be Plated and Electroformed, *Mater. Design Eng.*, 62: 93-94 (July 1965).
17. J. M. Criscione, J. Rexer, and R. G. Fenish, High-Temperature Protective Coatings for Refractory Metals, Progress Report No. 2 (N65-30457), Union Carbide Corp., Carbon Products Division, July 12, 1965.
18. K. Splichal, Electrocladding Uranium, USAEC Report SC-T-65-754 [translated from *Jaderna Energie*, 10: 287-291 (1964)].
19. I. M. Kvokova and V. I. Layner, Electrolytic Coating of Molybdenum and Tungsten with Rhenium, USAEC Report UCRL-TRANS-1212L [translated from *Izv. Vysshikh Uchebn. Zavedenii, Tsvetn. Met.*, No. 4: 142-146 (July–August 1964)].
20. H. T. Francis, Investigations of Random Thickness Variations in Chem-Milled 2219-T37 Aluminum, Final Report on Project B6031, Illinois Institute of Technology Research Institute, Apr. 29, 1965.
21. J. R. Lundquist and R. W. Stromatt, Nickel Electroplating on Uranium: Surface Preparation and Plating Solution Studies, USAEC Report BNWL-124, Battelle–Northwest, October 1965.
22. R. P. Levey, Isostatic Hot Pressing, USAEC Report Y-1487, Union Carbide Corp., Y-12 Plant, June 9, 1965.
23. C. B. Boyer, F. D. Orcutt, and R. M. Conway, Operation of High-Gas-Pressure Autoclaves at High Internal Pressures, Preprint 37C, paper presented at the American Institute of Chemical Engineers Symposium on High-Pressure Processes, Equipment and Research, December 1965.
24. W. H. Kearns and S. Thompson, The Structural Stability of Welds in Columbium Alloys, Quarterly Progress Report No. 6, General Electric Company, Re-Entry Systems Department, Apr. 15, 1965.
25. G. G. Lessmann and D. R. Stoner, Determination of the Weldability and Elevated-Temperature Stability of Refractory Metal Alloys, Report WANL-PR(P)-007, Westinghouse Electric Corp., Astronuclear Laboratory, Mar. 20, 1965.
26. F. St. Germain et al., Evaluation of RMSRP Tungsten Sheet, Final Report, Solar, a division of International Harvester Co., July 9, 1965.
27. N. Nagler, J. R. Crisci, and A. L. Frank, Out-of-Chamber Semiautomatic Welding of Ti–7 Al–2 Cb–1 Ta Alloy Titanium Plate, Technical Progress Report No. 4, U. S. Naval Applied Science Laboratory, Dec. 28, 1964.
28. H. Nagler, S. J. Castiglioni, and J. R. Crisci, Out-of-Chamber Welding of a 7-Foot-Diameter Cylinder of 2⅛-Inch-Thick Ti-721 Roll Formed Plate, Technical Progress Report No. 5, U. S. Naval Applied Science Laboratory, Oct. 18, 1965.
29. R. A. Rosenberg, K. J. Pulkonik, G. S. Irons, and R. D. Regan, Tungsten-Arc Welding Titanium Using a Nonreactive Flux, Report AFML-TR-65-174, Mitron Research and Development Corp., June 1965.
30. R. W. Briggs et al., SNAP-50/SPUR Generator Development Program Quarterly Technical Progress Report for Period Ending June 30, 1965, Report NP-15423, Westinghouse Electric Corp., Aerospace Electrical Division, July 15, 1965.
31. J. McDonald, Jr., E. B. Norris, P. D. Watson, and K. K. Speirs, Consulting Services on the Advanced BONUS Core Boiler-Superheater Fuel Element Weldments, USAEC Report TID-22425, Southwest Research Institute, Sept. 20, 1965.
32. J. R. Stewart, Space Radiator Fabrication Development. Status Report, USAEC Report PWAC-483, Pratt & Whitney Aircraft Division, United Aircraft Corp., Aug. 25, 1965.

33. H. Bowes, Atomic Energy Research Establishment, Harwell, unpublished.
34. R. S. Kirby and J. D. LaMotte, Feasibility of Brazed Joints Between Cb–1 Zr Alloy and Alumina Ceramics, USAEC Report LA-3302, Los Alamos Scientific Laboratory, Dec. 1, 1964.
35. J. F. Clarke et al., State-of-the-Art Review of Ceramic-to-Metal Joining, Report AFML-TR-65-143, Metals & Controls Inc., a division of Texas Instruments, Inc., March 1965.
36. J. Robertson, Molecular Bonding for Unweldables, *Metalworking News* (Sept. 13, 1965).
37. J. H. Gittus, The Evaluation of Nuclear Fuel Element Components, British Report TRG-Report-975, Apr. 13, 1965.
38. Argonne National Laboratory, Reactor Development Program Progress Report, August 1965, USAEC Report ANL-7090, Sept. 21, 1965.
39. D. C. Worlton, High Volume Nondestructive Test Applications at the Hanford Atomic Products Operation, USAEC Report BNWL-SA-97, Battelle–Northwest. Mar. 11. 1965.
40. P. Radislav, Problems of Detectoscopic Examination of Structural Materials for the Reactor of the First Czechoslovakian Atomic Power Station, Canadian Report AECL-2286 (from paper presented at the Symposium on Nondestructive Testing, Bucharest, Mav 17–21. 1965).
41. Argonne National Laboratory, Chemical Engineering Division Semiannual Report, USAEC Report ANL-6925, Mav 1965.
42. B. B. Brenden and J. C. Spanner, An Instrument for Measuring Bowing in Long Tubes, USAEC Report BNWL-59, Battelle–Northwest, August 1965.

LEGAL NOTICE

This journal was prepared under the sponsorship of the U. S. Atomic Energy Commission. Neither the United States, nor the Commission, nor any person acting on behalf of the Commission:

A. Makes any warranty or representation, expressed or implied, with respect to the accuracy, completeness, or usefulness of the information contained in this journal, or that the use of any information, apparatus, method, or process disclosed in this journal may not infringe privately owned rights; or

B. Assumes any liabilities with respect to the use of, or for damages resulting from the use of any information, apparatus, method, or process disclosed in this journal.

As used in the above, "person acting on behalf of the Commission" includes any employee or contractor of the Commission, or employee of such contractor, to the extent that such employee or contractor of the Commission, or employee of such contractor prepares, disseminates, or provides access to, any information pursuant to his employment or contract with the Commission, or his employment with such contractor.